1985

Motion and coalescence of gas bubbles in polymer solutions.

Abdulhamid Mabruk Fadhil. Dajan
University of Windsor

National Library of Canada
Canadian Theses Service
Ottawa, Canada
K1A 0N4

Bibliothèque nationale du Canada
Services des thèses canadiennes

CANADIAN THESES

THÈSES CANADIENNES

NOTICE

The quality of this microfiche is heavily dependent upon the quality of the original thesis submitted for microfilming. Every effort has been made to ensure the highest quality of reproduction possible.

If pages are missing, contact the university which granted the degree.

Some pages may have indistinct print especially if the original pages were typed with a poor typewriter ribbon or if the university sent us an inferior photocopy.

Previously copyrighted materials (journal articles, published tests, etc.) are not filmed.

Reproduction in full or in part of this film is governed by the Canadian Copyright Act, R.S.C. 1970, c. C-30. Please read the authorization forms which accompany this thesis.

AVIS

La qualité de cette microfiche dépend grandement de la qualité de la thèse soumise au microfilmage. Nous avons tout fait pour assurer une qualité supérieure de reproduction.

S'il manque des pages, veuillez communiquer avec l'université qui a conféré le grade.

La qualité d'impression de certaines pages peut laisser à désirer, surtout si les pages originales ont été dactylographiées à l'aide d'un ruban usé ou si l'université nous a fait parvenir une photocopie de qualité inférieure.

Les documents qui font déjà l'objet d'un droit d'auteur (articles de revue, examens publiés, etc.) ne sont pas microfilmés.

La reproduction, même partielle, de ce microfilm est soumise à la Loi canadienne sur le droit d'auteur, SRC 1970, c. C-30. Veuillez prendre connaissance des formules d'autorisation qui accompagnent cette thèse.

THIS DISSERTATION
HAS BEEN MICROFILMED
EXACTLY AS RECEIVED

LA THÈSE A ÉTÉ
MICROFILMÉE TELLE QUE
NOUS L'AVONS REÇUE

NL 339 (r. 86/01)

Canada

MOTION AND COALESCENCE OF GAS BUBBLES IN POLYMER SOLUTIONS

by

Abdulhamid Mabruk Fadhil Dajan

A Thesis
submitted to the
Faculty of Graduate Studies and Research
through the Department of
Mechanical Engineering in Partial Fulfillment
of the requirements for the Degree
of Master of Applied Science at
the University of Windsor

TO MY WIFE, GAZALA BUAHDIALA,

AND MY SON, YOUNIS.

ACKNOWLEDGEMENTS

My sincere thanks and gratitude are due to HIS ALMIGHTY, ALLAH, WHO helped and blessed me during the course of my studies in general.

The author wishes to express his appreciation and thanks to Dr. D.D. De Kee for his supervision, valuable guidance, and continuous encouragement during the course of this work.

Thanks are due to Dr. Gary W. Rankin, Dr. Robert A. Stager, and Dr. Robert G.S. Gaspar. Their constructive criticism was both enlightening and beneficial.

I would like to express my appreciation and gratitude to Dr. Krishnaswamy Sridhar and Dr. Zygmunt F. Reif for their continuous encouragement throughout the course of my study in the Mechanical Engineering Department, University of Windsor.

The author is grateful to the University of Garyounis, Benghazi-Libya, for the financial support and providing the opportunity to pursue graduate studies abroad.

I would also like to extend my thanks to Mrs. Petrona Parungo for her meticulous typing of the thesis.

I feel very grateful to my wife, Gazala Abas Buahdiala, for her encouragement, sacrifices, understanding, and valuable assistance. Special thanks go to my son, Younis, who provided me with company during the long hours of writing the thesis.

ABSTRACT

The motion and coalescence of gas bubbles in solutions of different polymer concentration has been studied. Experimental equipment has been modified to inject single and multiple gas bubbles simultaneously with a minimum disturbance to the test fluid.

Average terminal velocity data were gathered using a photographic technique for different solutions of polyacrylamide (0.5, 1.0 with surfactant, 1.0, and 1.5 (wt.%) PAA) in a 50/50 (wt.%) mixture of glycerine and water. No discontinuity in the case of the log-log plots of the average terminal velocity versus bubble volume has been observed. The effect of injecting different gases such as air, nitrogen, and carbon-dioxide on the bubble motion, as well as the effect of a surface active substance whether deliberately added or already present in the tested fluid was studied. Also, a study of the effect of polymer aging characteristics on the motion of air bubbles was carried out.

Different types of bubble shapes were observed in terms of the polymer concentration, namely: spherical, prolate-teardrop, oblate-cusped, oblate-spheroid, and spherical-cap. Oblate-spheroid shaped bubble was observed only in the case of 0.5 (wt.%) PAA solution. For a specific liquid, the shape of the bubble was a function of its volume and the fluid elasticity.

Bubble coalescence was examined for two gas bubbles injected simultaneously from a variety of orifice separation distances (S) at two different coalescence heights (H) in the

four polymer solutions, mentioned earlier. The effects of polymer concentration, volume of the fixed bubble (V_f), coalescence height, surfactant, and injecting different gases on the coalescence process were studied. Fluid elasticity was found to be the predominant factor because of its influence on the bubble shape transition and thus on the wake configuration behind the leading bubble (V_v). A discontinuity in the case of the semi-log plot of V_v/V_f versus S/H was observed at a transition separation distance (S_t) between the orifices.

A dimensional analysis was performed to obtain the parameters which can be used to describe the non-Newtonian and elasticity influence on the motion of a non-spherical gas bubble. The viscosities of the four polymer solutions were measured with the aid of a Contraves Rheomat-30 viscometer.

TABLE OF CONTENTS

LIST OF TABLES

LIST OF FIGURES

LIST OF APPENDICES

NOMENCLATURE

c	dimensionless rheological parameter in Equations (IV-14 and IV-15).
C_s	shear wave velocity, defined by Equation (II-2), m/s.
D	bubble diameter, m.
De	Deborah number.
E_o	Eotvos number.
f	friction factor or drag coefficient.
H	coalescence height, m.
I.P.	injection period, s.
Le	Levich number.
n	power-law index.
r_e	equivalent radius of bubble = $(\frac{3V}{4\pi})^{1/3}$, m.
R	radius of bubble, m.
Re	Reynolds number.
S	orifice separation distance, m.
S_t	transition separation distance between the orifices, m.
τ_p	time constant in De Kee's model (Eq. IV-1), s.
V	bubble volume, m^3.
V_f	volume of the trailing bubble (fixed volume bubble), m^3.
$\langle v_t \rangle$	average ("terminal") velocity of bubble rise, m/s.
V_v	volume of the leading bubble (variable volume bubble), m^3.
v_w	velocity of the wake, m/s.

$\langle v_1 \rangle$	terminal velocity of the leading bubble in Equation (II-16), m/s.
$\langle v_2 \rangle$	terminal velocity of the trailing bubble in Equation (II-16), m/s.
Ws	Weissenberg number.
$\bar{\dot{\gamma}}$	shear rate tensor, s^{-1}.
η_o	zero shear rate viscosity, Pa.s.
η	non-Newtonian viscosity, defined by Equation (IV-1), Pa.s.
η_∞	high shear rate limiting viscosity, defined by Equation (IV-2), Pa.s.
λ	wavelength = $2\pi r_e$, m.
λ_o	time constant in Equations (IV-6) and IV-10), s.
Λ_1	dimensionless time defined by Equation (IV-5).
Λ_2	dimensionless time defined by Equation (IV-6).
II	second invariant of the rate of deformation tensor, defined by Equation (IV-17), s^{-2}.
ρ	density of the liquid phase, kg/m^3.
σ	surface tension, N/m.
τ	injection period, s.
$-(\tau_{11}-\tau_{22})$	primary normal stress difference, Pa.
$\bar{\tau}$	extra stress tensor, Pa.
ψ_1	primary normal stress coefficient = $\frac{-(\tau_{11}-\tau_{22})}{\dot{\gamma}^2}$, Pa.$s^2$.

I. INTRODUCTION

The motion of gas bubbles in a continuous phase has been the subject of comprehensive investigations in the last three decades. Bubble motion is of great importance in the study of boiling, cavitation, electrolysis and design of process equipment which involve mass transfer such as sparge reactors and fermentors in the chemical and biochemical process industries.

The objectives of this work are to:

(i) investigate the shape and motion of gas bubbles in viscoelastic liquids as a function of bubble volume.
The viscoelastic liquids are:

(a) a 0.5 (wt.%) solution of polyacrylamide (PAA) in a 50/50 (wt.%) mixture of glycerine and water.

(b) a 1.0 (wt.%) solution of PAA in a 50/50 (wt.%) mixture of glycerine and water.

(c) a 1.0 (wt.%) solution of PAA in a 50/50 (wt.%) mixture of glycerine and water with surfactant.

(d) a 1.5 (wt.%) solution of PAA in a 50/50 (wt.%) mixture of glycerine and water.

(ii) investigate the effect of injecting different gases, other than air, such as carbon-dioxide and nitrogen.

(iii) perform a dimensional analysis of the problem relating bubble behaviour to the properties of the liquid.

(iv) study bubble coalescence using a simultaneous multiple bubble injection technique.

(v) interpret the results of the experimental program.

II. LITERATURE SURVEY

A large amount of work has been published in the field of bubble dynamics for Newtonian fluids. Much less emphasis has been placed on similar studies involving rheologically more complex fluids. The principal objective of this chapter is to give a comprehensive review of this literature as it applied to the fluid dynamics, heat transfer, and mass transfer. Numerous examples, related to bubble motion and mass transfer in non-Newtonian fluids are, however, of great importance in the chemical industry. Also, the use of gas bubbles for obtaining accurate data on velocities, streamline and pathline configurations, in steady and unsteady fluid flows.

The study of bubble coalescence using a simultaneous multiple bubble injection technique has received no attention. Studies so far have involved in-line coalescence only. Bubble coalescence is of major significance in gas-liquid contactors used in the polymer and the fermentation industries. The viscoelasticity has a tendency to increase both the collision and the coalescence times of gas bubbles. The overall coalescence rate can be reduced considerably with the addition of polymer additives.

This chapter will deal mainly with the motion and coalescence of gas bubbles in non-Newtonian fluids.

II.1 Bubble Motion and Shape

The first major contribution on the motion of gas bubble in viscoelastic fluids was performed by Astarita and Apuzzo (A1) and has indeed been a source of information and inspiration for the researchers in this field. The study essentially provided experimental information on gas bubble motion in the low and high Reynolds number region and demonstrated the dramatic appearance of a discontinuity in the velocity of rise-bubble volume relationship for elastic fluids. Astarita and Apuzzo (A1) presented experimental results on the rising velocity and shapes of bubbles in both purely viscous and viscoelastic non-Newtonian pseudoplastic liquids. They reported that the terminal rise velocity of small bubbles in certain viscoelastic liquids exhibited a discontinuity at some critical value of the bubble volume. For example, they observed an approximately six-fold jump in the terminal velocity at a critical volume of 0.1×10^{-6} m^3 for their typical solutions. Also, a series of bubble shapes were observed which differed considerably from those encountered in Newtonian liquids; specifically, with increasing bubble volume, the bubbles changed from a spherical shape to a prolate teardrop shape and further through an oblate cusp shape to a spherical cap with rounded edges and a cusp trailing surface.

The bubble motion can be classified into the following regimes:

(i) Stokes Regime:

A gas bubble moves in the Stokes regime when the bubble is in creeping flow; the bubble is spherical and the interface is rigid.

(ii) Hadamard Regime:

A gas bubble moves in the Hadamard regime when the bubble is in creeping flow; the bubble is spherical and the interface is free.

(iii)Levich Regime:

A gas bubble moves in the Levich regime when the Reynolds number is high; the bubble is spherical and the interface is free.

(iv) Taylor Regime:

A gas bubble moves in the Taylor regime when the Reynolds number is high; the bubble has a spherical cap shape and the interface is free.

A free interface is one at which continuity of shear stress is satisfied, so that if the gas is assumed to be inviscid, the components of the stress tensor are zero at a free interface. A rigid interface is such that the liquid velocity on it is everywhere equal to the velocity of the bubble's center of gravity.

Astarita and Apuzzo (A1) offered the plausible hypothesis that the observed velocity discontinuity was due to a sudden transition from the Stokes to the Hadamard regime and that viscoelasticity was somehow responsible for making

the transition abrupt rather than continuous as with Newtonian fluids. In addition, they implied that the magnitude of the velocity jump could be largely attributed to a variation of viscosity with shear-rate similar to that found in the so-called pseudoplastic fluids (with the power-law parameter $n < 1$).

Calderbank et al. (C1) reported similar results for a 1% aqueous polyethyleneoxide (Polyox) solution. In addition, they implied that the bubble shapes observed in the aqueous polyox solution go from spherical to prolate spheroidal to that of a top rounded inward (this last transition occurring at the critical bubble size), to that of an oblate spheroid with a tail, to that of a spherical cap. Calderbank et al. (C1) discussed the rise velocity data of carbon-dioxide bubbles in a non-Newtonian 1% aqueous polyox solution. The velocity data pertaining to the polyox solution show an abrupt increase in velocity, by a factor of over four at a critical bubble size (bubble volume $\simeq 1.0 \times 10^{-8}$ m^3). Also, the terminal rise velocity of large spherical cap bubbles in the polyox solution asymptotically approached the predictions of the Dumitrescu equation:

$$\langle v \rangle = 0.35 \, (gD)^{\frac{1}{2}} \qquad \text{(II-1)}$$

where $\langle v \rangle$ = average ("terminal") velocity of bubble rise, (m/s)

and D = bubble diameter, (m)

g = gravitational acceleration (m/s^2).

Acharya et al. (A2) confirmed that a region exists where the bubble undergoes a rapid increase in the velocity in a small volume range which indicates that its interface is free. At large volumes, the bubble velocity becomes more insensitive to the bubble volume.

Acharya et al. (A2) examined if the observed velocity discontinuity occurred at a bubble rise velocity value equal to the shear wave velocity. This was not the case. The shear wave velocity is defined as follows:

$$C_s = \frac{\mu}{\rho\lambda} \qquad \text{(II-2)}$$

where, μ = liquid viscosity (Pa.s)

ρ = liquid density, (kg/m^3)

λ = wavelength (2π x equivalent radius of bubble). (m)

For instance, in the case of the data by Leal et al. (L1), the shear wave velocity (calculated on the basis of an effective viscosity and relaxation time evaluated at the appropriate shear rate) was of the order of 0.04 and 0.05 m/s. for 0.5% and 1% polyacrylamide solution, respectively. The corresponding rise velocities at which the discontinuities arose were, approximately 0.022 and 0.005 m/s. A graphical representation of the velocity discontinuity phenomena is shown in Fig. (II-1).

Astarita et al. (A1), Calderbank et al. (C1) and Leal et al. (L1) all observed a steep and abrupt jump (some-

Figure (II-1) Typical Velocity Discontinuity at a Critical Bubble Volume.

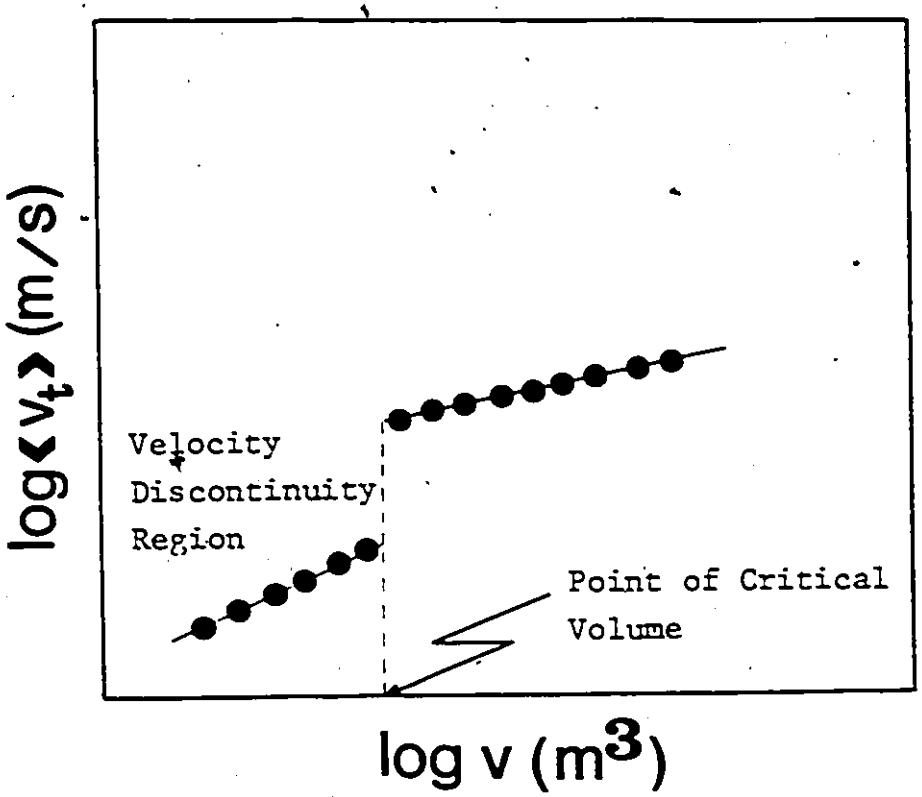
log⟨v_t⟩ (m/s)
Velocity
Discontinuity
Region
Point of Critical
Volume
log v (m³)

times up to ten fold) in the velocity at a critical volume. Acharya et al. (A2) hypothesized that the polymer molecules themselves act as large surfactants and the flow induced gradients of these large molecules may be responsible for generating the surface stresses which oppose the circulatory motion existing within the gas bubble; also, the partial cleansing of the surface responsible for the rapid velocity change is likely to occur much more abruptly in the case of a viscoelastic liquid.

Interesting observations concerning the motion of solid spheres and gas bubbles have been made by Leal et al. (L1) who showed that there was no observed discontinuity in the case of the motion of solid spheres of the same size range and the same absolute density difference as between the gas bubbles and the viscoelastic fluids being considered.

Leal et al. (L1) investigated the discontinuity in further detail and showed that, the discontinuity does occur because of a transition from the Stokes to Hadamard regime, just as Astarita and Apuzzo (A1) had concluded; that is the discontinuity mainly represents a changeover from a rigid interface to a free interface. As noted by Astarita and Apuzzo (A1), the slopes of the log <v> versus log V curves preceding the point of transition are larger in the viscoelastic solutions than in corresponding Newtonian liquids. Furthermore, the slope appears to be equal before and after this transition. Leal et al. (L1) observed the same trend.

This was shown by Astarita and Apuzzo (A1) to be partly due to the shear dependence of the viscosity for power-law fluids. Astarita and Apuzzo (A1) found that a satisfactory comparison existed between the power-law parameter n as calculated from the observed slope (d log <v>/d log V) and their equation:

$$\frac{d \log \langle v \rangle}{d \log V} = \frac{1 + n}{3n} \qquad \text{(II-3)}$$

provided that the liquid exhibited only weak normal stress effects. Calderbank et al. (C1) found good agreement between the two measured values of n for the case of 1% aqueous polyox solution. Acharya et al. (A2) discussed the plots of log <v> versus log D and log <v> versus log V which yield slopes of (n+1)/n and (n+1)/3n, respectively. The test of this observation for low Reynolds numbers (Re << 1) is made (a plot of d log <v>/d log V versus n) for both viscoinelastic solutions (such as carboxymethylcellulose solution, which did not exhibit any measurable normal stress differences) and viscoelastic solutions (such as polyethyleneoxide and polyacrylamide solutions) which exhibited large normal stress differences. This implies not only that the viscometric data were appropriate in the shear rate range covered, but also that the contribution of elastic stresses in the creeping flow range covered is negligible as far as the velocity-volume relationship is concerned.

Mendelson (M2) provided a wave analogy in predicting the bubble terminal velocity. The analogy is found to be in

quantitative agreement when the wave length is suitably interpreted in terms of bubble dimensions. This analogy relies heavily on the fact that when the motion is inviscid, the bubble may be thought of as an interfacial disturbance whose dynamic behaviour would be similar to the surface waves on an ideal fluid.

Mendelson (M2) introduced the wave equation, which is given as

$$\langle v \rangle = \sqrt{\frac{\sigma}{r_e \rho} + g r_e} \qquad \text{(II-4)}$$

where,

$\langle v \rangle$ = bubble terminal velocity, (m/s)

r_e = equivalent radius of bubble, (m)

ρ = density of liquid phase, (kg/m^3)

σ = surface tension. (N/m)

Mendelson (M2) concluded that the wave equation could predict the terminal velocity of bubbles. Acharya et al. (A2), who analyzed the behaviour of large gas bubbles in non-Newtonian media by using equation (II-4) observed good agreement between theory and experiment. The inviscid flow assumption in the wave theory is tantamount to the assumption that, the role of internal stresses in the high Reynolds number flows should be negligible.

Barnett et al. (B1) investigated the flow behaviour of the bubbles and instantaneous drag coefficients were calculated from diameter and velocity measurements. These data

were plotted against two different types of Reynolds numbers for non-Newtonian fluids:

(i) Power Law Fluid

$$Re_p = \frac{(\langle v \rangle)^{2-n} D^n}{K(3)^{n-1}} \qquad \text{(II-5)}$$

(ii) Ellis-Model Fluid, for which two Reynolds numbers can be derived:

$$Re_o = \phi_o \langle v \rangle \rho D \qquad \text{(II-6)}$$

and

$$Re_1 = \phi_1 \rho^{\alpha} (\langle v \rangle)^{2\alpha-2} \qquad \text{(II-7)}$$

where; $\phi_o (s^{-1} \cdot Pa^{-1})$, $\phi_1 (m^2 \cdot s^{-2} \cdot Pa^{-\alpha})$ and α(dimensionless) are empirical constants (model parameters).

Barnett et al. (B1) found that the power-law model does not fit the rheological data too well and that for Reynolds numbers less than one, the best fit to the "non-Newtonian bubble" data is given by:

$$F = \frac{28.6}{Re_E} \qquad \text{(II-8)}$$

where, F is the drag coefficient, and

$$Re_E = Re_o + Re_1 \qquad \text{(II-9)}$$

Barnett et al. (B1) concluded that the bubble-shaped transitions play a dominant role in the mass transfer characteristics of bubbles, for which they calculated the bubble diameter from the measured major and minor axes of the bubble photographic geometry. Assuming an oblate spheroid, they computed the diameter of the equivalent volume sphere. This technique is adopted by many of the authors of experimental research on bubble behaviour in non-Newtonian media.

Acharya et al. (A2) provided a mechanistic discussion of the bubble shapes in non-Newtonian fluids, in which the bubble shape was represented in terms of the eccentricity (D/H) of the bubble which is defined as the ratio of the maximum width to the maximum height. Bubble deformation in non-Newtonian media was discussed by Acharya et al. (A2) who provided comprehensive correlations of bubble shapes for eccentricity less than unity and bubble shapes for eccentricity greater than unity. The study essentially showed the following:

(i) For (D/H < 1), the Reynolds numbers are vanishingly small. The inertia forces are assumed to be negligible and the surface tension tends to maintain the shape perfectly spherical. Teardrop shaped bubbles appear when the liquids are elastic which evidently arise due to the interaction of the elastic and surface tension forces.

(ii) For (D/H > 1), at large Reynolds numbers, the fluid inertia causes major distortions from sphericity when the bubble moves in Newtonian media tending to make the bubble

shape approach an oblate spheroid. At large bubble volumes, the elastic stresses, the inertial stresses and the surface tension stresses will control the equilibrium shape of the bubble.

Wallis (W1) introduced a dimensionless group called the Eotvos number which is defined as follows:

$$E_o = \frac{\text{gravitational force}}{\text{surface tension force}}$$

$$E_o = \frac{g\, D^2\, (\rho_L - \rho_G)}{\sigma} \qquad \text{(II-10)}$$

where,

D = bubble diameter, (m)

ρ_L = density of the liquid phase, (kg/m^3)

ρ_G = density of the rising gas bubble, (kg/m^3)

σ = surface tension. (N/m)

The Eotvos number accounts for the effect of surface tension and plays a dominant role in the shape of a bubble rising in a viscous liquid and the breakaway of a bubble from a submerged horizontal orifice. Although most of the previous work with viscoelastic fluids has been experimental in nature, a few theoretical papers have been published related to this topic. Astarita (A4) presented an order of magnitude dimensional analysis of the problem of motion of a spherical gas bubble through a viscoelastic Maxwell liquid in terms of dimensionless groups such as:

(i) the Deborah number:

$$De = \frac{\text{time scale of flow}}{\text{relaxation time}} = \frac{RG}{\langle v \rangle \mu_L} \quad \text{(II-11)}$$

(ii) the Levich number:

$$Le = \frac{\text{viscous stress}}{\text{total stress}} = \frac{\mu_L \langle v \rangle}{\rho_L g R^2} \quad \text{(II-12)}$$

(iii) the Reynolds number:

$$Re = \frac{\text{inertia}}{\text{viscous force}} = \frac{\rho_L \langle v \rangle}{\mu_L} \quad \text{(II-13)}$$

(iv) the Weissenberg number:

$$Ws = (\text{relaxation time})(\text{shear rate}) = \frac{\mu_L \langle v \rangle}{GR} \quad \text{(II-14)}$$

(v) the A-groups:

$$A = \frac{\text{applied stress}}{\text{elastic modulus}} = \frac{\rho_L g R}{G} \quad \text{(II-15)}$$

where $\langle v \rangle$ = bubble terminal velocity, (m/s)

$\frac{\mu_L}{G}$ = relaxation time of the liquid, (s)

μ_L = liquid viscosity, (Pa·s)

G = elastic modulus, ($kg/m \cdot s^2$)

R = bubble radius, (m)

ρ_L = liquid density, (kg/m^3)

g = field acceleration, (m/s^2)

The study essentially provided a theoretical approach without

obtaining a rigorous solution to the problem. Astarita (A4) discussed the possible effect of choosing the Maxwell-type constitutive equation on establishing a rigid solution to the problem.

Kawase and Ulbrecht (K1) re-examined the mechanism of the abrupt transition of the terminal velocity in a purely viscous non-Newtonian fluid. They proposed a model based on the influence of the density difference between the gas and liquid phases, the purely viscous property of the ambient liquid in conjunction with the gradient of the surface tension and of the bubble volume. Kawase and Ulbrecht (K1) concluded that the model does not account for the sudden, discontinuous, transition which has been observed when bubbles rise in a polymer solution. Also, they suggested that elasticity plays an important role in this phenomenon but more experiments are needed to clarify this matter.

Shima and Tsujino (S1) investigated the effects of polymer concentration on the bubble behaviour and the coalescence rate in 0.67% and 1.01% CMC aqueous solutions. They found that the bubble oscillations were reduced with increasing polymer concentration. Also, the larger the concentration, the smaller the coalescence rate.

Shima and Tsujino (S1) concluded that an increase in polymer concentration is very effective on the suppression of cavitation damage.

Skelland and Caenepeel (S2) studied the effects of anionic and cationic surface active agents (S.A.A.) on mass transfer during drop formation, fall, and coalescence for both continuous and disperse phase-controlled systems. Their results exhibit a dramatic reduction in the mass transfer coefficient with increasing S.A.A. concentration. For the disperse phase-controlled system, transfer rates in all three stages were reduced by either anionic or cationic S.A.A. to less than 10% of that in uncontaminated systems. Also, they observed similar but less severe reductions for both surfactants in the continuous phase-controlled system during formation and free fall. Skelland and Caenepeel (S2) concluded that the surface active molecules migrate to the interface causing an interfacial blockage which in turn reduce circulation and oscillation during drop formation and free-fall. It also introduces waves modification at the coalescence interface.

Miller (M4) examined bubble coalescence in bubble swarms. Relationships are developed for determining interfacial areas as a function of bubble coalescence and for predicting liquid-film-controlled mass transfer between gas and liquid phases. Miller (M4) confirmed that the mass transfer rate is directly dependent on bubble size.

II.2 Bubble Coalescence

The in-line interaction of two bubbles in viscous liquids has been studied by Crabtree et al. (C2), de Nevers et al. (D1) and Narayanan et al. (N2). Their results can be considered in terms of the dimensionless groups such as the Reynolds number (Re), the Eotvos number (E_o) and the Morton number ($M = g\mu_L^4/\rho_L\sigma^3$).

Crabtree et al. (C2) studied the coalescence of two spherical cap bubbles for a Morton number of 2.89×10^{-2} with $40 < Re < 86$ and $5 < x/d_e < 40$ where x is the separation distance of bubbles, distance behind the leading bubble, and d_e is the volume-equivalent diameter of bubble [$d_e = (6V/\pi)^{1/3}$].

They attempted to predict the position of the trailing bubble by superposition, i.e., by assuming that the trailing bubble rises towards the leading bubble at a coalescence rate determined by

$$\frac{dx}{dt} = (\langle v_2 \rangle - \langle v_1 \rangle) + v_w \qquad \text{(II-16)}$$

where x = separation distance of bubbles, distance behind the leading bubble, (m)

t = time to coalesce, (s)

$\langle v_1 \rangle$ = terminal velocity of the leading bubble, (m/s)

$\langle v_2 \rangle$ = terminal velocity of the trailing bubble, (m/s)

and v_w = velocity of the wake, (m/s)

Crabtree et al. (C2) used their velocity data and the experimental coalescence rate to obtain values for the wake velocity from equation (II-16), which were then correlated by

$$\frac{v_w}{\langle v_1 \rangle} = 3.1 \ (d_{el}/x) \qquad \text{(II-17)}$$

They found better agreement when the wake velocity was derived from Batchelor's asymptotic wake velocity profile:

$$v_w = \frac{V\rho g}{4\pi\mu x} \exp\left[\frac{-\langle v \rangle . y^2 \rho}{4\mu x}\right] \qquad \text{(II-18)}$$

where, $\langle v \rangle$ = terminal rise velocity of which bubble is in isolation, (m/s)

y = radial distance from the axis of rise, (m)

V = bubble volume, (m^3)

μ = liquid viscosity, (Pa·s)

and ρ = liquid density. (kg/m^3)

Crabtree et al. (C2) found poor agreement with their data when the wake velocity was taken to be the potential flow velocity behind the leading bubble and its wake.

In-line coalescence of two bubbles during chain bubbling in glycerine (Morton number = 32) was studied by de Nevers et al. (D1). They proposed a model based on two different wake configurations. Both geometries are based on the following assumptions:

(i) The wake behind the bubble is conical.

(ii) The first bubble trails a wake in the form of an "exponential cone" whose radius decreases exponentially with distance.

de Nevers et al. (D1) presented their results in terms of coalescence time versus separation distance. They concluded that the experimental data seem to agree about equally well with the predictions of the model, based on two different assumed wake geometries. This indicates that the assumed shape of the wake is not particularly significant.

Narayanan et al. (N2) measured bubble positions during in-line coalescence of two bubbles of equal size in three liquids of different Morton numbers ($M = 1.8 \times 10^{-3}$, $M = 95 \times 10^{-2}$ and $M = 19.5$) for $2 < x/d_e < 6$ and for $Re < 7$ the interaction was adequately described by the theory for two weightless spheres. For larger Re, however, there is no theory available.

Narayanan et al. (N2) used the superposition principle of equation (II-16) and they derived the wake velocity from their data and presented a graphical correlation of $(\langle v_l \rangle / v_w)$ versus (x/d_{el}) for $7 < Re < 80$.

Bhaga et al. (B2) checked the validity of equation (II-16) for in-line bubble coalescence. They arrived at the following conclusions:

(i) if the column is sufficiently tall, two bubbles of equal size will always coalesce.

(ii) if the trailing bubble is smaller than the leading bubble, it will coalesce if it is larger than a critical size.

Bhaga et al. (B2) confirmed the validity of equation (II-16). Crabtree et al. (C2) used a wake velocity function based on the far-wake solution described by Batchelor's asymptotic wake velocity profile. Batchelor's theory is only valid for viscous wakes, which means behind bubbles with a Reynolds number less than unity or far downstream in the wake for higher Reynolds numbers. Crabtree and Bridgewater's theory differs quite considerably from their experimental results, probably due to the high Reynolds numbers encountered: Re ε (40-90).

The results of these papers lead to a conclusion that increased viscosity of the ambient liquid enhances the coalescence rate and results in a reduced interfacial area.

Acharya et al. (A3) presented their data in terms of coalescence times of bubbles in inelastic carboxymethylcellulose (CMC) and visoelastic polyacrylamide (PAA) solutions versus the basal bubble diameter. The data show that the coalescence time of bubbles is longer in a viscoelastic PAA solution than in an inelastic CMC solution, which suggests that elasticity delays the coalescence process. They attempted to interpret the delayed coalescence, but noting that a viscoelastic fluid has a resistance towards being stretched which an inelastic fluid does not have.

Because the age and rheology of polymer solutions play a dominant role in the study of dynamics of bubbles in viscoelastic media, Naik et al. (N1) studied the rheological behaviour of aqueous CMC solutions and the changes that occur with time.

They observed the following:

(i) The viscosity of an unpreserved CMC solution decreased with time;

(ii) Aqueous CMC solutions have high degrees of pseudopolasticity and high shear stability over long periods.

Naik et al. (N1) reported that the decrease of viscosity with time is due to a decrease in molecular weight resulting from degradation. The greatest decrease was exhibited by a solution stored at 343 K.

III. EXPERIMENTAL PROCEDURE

A schematic diagram of the entire single bubble system is given in Figure (III-1) showing the description of the test facilities. The multiple injection system is basically of the same orientation except for the stroke adjustment mechanism as shown in Figure (III-2).

III.1 Apparatus

The experimental apparatus has been designed to:

(i) produce bubbles of varying volumes. (0.01×10^{-6} m^3 to 30×10^{-6} m^3)

(ii) produce bubbles at selected injection periods.

(iii) inject bubbles simultaneously.

(iv) determine the terminal velocity of the produced bubbles.

Since photographic work had to be undertaken during bubble ascent in the column, two plexiglass tanks were constructed to help visualize the motion of single and multiple gas bubbles. The single bubble tank is 20.3×10^{-2} m in length and 61×10^{-2} m in height. The multiple bubble tank is 23×10^{-2} m in length and 76.2×10^{-2} m in height.

The pressure exerted by the fluid upon the orifice in which the bubble is to emerge is counterbalanced by an equivalent gas pressure. This technique has been used by Mordarski (M3). A Union Carbide pressure regulator (0.0 - 14.0 kPa) is utilized to balance the fluid head above the

Figure (III-1) A Schematic Flow Diagram of the Single Bubble Injection System and the Test Facilities.

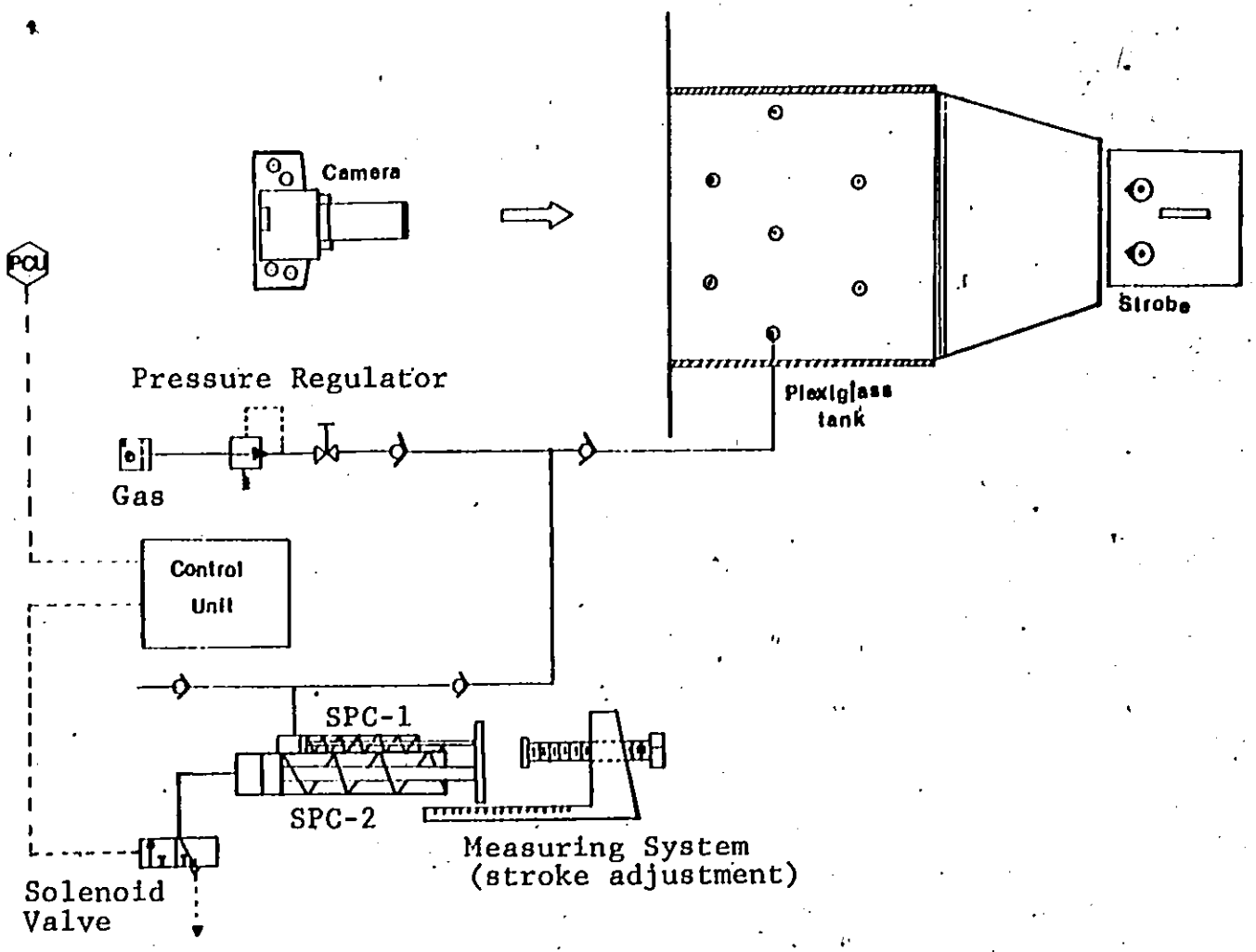
Camera
PCU
Strobe
Pressure Regulator
Plexiglass tank
Gas
Control Unit
SPC-1
SPC-2
Measuring System (stroke adjustment)
Solenoid Valve

Figure (III-2) Measuring Systems for the Experiments of Bubble Coalescence.

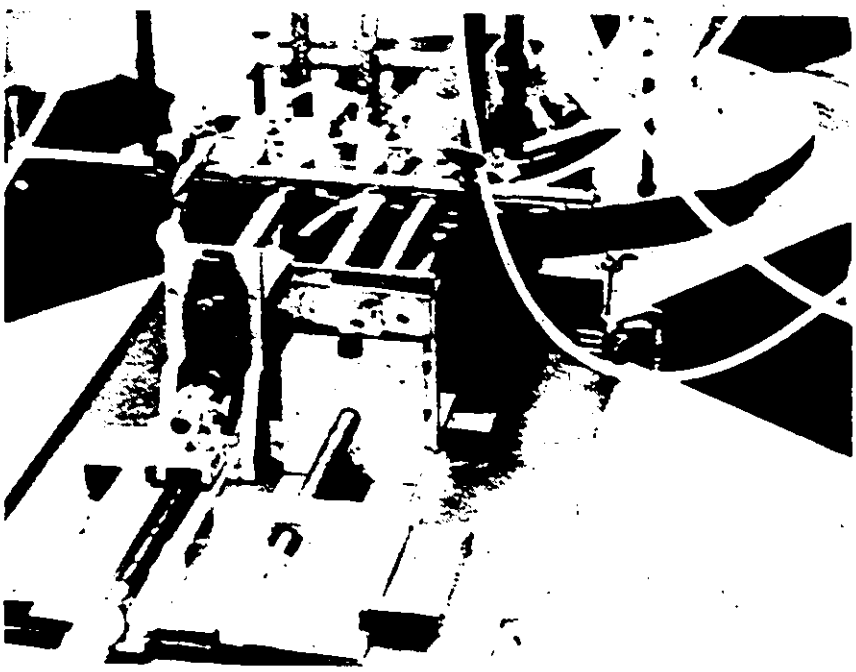

orifice plane. This regulator would allow for very fine pressure adjustment at the orifices with normal supply gas pressures provided by the gas cylinders. In the multiple bubble case, a cylindrical gas distributor provides ports for up to six simultaneous injections. Thereafter, gas bubbles can be injected with minimal disturbance to the polymer solutions.

Gas bubbles were released through a special designed orifice. The orifice tip was chamfered (beveled edge) to avoid capillary waves or ripples which might cause drastic changes in the gas flow rate (A5). The lower portion was fitted with an adaptor for union with a 6×10^{-3} m outside diameter polyflo tubing system. Orifices were selected carefully to match the desired range of bubble volumes. Figure (III-3) shows a schematic diagram of orifices arrangement and inside diameters for the single bubble tank. In the case of the multiple bubble tank, injection was restricted to an intermediate volume range ($V \geq 1 \times 10^{-6}$ m^3) and employed only the 3.175×10^{-3} m inside diameter orifice. A schematic diagram of the multiple bubble configuration is presented in Figure (III-4) showing the possible spatial separation distance between orifices. Moreover, Figures (III-3 and III-4) are not drawn to scale

The injection system described here uses two commercially available units. A pneumatic cylinder and a check-valve. The pneumatic cylinder can expand and compress the gas

Figure (III-3) Schematic Diagram of Orifices Configuration.

SINGLE BUBBLE INJECTION SYSTEM

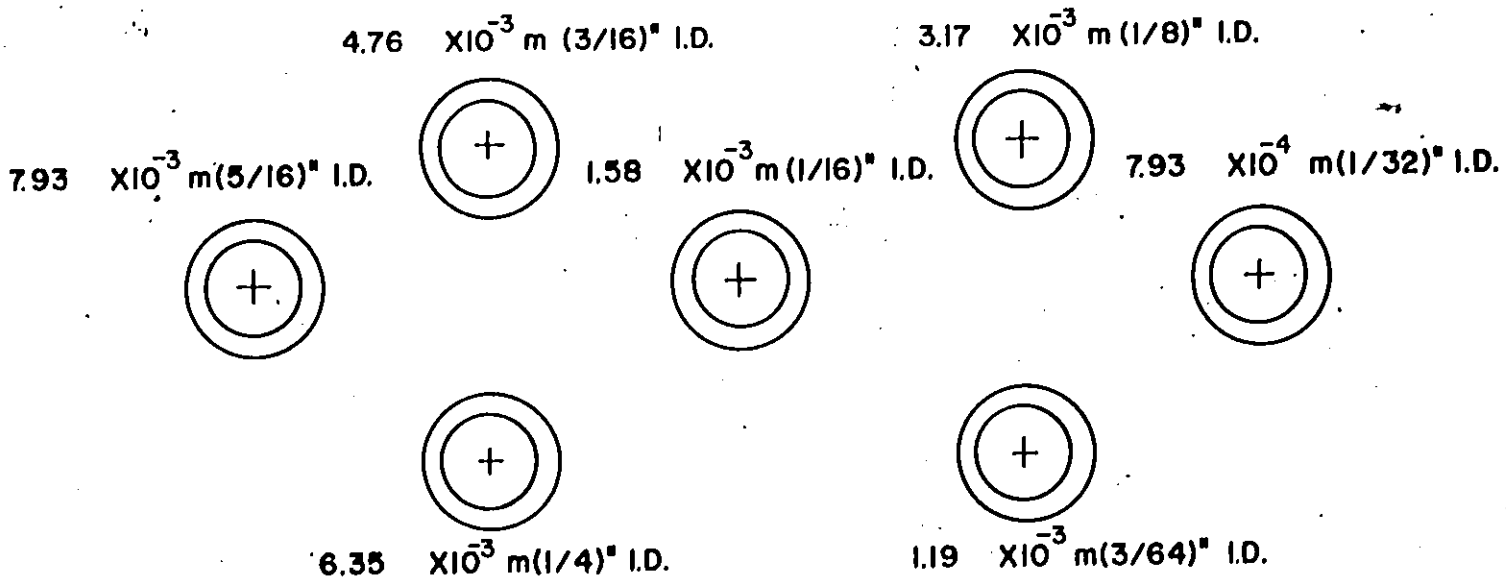

Figure (III-4) Schematic Diagram of Orifices Spatial Separation Distance Configuration.

MULTIPLE BUBBLE INJECTION SYSTEM

ALL ORIFICES ARE 3.17 $X10^{-3}$ m (1/8)" I.D.

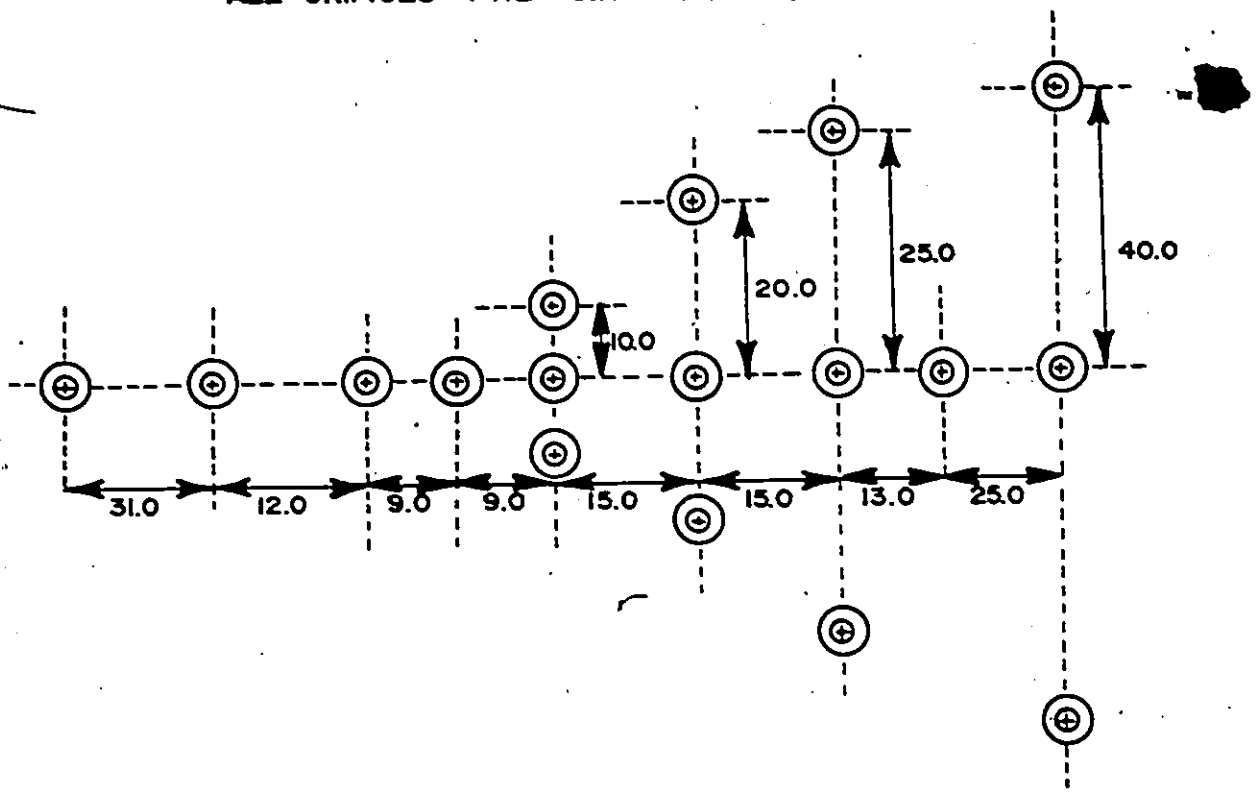

ALL DIMENSIONS ARE IN (mm)

in a cyclic manner for the purpose of injecting reproducible and different gas volumes. The role of the check-valve is to allow gas flow in one direction only.

Different types of pneumatic cylinders employed in this work are summarized as follows:

(i) a cylinder of 2.60×10^{-3} m in diameter is capable of producing bubble volumes from 0.01×10^{-6} m^3 to 0.3×10^{-6} m^3.

(ii) a cylinder of 6.00×10^{-3} m in diameter is capable of producing bubble volumes from 0.3×10^{-6} m^3 to 1×10^{-6} m^3.

(iii) a cylinder of 14.30×10^{-3} m in diameter is capable of producing bubble volumes from 1×10^{-6} m^3 to 10×10^{-6} m^3.

(iv) a combination of two or three cylinders is capable of producing bubble volumes from 10×10^{-6} m^3 to 30×10^{-6} m^3.

The present system uses two types of check-valves:

(i) the Harris check-valve, made of brass, which utilizes a ball and spring mechanism for operation.

(ii) the Norgren check-valve, made of polyproplyene, which utilizes a silicon cup-shield.

By placing the Norgren check-valve at the entrance to the orifice, back-flow of polymer into the orifice assembly was prevented from reaching the Harris check-valve. This method of

valves connection provides a reliable way of experimentation for the following reasons:

(i) the polymer solution could change the spring characteristics of the Harris check-valve if the polymer were to flow in it. Also, corrosion would take place with time.

(ii) alteration of the gas flow causes the formation of small satellite gas bubbles with every injected bubble and hence increases the uncertainty of the bubble volume.

(iii) loss of fluid at the bottom of the tank is minimized.

To inject a sample gas stored at atmospheric pressure (zero gauge pressure), a single acting spring return pneumatic cylinder (SPC-1) is utilized which delivers the compression injection action. Another pneumatic spring return cylinder (SPC-2) is responsible for generating the necessary suction action in SPC-1, thereby admitting sample gas through the Harris check-valve. A two port solenoid-valve is used in conjunction with SPC-2 to initiate the required action. The solenoid-valve allows the system to inject a sample gas at any selected time period. Moreover, the solenoid-valve, SPC-1 and SPC-2 are shown in Figure (III-1).

The volume of gas which is to be injected may be calibrated by using a simple stroke adjustment mechanism which is basically a stop for the extended pneumatic cylinder rod.

This measuring system is flexible as it allows for the interchanging of pneumatic cylinders of different diameters. For each grouping of cylinder and orifice, a calibration curve of volume versus actual stroke is obtained. In the case of the multiple injection system, the stroke adjustment mechanism is different in that it must accommodate three pneumatic cylinders. Both measuring systems are combined together for the study of bubble coalescence as shown in Figure (III-2).

An inverted bubble collector was built by joining a burette to the bottom of a graduated cylinder for measuring the volume of the released bubble. The volume of one bubble is calculated from the ratio of the total volume of liquid displaced in the collector and the total number of bubbles collected. Bubble volume was obtained for atmospheric conditions by applying a correction for the fluid head in the tank.

To measure the bubble terminal velocity, a Ricoh-35 mm camera set on a low shutter speed registers the motion while a stroboscope will intermittently illuminate the rising bubble. The camera was mounted on a tripod to avoid vibrations at the time of filming due to the low shutter speed (one-second). A dark room was also assembled for processing the film. By knowing the stroboscope frequency (6.00 Hz) and the distance between two successive bubbles on the developed film, one can easily determine the bubble terminal velocity. Projection of the negatives on the wall allow us to measure the eccentricity (D/H) of the bubble within a few percent. Also, each picture includes the projection of a ruler.

The rheological properties of the viscoelastic fluids were ascertained by using the Contraves Rheomat-30 viscometer shown in Figure (III-5). As a rotational rheometer, it is used in conjunction with either a coaxial cylindrical measuring system or a cone and plate system. The rheometer can measure viscosity as a function of shear rate. Since shear rate is a function of rotational speed and measuring system dimensions; and shear stress as a function of torque, the flow behaviour and viscosity can be evaluated. Furthermore, an anti-bacterial agent (0.01 wt.%) was added to the four polymer solutions. This preservative (phenylmercuric acetate) prevents biological degradation with time which could alter the molecular weight and hence decrease the viscosity.

Figure (III-6) shows the Fisher Autotensiomat surface tension analyzer which has been employed to measure the surface tension of:

(i) a 1.0 (wt.%) solution of polyacrylamide (PAA) in a 50/50 (wt.%) mixture of glycerine and water.

(ii) a 1.0 (wt.%) solution of PAA in a 50/50 (wt.%) mixture of glycerine and water with 0.0417 (wt.%) of surfactant (Sorbitan Monolaurate).

The values of surface tension and density are listed in Table (III-1).

A general guide to the chemicals used in mixing the four polymer solutions with molecular representation and chemistry outline is presented in Table (III-2). Finally, a complete list

Figure (III-5) - Contraves Rheomat-30 Viscometer with Programming Unit and X-Y Recorder.

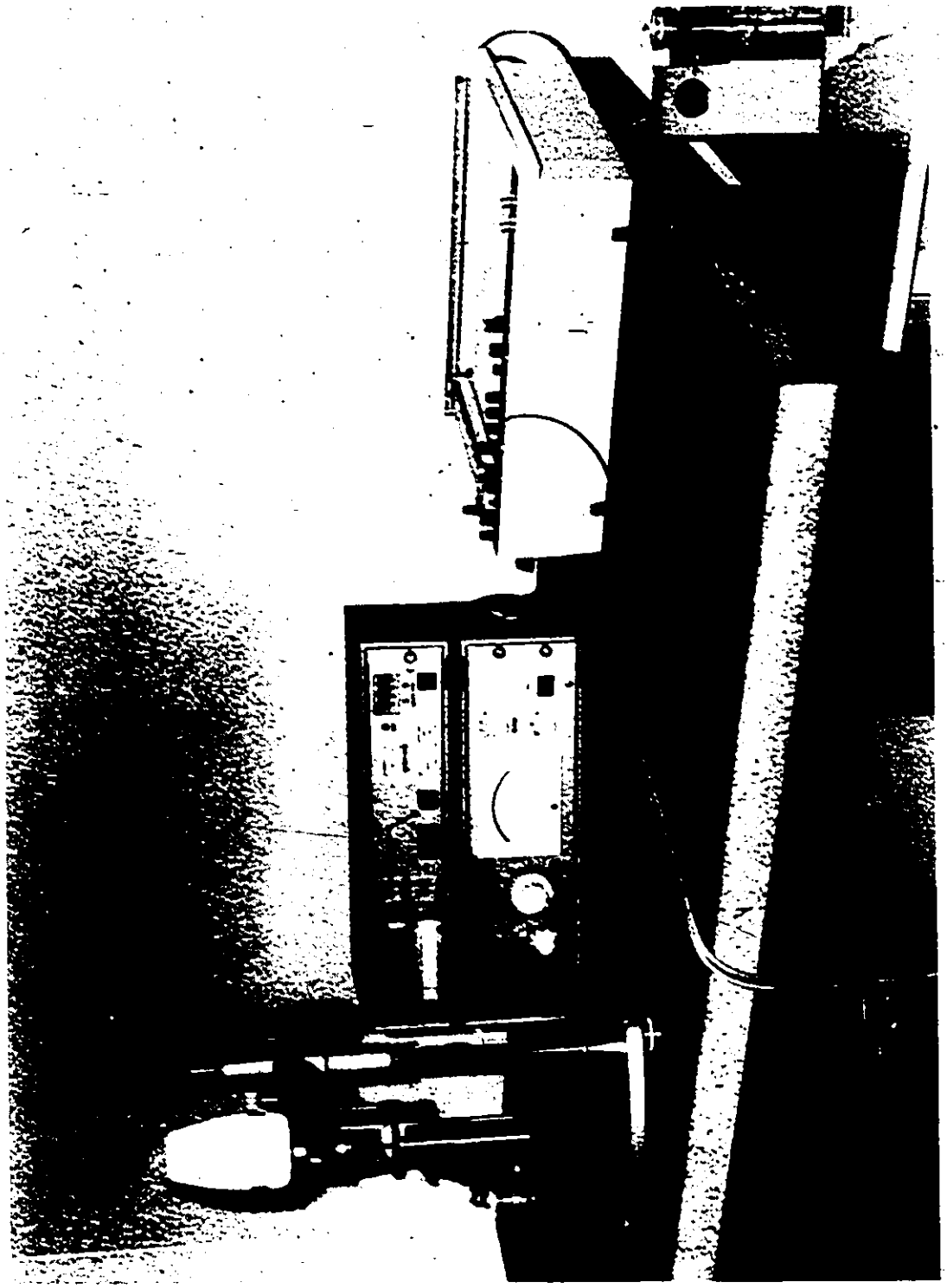

Figure (III-6) Fisher Autotensiomat Surface Tension Analyzer.

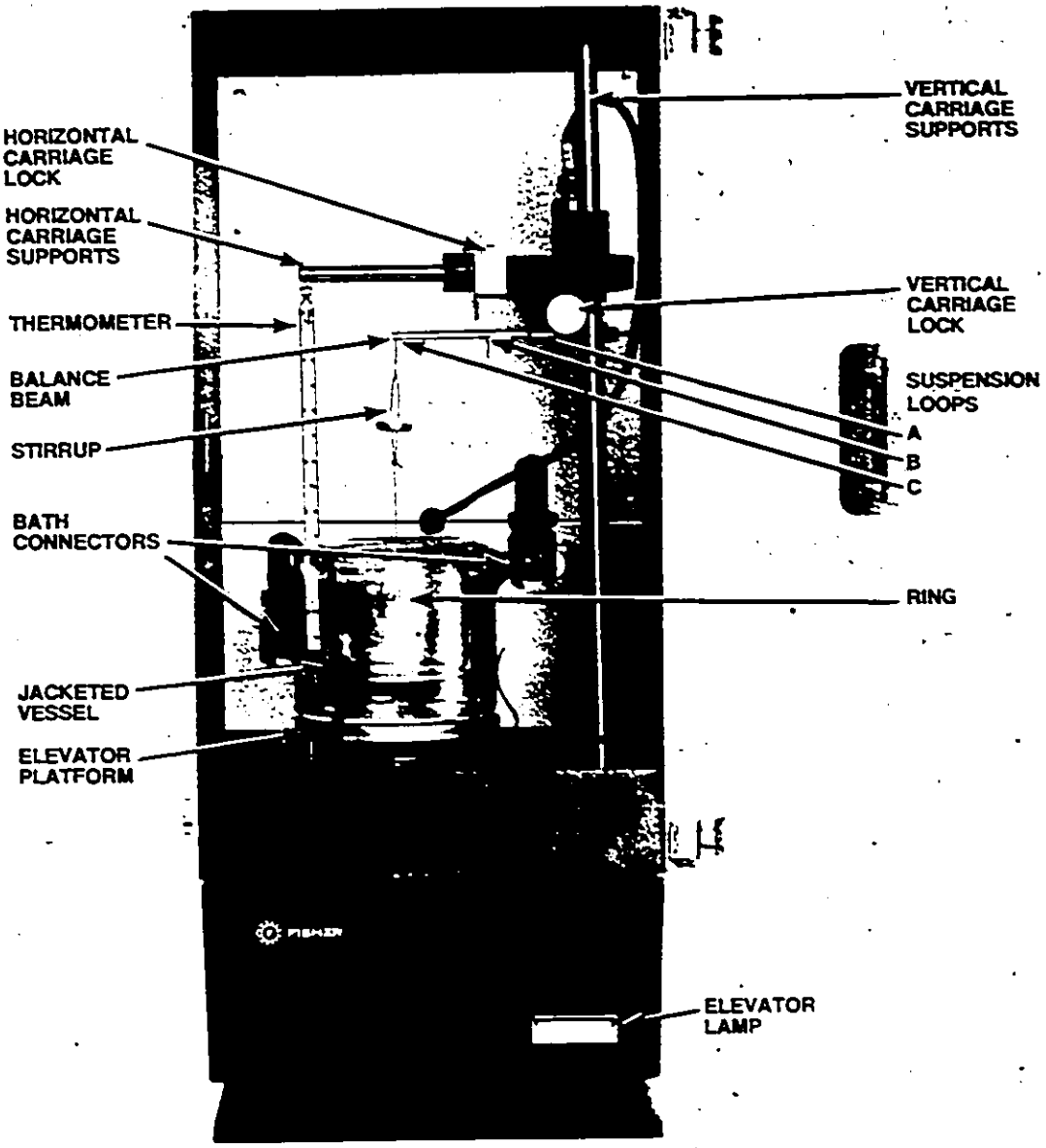

Sample Module

TABLE (III-1) Values of Density and Surface Tension at Room Temperature and Pressure (15°C and 101.30 kPa)

Fluid	ρ (Kg/m^3)	σ (N/m)
1.0 (wt.%) solution of polyacrylamide (PAA) in a 50/50 (wt.%) mixture of glycerine and water	1129.50	0.0653
1.0 (wt.%) solution of PAA in a 50/50 (wt.%) mixture of glycerine and water with surfactants	1129.00	0.0343
0.5 (wt.%) solution of PAA in a 50/50 (wt.%) mixture of glycerine and water	1126.20	
1.5 (wt.%) solution of PAA in a 50/50 (wt.%) mixture of glycerine and water	1131.10	
Sorbitan Monolaurate (Surfactants)	1119.60	
Glycerol	1255.30	0.0631
Distillate Water	997.60	0.0728

TABLE (III-2) General Guide to the Chemicals Used for Preparing the Polymer Solutions

Name of Chemical	Chemistry Background	Identification & Manufacturer
Polyacrylamide (PAA) $[-CH_2CH(CONH_2)-]_n$ (Separan AP-30)	Granular (non-ionic) Nominal M.W. $5x10^6$-$6x10^6$ Soluble in Water and Glycerol	Lot No. 0324MJ Aldrich Chemical Company, Inc. Milwaukee, Wisconsin 53201 U.S.A.
Phenylmercuric acetate $CH_3CO_2HgC_6H_5$ (Preservatives)	Crystalline Highly Toxic Corrosive Poor Solubility in Water and Glycerol	Lot No. 1804BE Aldrich Chemical Company, Inc. Milwaukee, Wisconsin 53201 U.S.A
Glycerol $CH_2OHCHOHCH_2OH$ (Glycerine)	Reagent Irritant Hygroscopic Soluble in Water	Cat. No. 5350-1 Caledon Laboratories Ltd. 40 Armstrong Avenue Georgetown, Ontario L7G 4R9
Sorbitan Monolaurate (Surfactants)	Liquid @ 25°C Hydrophilic ("water-loving") Highly Soluble in Water and Glycerol Anionic Surface Active Agent	Emsorb 6915 POE(20) Emery Industries Ltd. 565 Evans Avenue Toronto, Ontario M8Z 1K2

of the experimental equipment utilized in this project is given in Table (III-3).

III.2 Operation

Before proceeding with any experimental work, the terminal velocity region should be determined on the plexiglass tank. The tank is marked to different heights above the tip of the orifice. By using a stop-watch, one could determine the amount of time elapsed for the bubble to pass the marked distance. Knowing the bubble velocity and the corresponding height, a plot of velocity versus height can easily locate the "steady state" region as shown in Figure (III-7).

The experimenter has only to pressurize the necessary injection lines and select an injection period. Set the stroke adjustment mechanism for the desired bubble volume. This then allows the experimenter to position the camera and the stroboscope to take the necessary photographs. Finally, for the interest of reproducibility and firmness of the experimental data, the plexiglass tanks, fluid containers, and every tubing circuit should be periodically cleaned and free from any surface active substances. These materials can be detergents, plasticizers from tubing used in the equipment, impurities, or metallic colloids from fittings.

TABLE (III-3) Equipment Schedule

Item	Manufacturer/Supplier	Identification
Autotensiomat (Surface Tension Analyzer)	Fisher Scientific Co. Pittsburgh, PA 15219	Model 215 Cat. No. 14-811
RICOH-35 mm camera	Turek Ltd.	Model No. KR-10
SIGMA Macrozoom Lens	Turek Ltd.	Model No. 641-458
RICOH Electric XR Winder-1	Turek Ltd.	Model No. XR-1 (47 152002)
Stroboscope	Sargent-Welch Scientific Co. Ltd.	Cat. No. S-77545
Harris Check Valve	Essex Welders Supply	Model No. 88-3CVL
Norgren Check Valve	Checker Industrial Ltd.	Model No. 4LD-061 -D00
Pneumatic Cylinder 6.0×10^{-3} m (6 mm)	Nopak Canada Ltd.	Model No. CJB6-605
Pneumatic Cylinder 1.43×10^{-2}m (9/16") bore	Industrial Air and Hydraulic Equipment Co.	Model No. 015
Pneumatic Cylinder 1.27×10^{-2}m (1/2")	Canadian Power and Rubber Supply Co.	Model No. DCPS -05-3
Agastat Electric Timer	Petersons Electronics Ltd.	Model No. STMNHAG
Threeway Solenoid Valve	Checker Industrial Ltd.	Model No. H41AA02 -HSI-HDO
Low Pressure Line Regulator	Union Carbide Ltd.	Model No. SSC-1
Pneumatic Cylinder 2.6×10^{-3}m (2.6 mm) bore	Windsor Factory Supply	Model No. DM 112 x3
Electric Relay	Industrial Control Equipment	Model No. A-10B
Rheomat-30 (Viscometer)	Contraves AG Zurich Schaffhauserstrasse 580 8052 Zurich P.O. Box	Bull. T361e-7504

Figure (III-7) Determination of the Terminal Velocity Region.

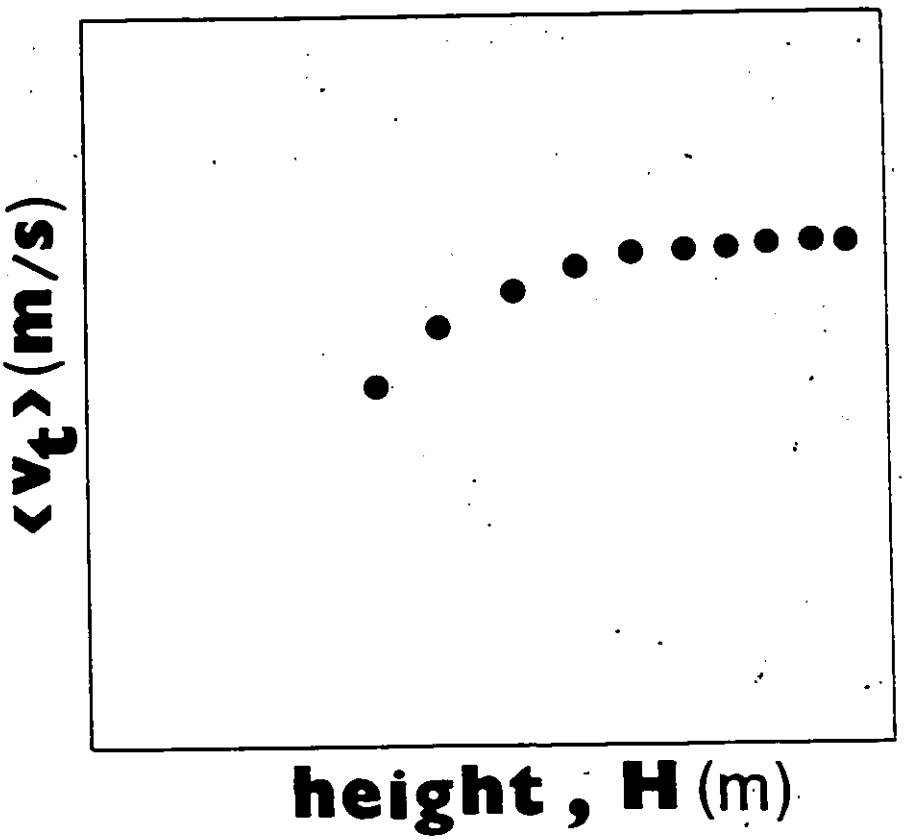
$\langle v_t \rangle$ (m/s)
height , H (m)

IV. RESULTS AND DISCUSSION

The average terminal velocity data of air, carbon-dioxide, and nitrogen bubbles in four polymer solutions are presented in Appendix I. The experimental results are discussed in the following section.

IV.1 Bubble Motion and Shape

Figures (IV-1,2,3,4, and 5) show the data on ascending velocity versus volume. The data have the same general characteristics. The terminal velocity of the gas bubbles increased with increasing volume. No region exists where the bubble undergoes a rapid increase in the velocity at a volume of about 0.10×10^{-6} m^3 as reported by several authors (A1, A2, C1, L1, and K1). At small volumes, the gas bubbles are spherical and are moving under creeping flow conditions. Also, at large volumes, the terminal velocity of the gas bubbles becomes more insensitive to the bubble volume.

Figure (IV-1) illustrates the effect of polymer concentration on the motion of air bubbles in the 0.5, 1.0, and 1.5 (wt.%) PAA solutions. Major differences in terminal velocity are predominant in the small volume range. The motion of small volume gas bubbles in a viscoelastic medium is confined to a low shear-rate range at which the viscosity is very high (see Section IV.3), hence the terminal velocity of small gas bubbles appreciably decreases as the fluid

FIGURE (IV-1): The Effect of Polymer Concentration on the Motion of Air Bubbles.

○ 0.5 (wt. %) PAA ($\langle v_t \rangle$ ± 5.91% max.)

△ 1.0 (wt. %) PAA ($\langle v_t \rangle$ ± 2.97% max.)

□ 1.5 (wt. %) PAA ($\langle v_t \rangle$ ± 5.98% max.)

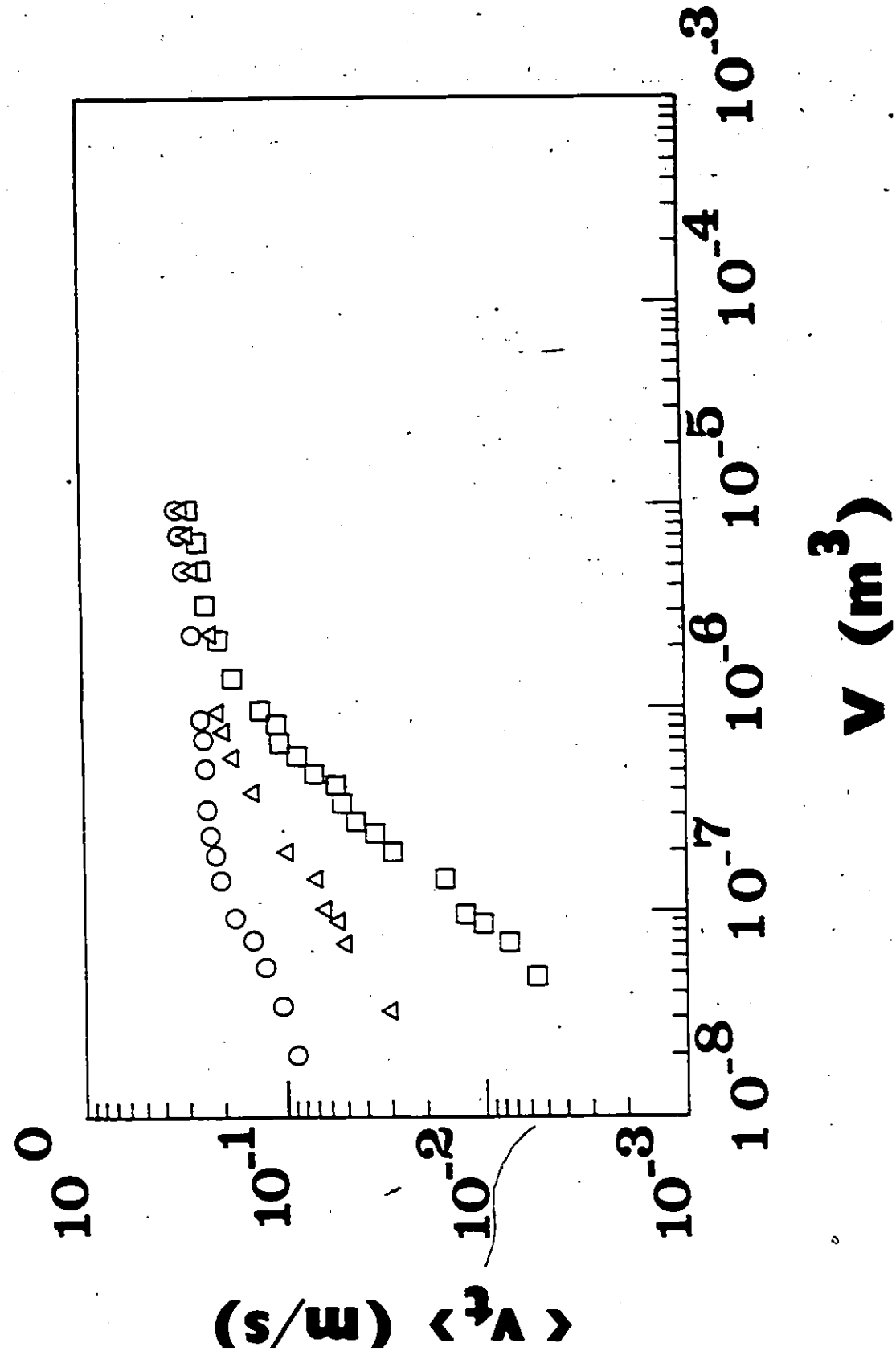
10^{0}
10^{-1}
10^{-2}
10^{-3}
$\langle v_3 \rangle$ (m/s)
10^{-8}
10^{-7}
10^{-6}
10^{-5}
10^{-4}
10^{-3}
V (m^3)

becomes more elastic. Ting (T1) postulated that the visco-elastic retardation effect becomes more pronounced at small bubble volume. At the bubble surface, normal stresses will build up to cause viscoelastic retardation. These stresses increase with increasing shear-rate (M5). Levan and Newman (L2) pointed out that a viscoelastic film at the interface can reduce the shear stresses transmitted inside the bubble and thus attenuate internal circulation.

In addition, Figure (IV-1) demonstrates the negligible effect of elasticity on the motion of large volume air bubbles. For the three different concentrations of polymer solutions, the terminal velocity of air bubbles asymptotically approach the Dumitrescu prediction (Equation II-1). This asymptotic rising velocity may be due to the stable shape (spherical-cap) adopted by the large volume air bubbles.

Elasticity plays a significant role in controlling the shape of gas bubbles moving in a viscoelastic fluid. The shape of air bubbles were observed in terms of the concentration:

(i) air bubbles moving in a 0.5 (wt.%) PAA solution, the shape goes from spherical ($V < 0.04 \times 10^{-6}$ m^3) to prolate-teardrop shaped ($0.04 \times 10^{-6} < V < 0.15 \times 10^{-6}$ m^3) to that of an oblate-cusped shape ($0.15 \times 10^{-6} < V < 0.45 \times 10^{-6}$ m^3) into an oblate-spheroid ($0.45 \times 10^{-6} < V < 2.5 \times 10^{-6}$ m^3) and finally to spherical-cap ($V > 2.5 \times 10^{-6}$ m^3).

(ii) the shape of air bubbles moving in the 1.0 (wt.%) PAA solution goes from spherical ($V < 0.05 \times 10^{-6}$ m^3) to prolate-teardrop shaped ($0.05 \times 10^{-6} < V < 0.50 \times 10^{-6}$ m^3) to that of an oblate-cusped shape ($0.50 \times 10^{-6} < V < 7.5 \times 10^{-6}$ m^3) and finally to spherical-cap ($V > 7.5 \times 10^{-6}$ m^3).

(iii) air bubbles shape observed in a 1.5 (wt.%) PAA solution go from spherical ($V < 0.07 \times 10^{-6}$ m^3) to prolate-teardrop shaped ($0.07 \times 10^{-6} < V < 2 \times 10^{-6}$ m^3) into an oblate-cusped shape ($2 \times 10^{-6} < V < 11 \times 10^{-6}$ m^3) and finally to that of a spherical-cap ($V > 11 \times 10^{-6}$ m^3).

Figure (IV-9) shows the bubble shapes observed in the 0.5, 1.0, and 1.5 (wt.%) PAA solutions.

The above observations reveal that elasticity is associated with the shape transition and the tailing phenomena. The tailing of the downstream surface of gas bubbles has been

reported by Barnett et al. (B1), and is known to be peculiar to non-Newtonian fluids only. A possible explanation of this phenomenon was given by Barnett et al. (B1) who quoted that the fluid displaced by the bubble movement fails to recover rapidly enough. The result is a "hole" at the rear of the gas bubble. This, in turn, sets up an adverse pressure gradient and separation, thereby resulting in a wake behind the bubble.

Bubble shape transition plays an important role in studying wake configurations. The changes in the bubble wake were investigated by Narayanan et al. (N2) who established the existence of three classes of wakes; in class (1), a thin trailing wake behind a spherical shaped bubble can be regarded as a result of creeping flow conditions. In class (2), a wake with a small vortex behind the prolate-teardrop and oblate-cusped shaped bubbles is formed. The difference between the two bubble shapes is associated with the vortex length and with the bubble size. In class (3), a wake with stable vortex behind the spherical-cap shaped bubble is formed.

Furthermore, stress relaxation contributes to the failure of the displaced fluid from being quickly recovered. The stress relaxation time at a certain shear-rate increases with increasing polymer concentration. Polymer solutions are composed of long chain molecules which tend to get more entangled as the concentration increases. The more entangled the system, the longer it will take to achieve thermodynamic

equilibrium after a disturbance such as an applied shear-rate. Qualitatively, it can be said that in elastic liquids, the size of the wake is much larger than in the case of inelastic liquids. Since a larger wake dissipates more energy, the drag coefficient in an elastic fluid is higher.

The surface tension tends to maintain the shape perfectly spherical when the inertia forces assume a negligible value as reported by Acharya et al. (A2).

Clift et al. (C3) discussed the effect of internal circulation on wake formation. Internal circulation delays the onset of flow separation and wake formation in the external fluid. They justified their observation by referring to the well-known method of delaying boundary layer separation on solid bodies if the surface moves in the same direction as the fluid.

Figure (IV-2) illustrates the effect of the polymer aging characteristics on the motion of air bubbles. Terminal velocity data were obtained for the 1.0 (wt.%) PAA solution. The terminal velocity of air bubbles increases with age. It is possible that the polymer solution exhibits a reduction in viscosity with age. This is most likely due to a decrease in molecular weight resulting from polymer degradation with time.

The effect of a surfactant on the motion of gas bubbles is illustrated in Figure (IV-3). A reduction in the terminal velocity of carbon-dioxide bubbles was shown by

adding 0.0417 (wt.%) of a surface active agent (Sorbitan Monolaurate) to the 1.0 (wt.%) PAA solution. Because of the structure of the surfactant molecule, it will migrate toward and concentrate at the liquid-gas interface, thereby lowering the surface tension. Surface active molecules arrange themselves like bridges across the interface, effectively riveting the two surface films together. At first they are not strong enough to withstand the viscous drag but as more and more molecular bridges form, the strength of the lattice is built-up and eventually resisting the transfer of shear stresses across the interface and thus suppress internal circulation (G1). Johnson and Hamielec (J1) have shown experimentally that much higher mass transfer rates occur for circulating than for noncirculating drops as they travel through a continuous phase. Clift et al. (C3) also reported that traces of surface active impurities may have a profound effect on reducing the internal circulation, thereby increasing the drag and decreasing the overall mass transfer. In addition, Figure (IV-3) shows the volume range (0.10×10^{-6} m^3 - $10 \times 10^{-6} m^3$) for which the surfactant has little effect on the motion of carbon-dioxide bubbles. As the surfactant molecule reaches the bubble surface, it is swept to the rear of the bubble by the tangential velocity leaving the frontal region relatively uncontaminated. The only possibility that could cause a concentration gradient on the surface is molecular diffusion of the surfactant molecules themselves in the direction countercurrent to the tangential velocity which in turn tends to retard the surface motion (H1).

FIGURE (IV-2): The Effect of the Polymer Ageing Characteristics on the Motion of Air Bubbles.

For the 1.0 (wt. %) Solution of Polyacrylamide (PAA) in a 50/50 (wt. %) Mixture of Glycerine and Water.

◇ one month ($\langle v_t \rangle$ ± 2.97% max.)

▲ eight months ($\langle v_t \rangle$ ± 6.18% max.)

□ ten months ($\langle v_t \rangle$ ± 7.24% max.)

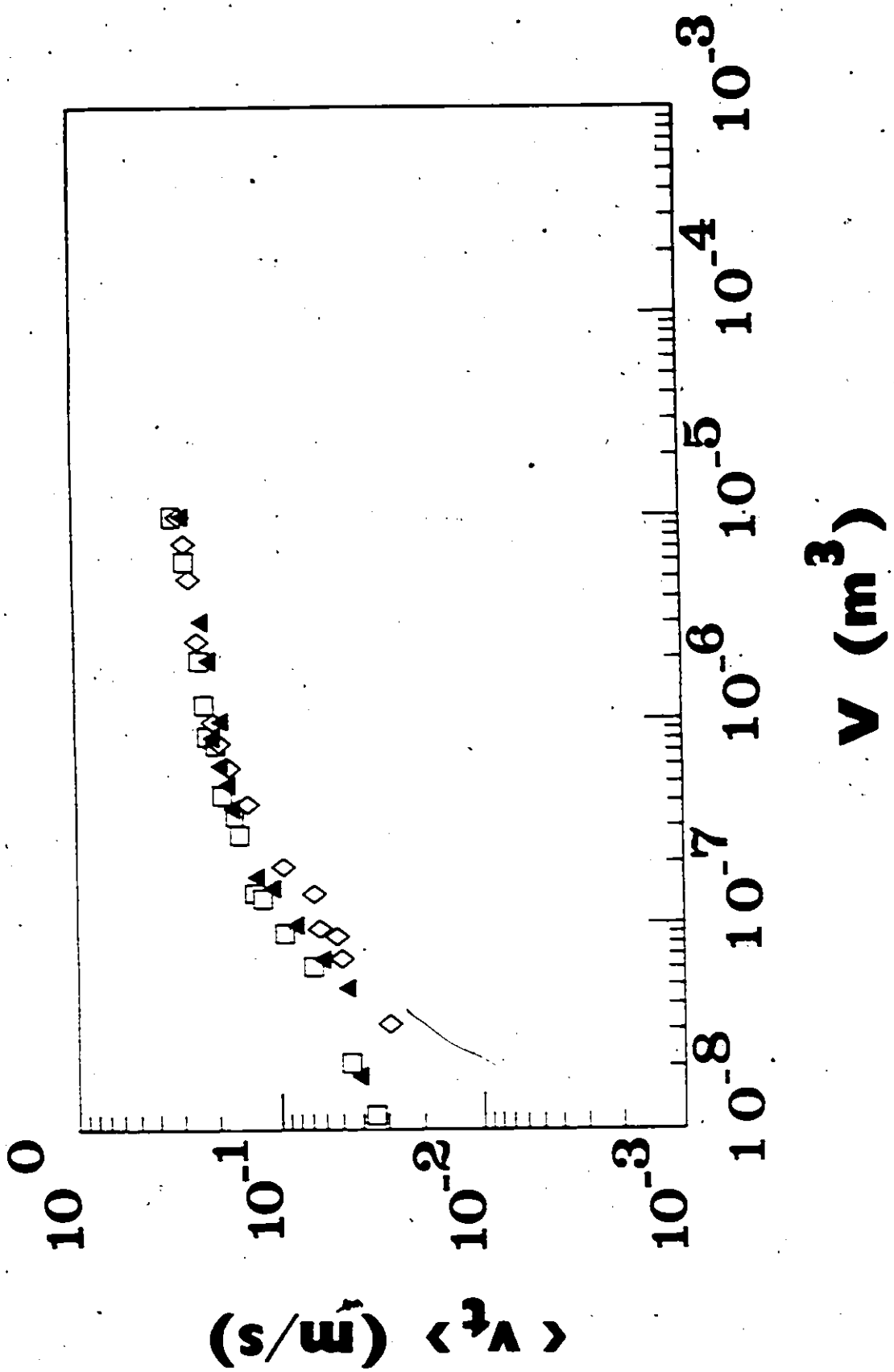
$\langle \nu_t^3 \rangle (s/\tilde{m})$
10^0
10^{-1}
10^{-2}
10^{-3}
10^{-8}
10^{-7}
10^{-6}
10^{-5}
10^{-4}
10^{-3}
$v\ (m^3)$

FIGURE (IV-3): The Effect of Surfactant on the Motion of Carbon Dioxide Bubbles.

△ 1.0 (wt. %) PAA ($\langle v_t \rangle$ ± 4.16% max.)

▲ 1.0 (wt. %) PAA with Surfactant ($\langle v_t \rangle$ ± 3.48% max.)

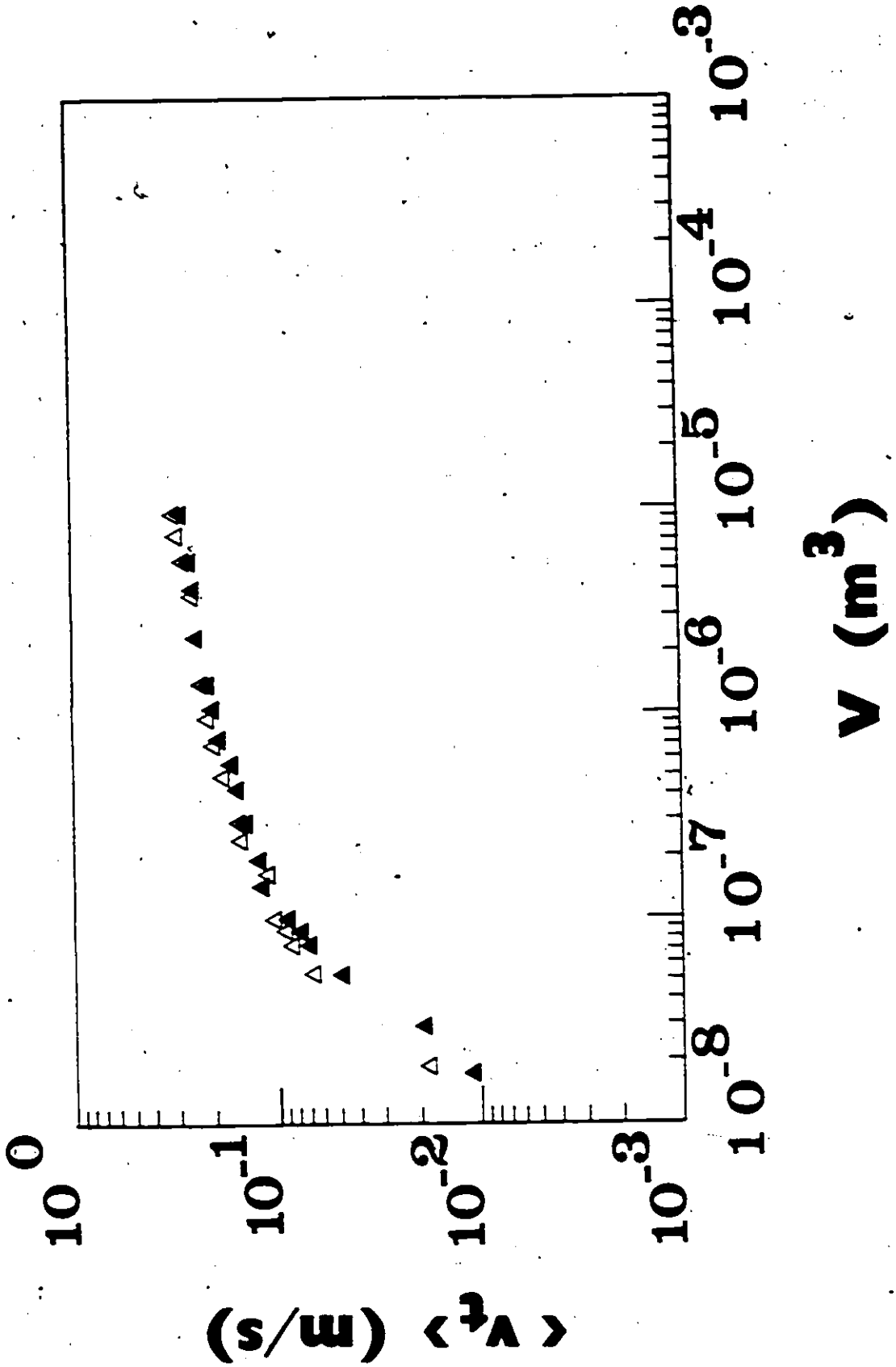
$\langle v_s^3 \rangle$ (m/s)
10^0
10^{-1}
10^{-2}
10^{-3}
10^{-8}
10^{-7}
10^{-6}
10^{-5}
10^{-4}
10^{-3}
v (m^3)

Figure (IV-4) confirms the earlier conclusion that minute traces of surface active substance whether deliberately added or already present in the tested fluid as in the case of the motion of air bubbles in 1.0 (wt.%) solution of poly-acrylamide (PAA) in a 50/50 (wt.%) mixture of glycerine and tap-water. A greater reduction in the terminal velocity of air bubbles was exhibited in comparison with the data which are shown in Figure (IV-3). This may be due to the higher concentration of impurities carried by the tap-water. Moreover, Figure (IV-4) demonstrates the effect of injecting different gases. Terminal velocity of carbon-dioxide bubbles were compared with the one of air bubbles in the 1.0 (wt.%) PAA solution. It seems that the polarizability of the carbon-dioxide molecule is more pronounced in the small volume range. This effect may be responsible for the retardation and hence reducing the bubble terminal velocity (A5 and A6). Increasing the bubble volume this effect is no longer predominant and the buoyant force is prevailing.

Figure (IV-5) shows another comparison between the motion of air and nitrogen bubbles in 0.5 (wt.%) PAA solution. Nitrogen bubbles exhibit a reduction in the terminal velocity. This is possibly due to the diamagnetic property of the nitrogen molecule in which the repulsive forces come into operation and therefore cause a retardation.

FIGURE (IV-4): The Effects of Surface Active Impurities and Injecting Different Gases on the Motion of Gas Bubbles.

△ Air Bubbles in 1.0 (wt. %) PAA

($\langle v_t \rangle$ ± 2.97% max.)

▲ Air Bubbles in 1.0 (wt. %) PAA with Tap Water

($\langle v_t \rangle$ ± 5.05% max.)

□ Carbon Dioxide Bubbles in 1.0 (wt. %) PAA

($\langle v_t \rangle$ ± 4.16% max.)

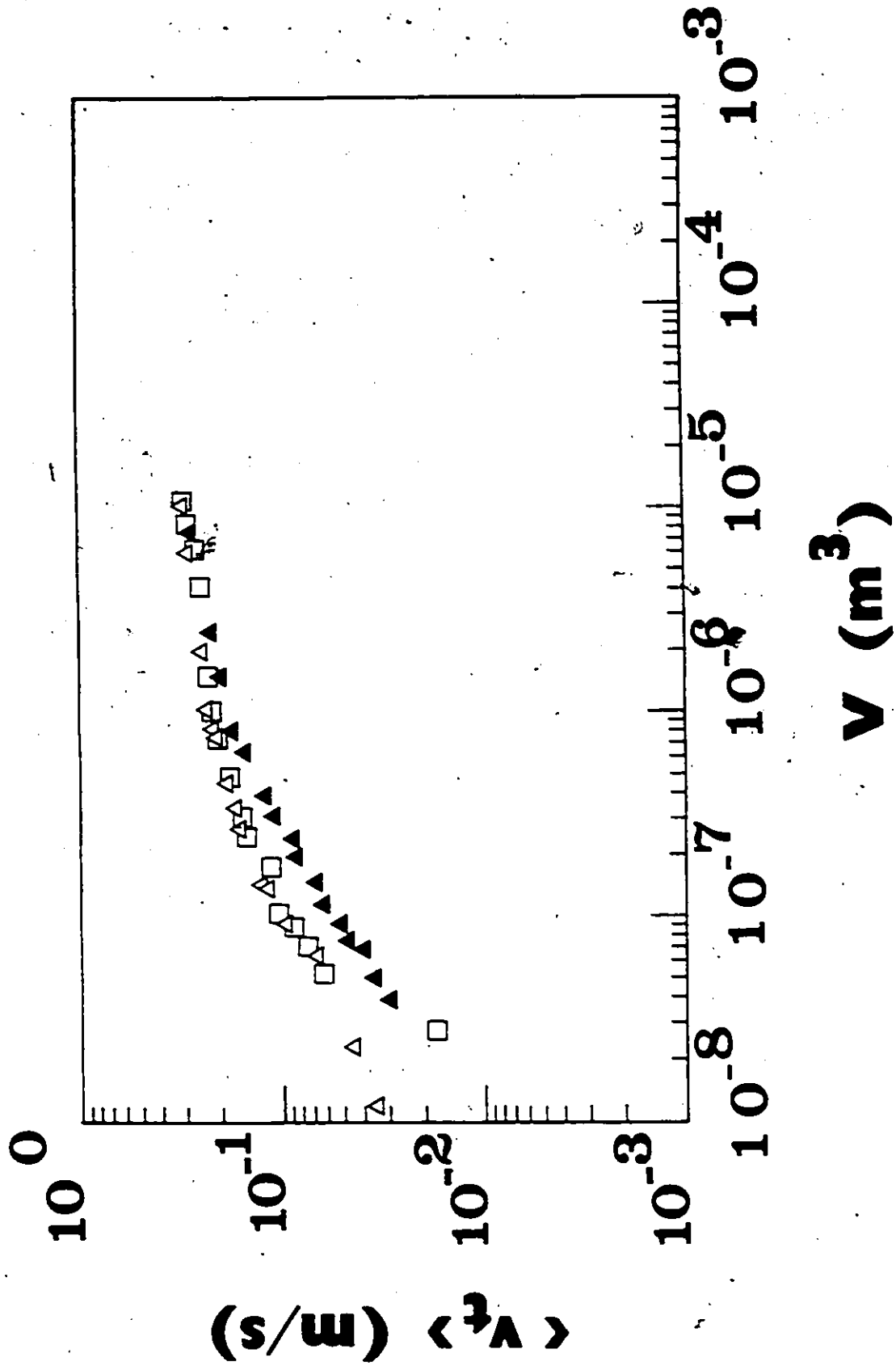
10^{0}
10^{-1}
10^{-2}
10^{-3}
$\langle v_z^3 \rangle$ (m/s)
10^{-8}
10^{-7}
10^{-6}
10^{-5}
10^{-4}
10^{-3}
V (m^3)

FIGURE (IV-5): Comparison Between the Motion of Air and Nitrogen Bubbles in 0.5 (wt. %) PAA.

○ Air Bubbles ($\langle v_t \rangle$ ± 5.91% max.)

● Nitrogen Bubbles ($\langle v_t \rangle$ ± 2.21% max.)

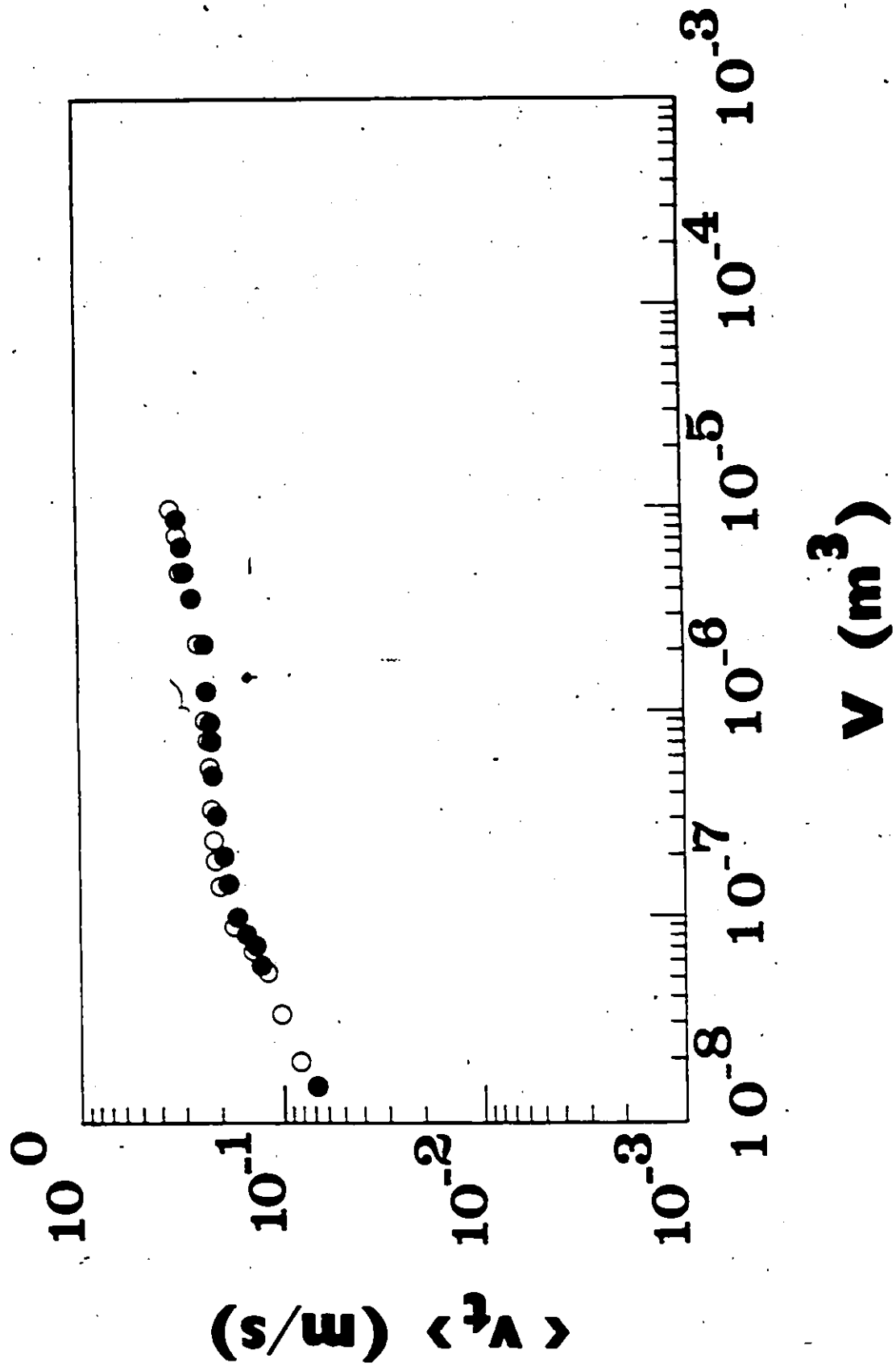
10^{0}
10^{-1}
10^{-2}
10^{-3}
10^{-8}
10^{-7}
10^{-6}
10^{-5}
10^{-4}
10^{-3}
V (m^3)
$\langle v_t \rangle$ (m/s)

IV.2 Bubble Coalescence

A study of gas bubble coalescence using a multiple-bubble injection technique in the four fluids, mentioned earlier, has been carried out. Different gases such as air, nitrogen, and carbon-dioxide were injected from a variety of orifice separation distances (S). Bubble coalescence phenomena have been examined at two different heights (H = 0.25 m and H = 0.50 m) measured from the orifice plane in the tank.

Attention in this work was focused on the coalescence of two bubbles, one of which was fixed at a certain volume (V_f = 1,2, or 3×10^{-6} m^3). A second bubble was injected simultaneously from another orifice. The volume of this bubble was increased until it reached a volume (V_v) which coalesced with the fixed volume bubble at a selected height in the tank.

The process of coalescence takes place in three different stages:

(i) the approach of the trailing bubble (fixed volume bubble, V_f) from a distance behind the leading bubble (variable volume bubble, V_v) until it reaches the wake region behind the leading bubble.

(ii) the movement of the trailing bubble in the wake of the leading one until they are separated by a thin liquid film.

(iii) thinning and final rupturing of the liquid film between the leading bubble and the

trailing one.

Typical coalescence data are plotted in a dimensionless form and presented in Figures (IV-6, 7,8,10,11,12 and 13). These figures demonstrate the appearance of a discontinuity in the semi-log plot of (V_v/V_f) versus (S/H) at a transition separation distance (S_t) between the orifices.

To achieve coalescence for a large range of orifice separation values, the volume of the leading bubble (V_v) becomes rapidly very large and a discontinuity in the linear relationship between V_v and S is expected. The observed transition occurs at a separation distance varying from about 15×10^{-3} m to 33×10^{-3} m.

Variables associated with the coalescence process are:

(i) the height (H) above the orifice plane at which the coalescence will take place.

(ii) the volume of the fixed bubble (V_f).

(iii) the polymer concentration (c, wt. %).

Figures (IV-6,7,8,10 and 11) illustrate the response of the leading bubble (V_v) to the changes in the coalescence height (H), the volume of the fixed bubble (V_f), and the continuous phase elasticity.

The effect of changing the coalescence height is shown in Figures (IV-6-8). For the coalescence to take place, a smaller leading bubble volume was observed in the case of the large coalescence height. This is due to the

FIGURE (IV-6): The Effect of Polymer Concentration and Surfactant on the Coalescence Process of Air Bubbles for H = 0.50 m and V_f = 1 x 10^{-6} m^3.

△	0.5 (wt. %) PAA	(V_v ± 18.67% max.)
○	1.0 (wt. %) PAA with Surfactant	(V_v ± 7.54% max.)
●	1.0 (wt. %) PAA	(V_v ± 8.15% max.)
▲	1.5 (wt. %) PAA	(V_v ± 9.71% max.)

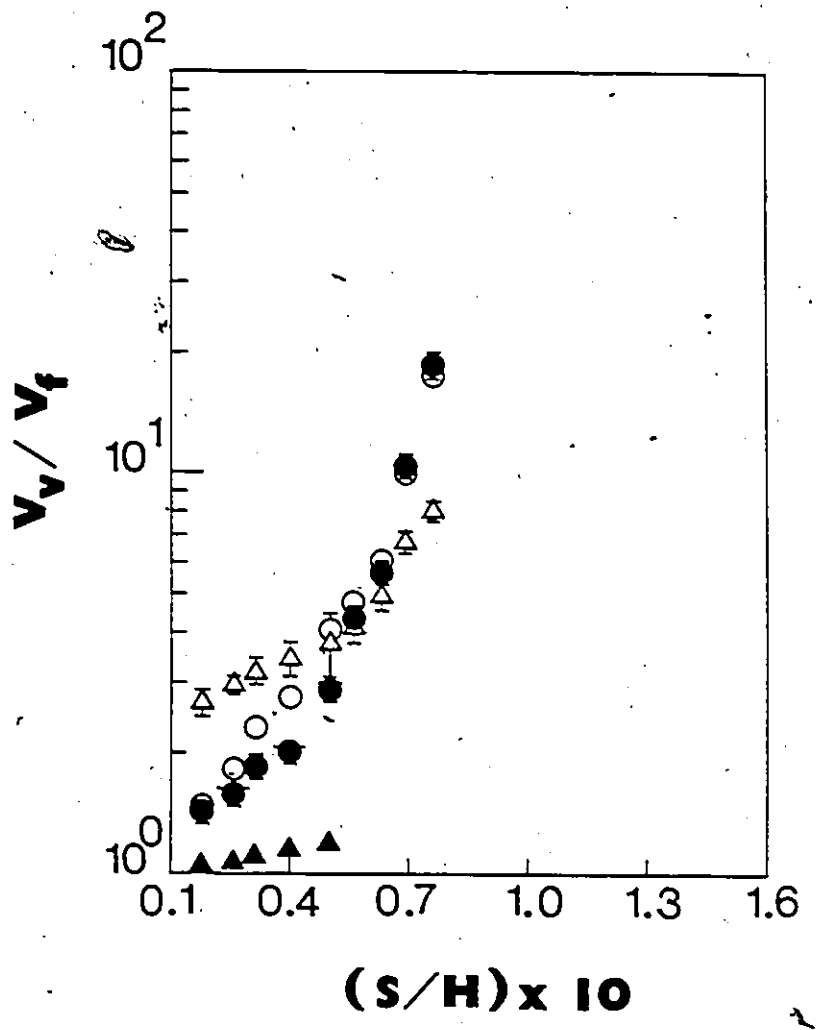
10^2
10^1
10^0
V_v / V_f
0.1
0.4
0.7
1.0
1.3
1.6
(S/H)x 10

FIGURE (IV-7): The Effect of Polymer Concentration and Surfactant on the Coalescence Process of Air Bubbles for H = 0.25 m and V_f = 4 x 10^{-6} m^3.

△ 0.5 (wt. %) PAA (V_v ± 9.14% max.)

○ 1.0 (wt. %) PAA with Surfactant (V_v ± 7.74% max.)

● 1.0 (wt. %) PAA (V_v ± 7.63% max.)

▲ 1.5 (wt. %) PAA (V_v ± 9.35% max.)

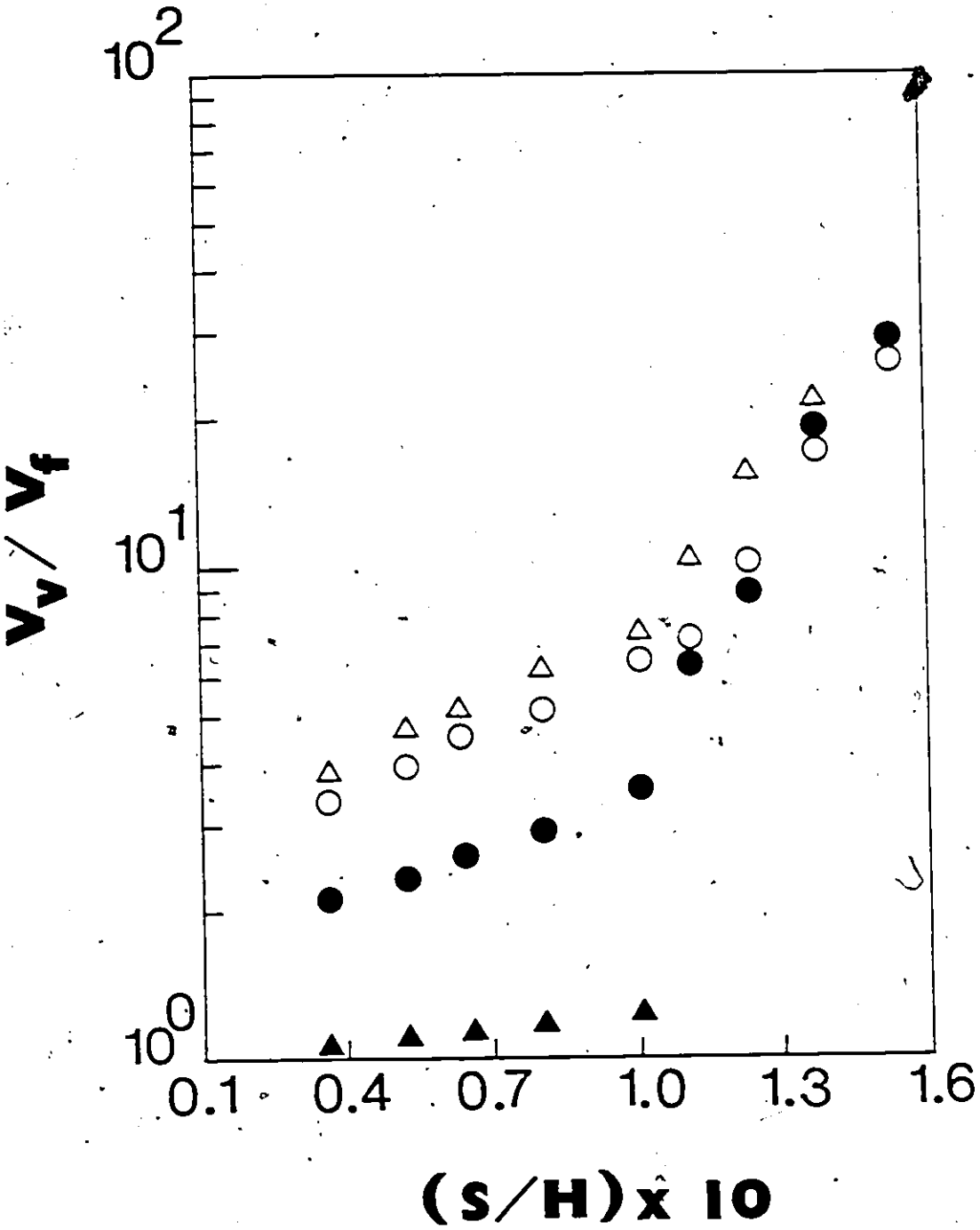
10^2
10^1
10^0
V_v / V_t
0.1
0.4
0.7
1.0
1.3
1.6
(S/H) x 10

FIGURE (IV-8): Summary of the Effect of Changing the Coalescence Height (H = 0.50 m and H = 0.25 m) and the Volume of the Fixed Bubble (V_f = 1, 2 and 3 x 10^{-6} m^3) on the Coalescence Process of Air Bubbles in 1.0 (wt. %) PAA.

For H = 0.50 m:

○ V_f = 1 x 10^{-6} m^3 (V_v = 8.15% max.)

△ V_f = 2 x 10^{-6} m^3 (V_v = 7.14% max.)

□ V_f = 3 x 10^{-6} m^3 (V_v = 6.98% max.)

For H = 0.25 m:

● V_f = 1 x 10^{-6} m^3 (V_v = 7.63% max.)

▲ V_f = 2 x 10^{-6} m^3 (V_v = 9.53% max.)

■ V_f = 3 x 10^{-6} m^3 (V_v = 12.66% max.)

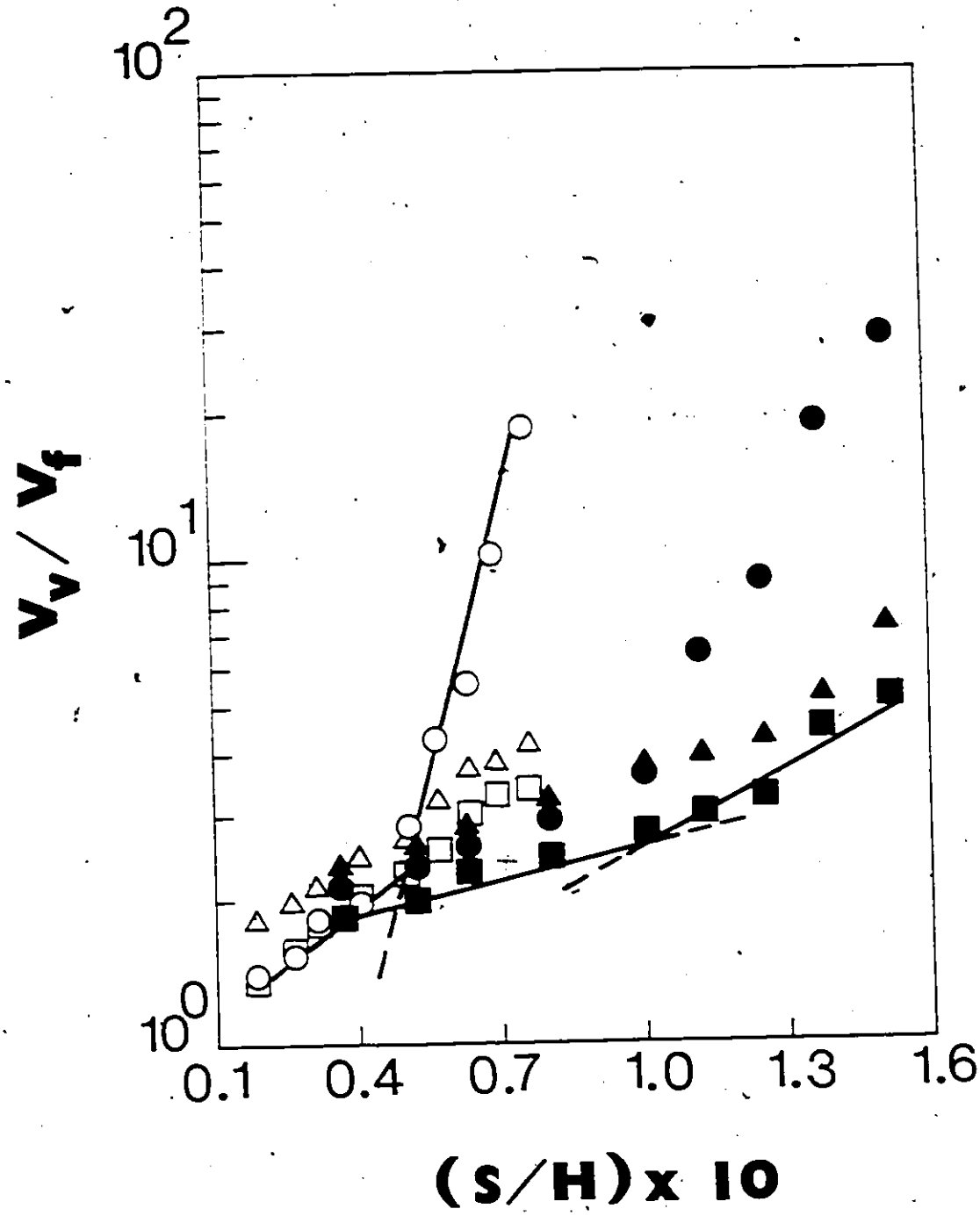
10^2
10^1
10^0
V_v / V_f
0.1
0.4
0.7
1.0
1.3
1.6
(S/H) x 10

fact that for large coalescence heights, the time required by the leading bubble (V_v) to reach the coalescence height is superior to the time required in the case of smaller coalescence heights. The longer the required time the greater the chance for the trailing bubble (V_t) to enter the wake behind the leading one in order to complete the coalescence process. To compensate for the shorter time exhibited in the case of smaller coalescence heights, a broader wake capable of trapping the trailing bubble is needed to achieve coalescence; that is to say: a larger leading bubble is required. In addition, this could be a possible explanation to the more frequent occurrence of this transition in the case of 0.25 m coalescence height.

Figure (IV-8) shows the result of changing the volume of the trailing bubble (V_t = 1,2, and 3 x 10^{-6} m^3). The larger the volume of the trailing bubble the more volume of the leading bubble is required for coalescence to take place. This is because larger volume bubbles exhibit higher terminal velocity, thereby larger leading bubble volumes are required in order to produce a broader wake capable of trapping these fast trailing bubbles.

The fluid elasticity plays a dominant role in controlling the coalescence process because of the great influence of elasticity on the shape of the leading bubble (V_v) and thus its wake configurations, that is, elasticity delays the shape transition (see Section IV.1).

The coalescence data presented in Figures (IV-6, 7, 10, and 11) will be studied in terms of two different regions:

(i) Small orifice separation:

The shape transition of the leading bubble (V_v) and its influence on the type of wake plays a dominant role in controlling the coalescence process in this region. For different values of V_f and H, the smallest leading bubble volume required to achieve coalescence was observed in the case of 1.5 (wt.%) PAA. This is due to the low terminal velocity exhibited by the trailing bubble (V_f) and the longer wake region behind the leading bubble due to the highly elastic nature of this fluid, that is, the trailing bubble is caught up in the wake at a longer distance from the leading one than would be the case in a less elastic fluid. In the case of 0.5 and 1.0 (wt.%) PAA, Figures (IV-6 and IV-7) show that the largest leading bubble volume required for coalescence to occur was observed in the case of 0.5 (wt.%) PAA for $V_f = 1 \times 10^{-6}$ m^3. The shape of the trailing bubble (V_f) in this concentration is oblate-spheroid (see Figure IV-9). If the leading bubble (V_v) falls within this shape range, coalescence no longer takes place. This particular bubble shape shows irregular vortex shedding. Narayanan et al. (N2) concluded that the influence of the wake on coalescence of bubbles in this shape configuration is small, due to the unsystematic pattern of the wake. It is, however, necessary that the volume of the leading bubble be larger and transition to a

Figure (IV-9) Shape of Bubbles in 0.5, 1.0 and 1.5 (wt.%) Solutions of Polyacrylamide (PAA) in a 50/50 (wt.%) Mixture of Glycerine and Water

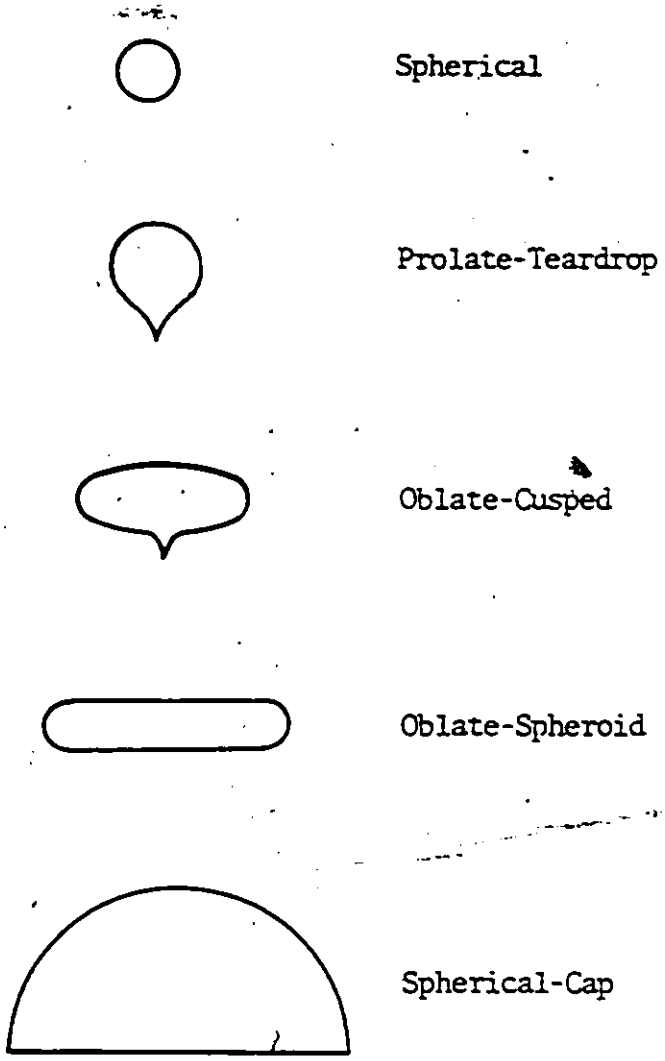

Note: Oblate-Spheroid Shaped Bubbles were Observed Only in the Case of 0.5 (wt. %) PAA.

spherical-cap shaped bubble is attained. The influence of the wake on coalescence is now working over a long distance and thus coalescence can be achieved. For V_f = 2 and 3 x 10^{-6} m^3, Figures (IV-10 and IV-11) show that the largest leading bubble volume (V_v) was exhibited in the case of 1.0 (wt.%) PAA compared to the 0.5 (wt.%) PAA. The shape of the two considered V_f bubbles is spherical-cap in 0.5 (wt.%) PAA and oblate-cusped in 1.0 (wt.%) PAA. If the shape of the leading bubble in 1.0 (wt.%) PAA is still in the range of oblate-cusped, a shape transition to spherical-cap is required in order to achieve coalescence. This is because of a more effective wake which exists behind a spherical-cap shaped bubble (N2).

(ii) Large orifice separation:

A stable shape (spherical-cap) adopted by the large leading bubble volumes (V_v) is required in this region. Therefore, the only effects associated with elasticity are the length of wake behind the leading bubble (see Section IV.1) and the velocity of the trailing bubble (V_f). Figures (IV-6 and IV-7) show that coalescence no longer takes place in the case of 1.5 (wt.%) PAA for V_f = 1 x 10^{-6} m^3. This is due to the high sensitivity of $\langle V_t \rangle$ to volume changes of the leading bubble. If the volume of the leading bubble is below the volume required for coalescence to occur, the generated wake fails to trap the trailing bubble. On the other hand, if the

volume of the leading bubble is above the coalescence volume, the leading bubble accelerates too rapidly leaving the trailing bubble behind. An increase in the volume of the leading bubble causes coalescence to occur at a different height in the tank. For V_f = 2 and 3 x 10^{-6} m^3, coalescence for the 1.5 (wt.%) PAA case could be achieved as shown in Figures (IV-10 and IV-11) in which the transition occurred at smaller orifice separation compared to the 0.5 and 1.0 (wt.%) PAA cases. This is because of the very large leading bubble volumes required in order to avoid the no coalescence conditions for the 1.5 (wt.%) PAA case. The combined effect of the length of wake behind the leading bubble (V_v) and the velocity of the trailing bubble (V_f) is shown in Figure (IV-6) for V_f = 1 x 10^{-6} m^3 and H = 0.50 m. Larger values of V_v were observed in the case of 1.0 (wt.%) PAA compared to the 0.5 (wt.%) PAA case. That is, the filled circles are now clearly above the open triangles. Error bars are included for comparison. This situation is the opposite of the condition shown at small orifice separation. The interplay of spherical-cap shaped bubbles and oblate-spheroid shaped bubbles in the 0.5 (wt.%) PAA case at "large" S values is such that a relatively low volume V_v is required because the oblate-spheroid shape (large horizontal projection) gets caught more easily in the wake of the leading bubble V_v. On the other hand, the 1.0 (wt.%) PAA case involving a large spherical-cap (V_v) bubble and a fixed oblate-cusped (V_f) bubble really requires a large V_v volume in order to guide the trailing bubble in its wake. Figures (IV-7 , 10 and

FIGURE (IV-10): The Effect of Polymer Concentration on the Coalescence Process of Air Bubbles for $V_f = 2 \times 10^{-6}$ m^3 and H = 0.25 m.

○ 0.5 (wt. %) PAA ($V_v \pm 8.85\%$ max.)

△ 1.0 (wt. %) PAA ($V_v \pm 9.53\%$ max.)

□ 1.5 (wt. %) PAA ($V_v \pm 6.93\%$ max.)

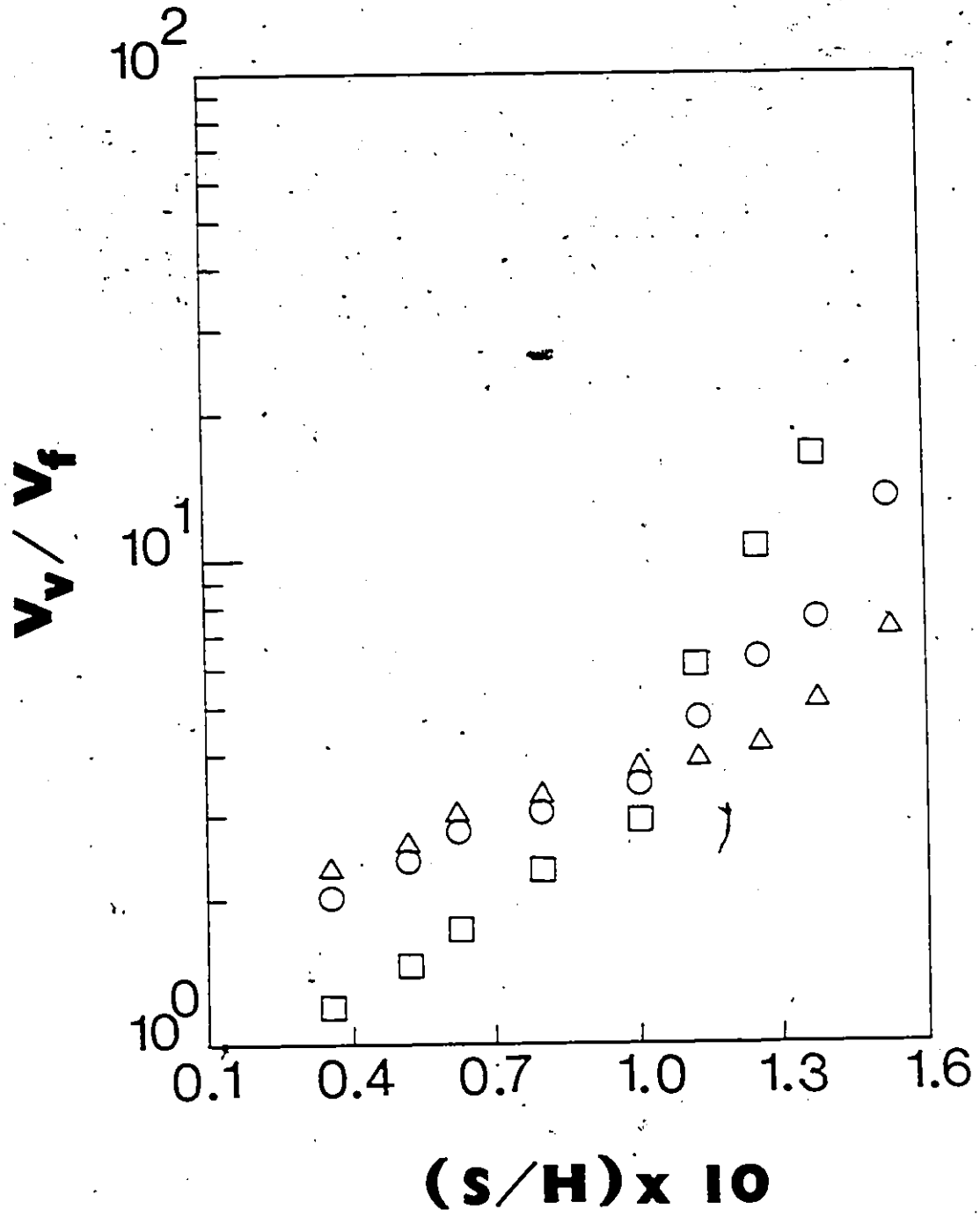
10^2
10^1
10^0
V_v / V_f
0.1
0.4
0.7
1.0
1.3
1.6
(S/H)x 10

FIGURE (IV-11): The Effect of Polymer Concentration on the Coalescence Process of Air Bubbles for $V_f = 3 \times 10^{-6}$ m^3 and H = 0.25 m

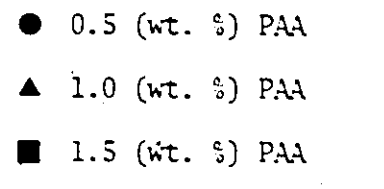

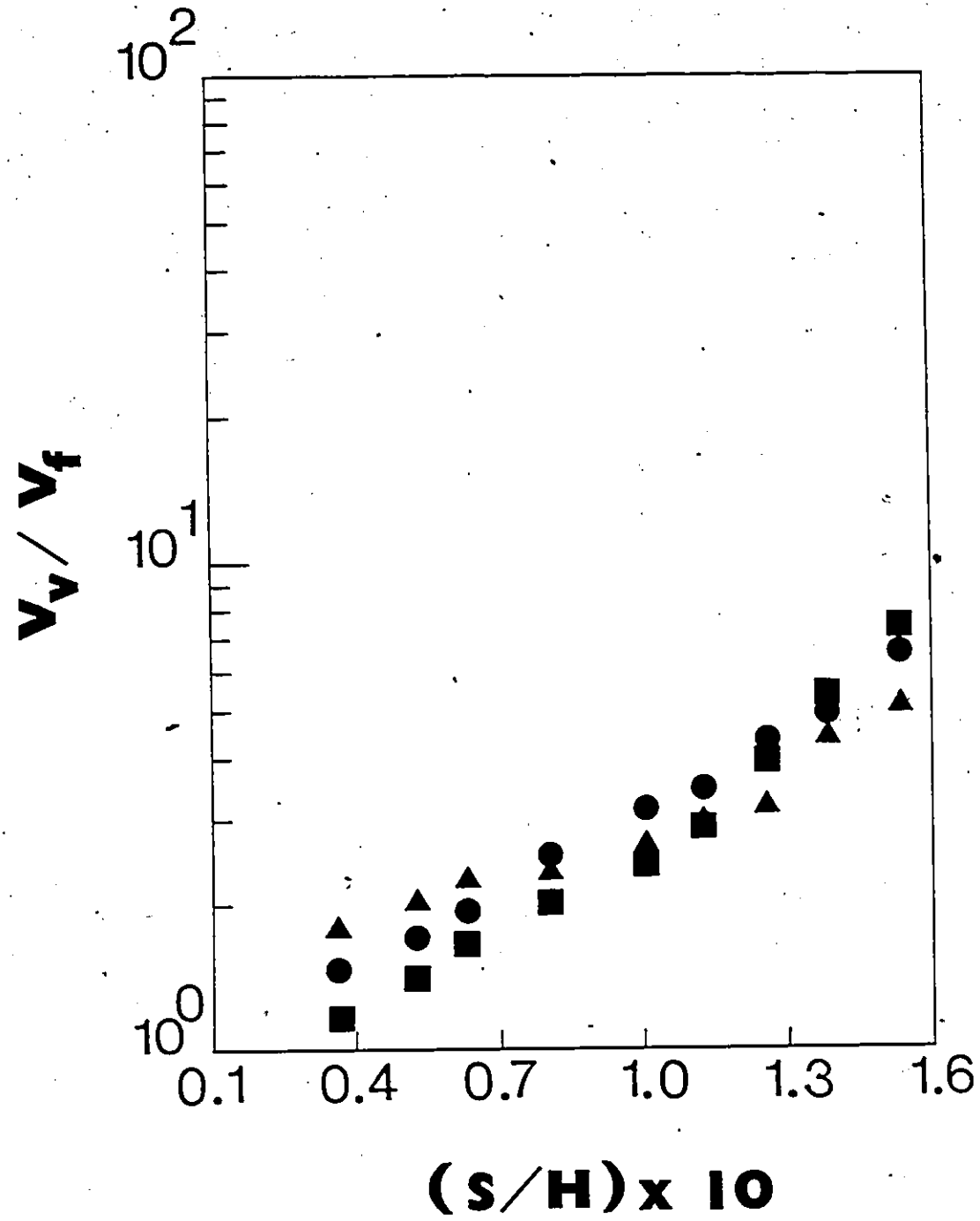
10^2
10^1
10^0
V_v / V_f
0.1
0.4
0.7
1.0
1.3
1.6
(S/H) x 10

11) show results for $\forall_f$ = 1,2, and 3 x 10^{-6} m^3 and H = 0.25 m. Again, the observed trends are due to the interplay of elasticity (polymer concentration), coalescence height (H), and bubble terminal velocities, wake and shape.

The effect of surfactant on coalescence is also shown in Figures (IV-6 and IV-7). It is seen that the leading bubble in 1.0 (wt.%) PAA with surfactant exhibits a larger volume than the one without surfactant. Thinning and final rupturing of the liquid film separating two coalescing bubbles decreases markedly with the addition of even a small amount of surfactant (G2). It is apparent that the surfactant suppressed internal circulation in the rising gas bubble (see Section IV.1). This suggests that the reduction in the rate of film thinning with the presence of surfactant resulted not only from the reduction in the surface tension but also from the interface acting as an elastic membrane which is capable of resisting shear stresses. Therefore, a larger leading bubble volume (V_v) is required, that is, the two coalescing bubbles will be subjected to high tangential surface stresses which in turn promote internal circulation, thus indicating that surface motion starts and quicker film thinning could be achieved.

Figures (IV-12 and IV-13) illustrate the effect of injecting different gases (air, nitrogen, and carbon-dioxide) on the coalescence process for V_f = 1 x 10^{-6} m^3 in two different polymer solutions, namely, 1.5 and 1.0 (wt.%) PAA with surfactant.

Nitrogen bubbles exhibit larger V_v values, in order to complete the coalescence process. This may be due to the diamagnetic property of the nitrogen molecule. This property causes a repulsion between the two touching bubbles (B3), and thus reduces the rate of thinning and rupturing of the liquid film between the two coalescing bubbles. To overcome this effect, a larger V_v (i.e. larger stresses) is needed for coalescence to occur. Figure (IV-12) shows that the carbon-dioxide bubbles exhibit larger V_v than in the case of air-bubbles. It appears that the polarizability of the carbon-dioxide molecule is significant, at small orifice separation, which in turn promotes repulsion between the two touching bubbles. At large orifice separation, large bubble volumes were involved and thus a greater momentum can overcome the effect of electrostatic forces. The data presented in Figure (IV-13) for the case of carbon-dioxide bubbles in 1.0 (wt.%) PAA with the surfactant are lying within a higher uncertainty ($\pm$19.86%). Finally, Figures (IV-12 and IV-13) show that the elastic forces mask the effect of different gases in the case of 1.5 (wt.%) PAA.

FIGURE (IV-12): The Effect of Injecting Different Gases on the Coalescence Process for H = 0.50 m and $V_f = 1 \times 10^{-6}$ m^3.

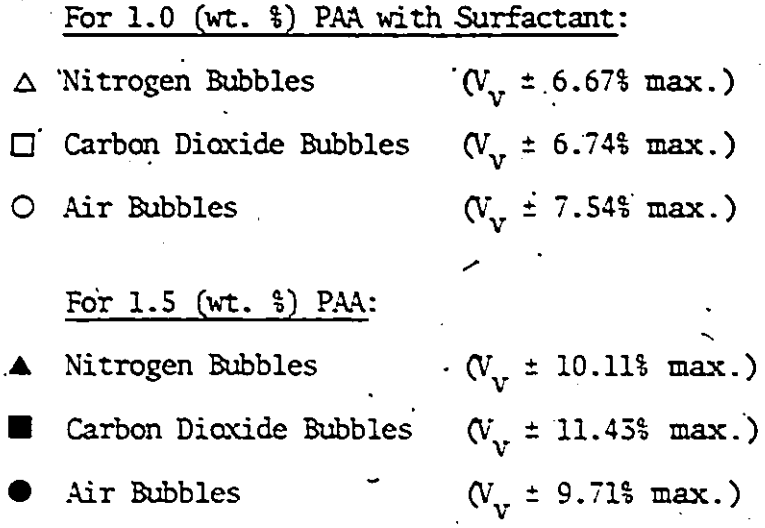

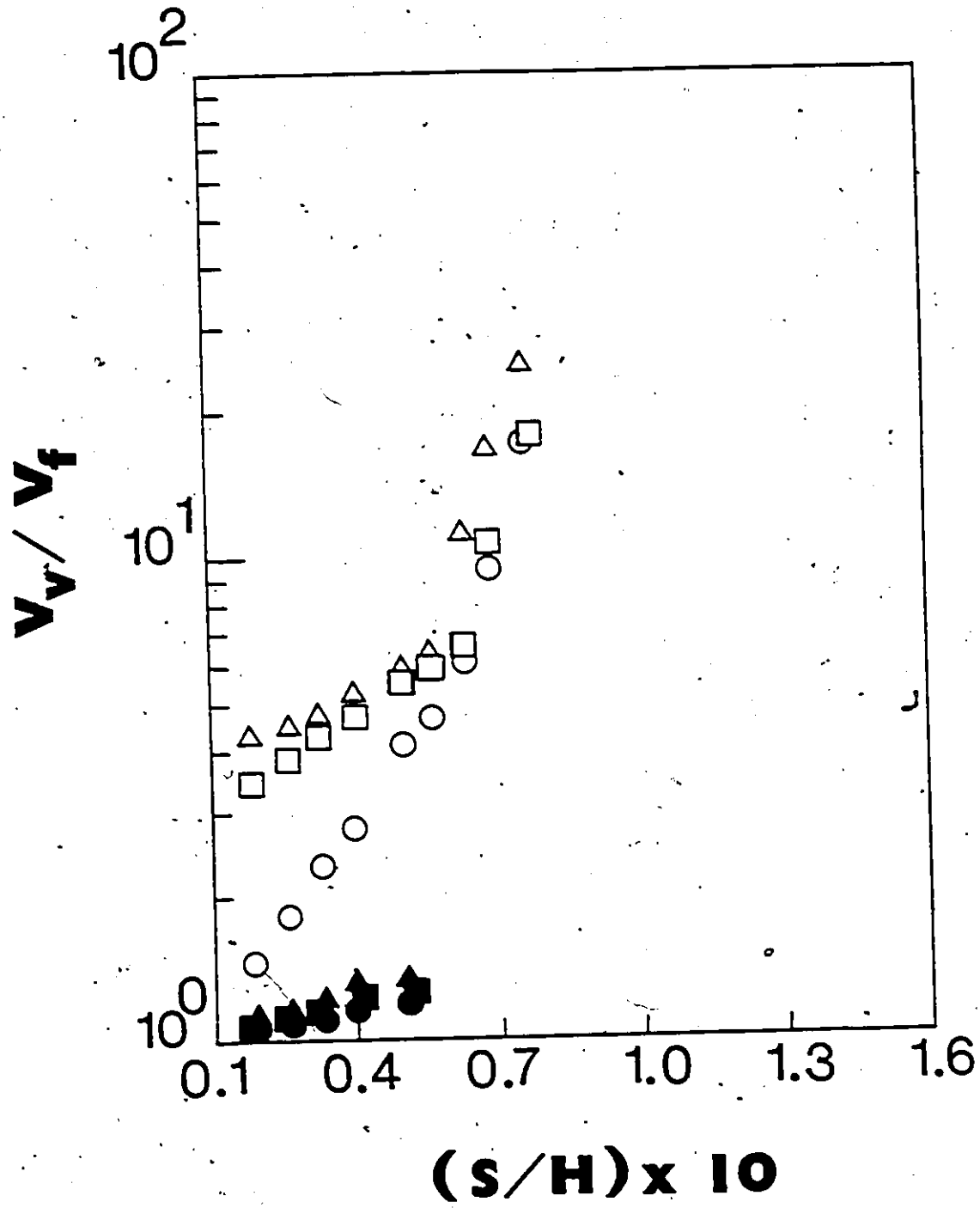
10^2
10^1
10^0
V_v / V_f
0.1
0.4
0.7
1.0
1.3
1.6
(S/H) x 10

FIGURE (IV-13): The Effect of Injecting Different Gases on the Coalescence Process for H = 0.25 m and $V_f = 1 \times 10^{-6}$ m^3.

For 1.0 (wt. %) PAA with Surfactant:

△ Nitrogen Bubbles ($V_v \pm 9.73\%$ max.)

□ Carbon Dioxide Bubbles ($V_v \pm 19.86\%$ max.)

○ Air Bubbles ($V_v \pm 7.74\%$ max.)

For 1.5 (wt. %) PAA:

▲ Nitrogen Bubbles ($V_v \pm 9.36\%$ max.)

■ Carbon Dioxide Bubbles ($V_v \pm 10.62\%$ max.)

● Air Bubbles ($V_v \pm 9.35\%$ max.).

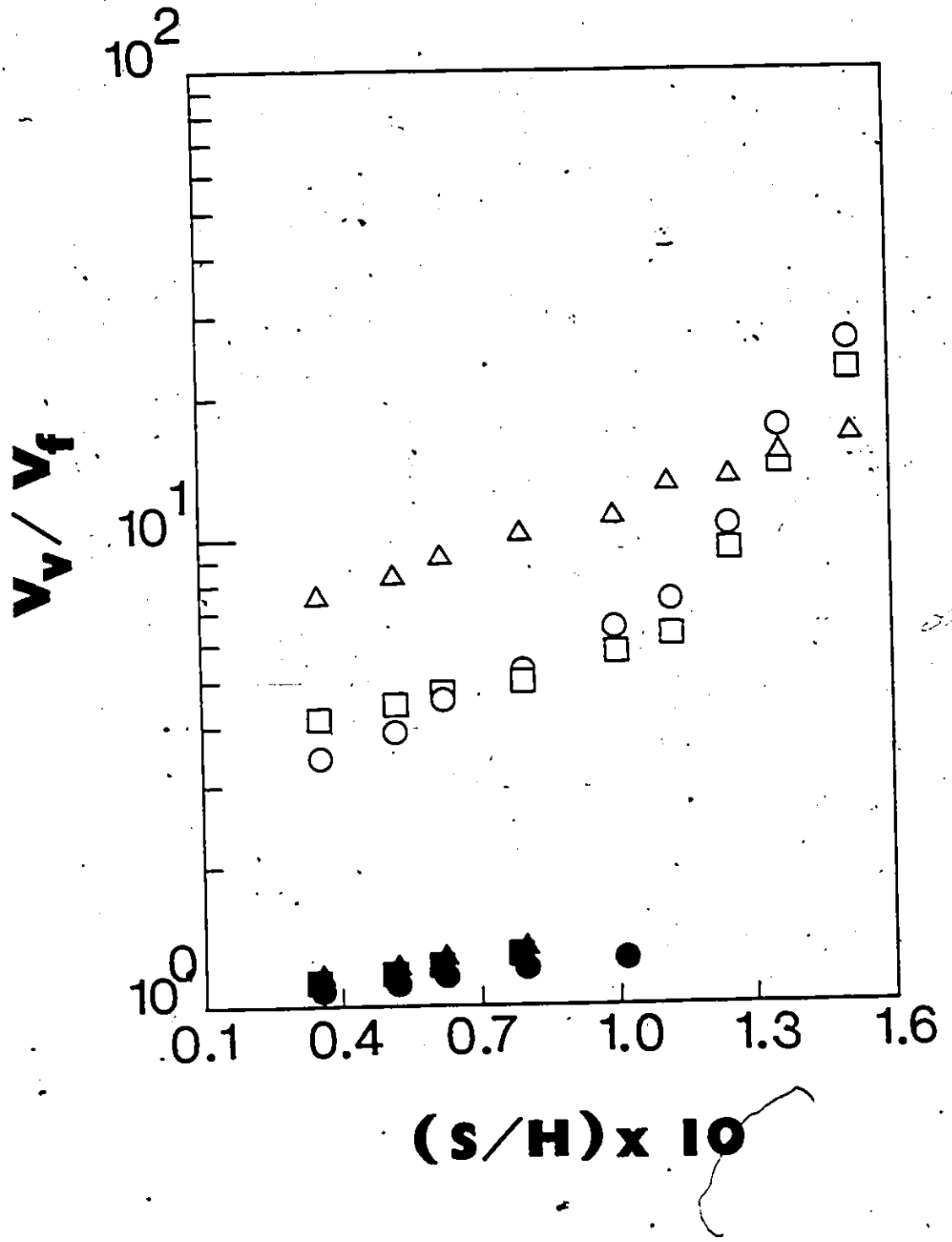
10^2
10^1
10^0
V_v / V_f
0.1
0.4
0.7
1.0
1.3
1.6
(S/H) x 10

IV.3 Viscosity Measurements

The experimental data obtained from the Rheomat-30 viscometer are presented in Appendix IV.

The four polymer solutions used were, 0.5, 1.0, 1.0 with surfactant, and 1.5 (wt.%) solutions of polyacrylamide (PAA) in a 50/50 (wt.%) mixture of glycerine and water. The chemical formula and the average molecular weight of the polyacrylamide used in preparing these solutions are presented in Table III-2. The polymer solution contains macromolecules, which are long chain molecules of varying lengths and are classified on an average molecular weight (M.W.) basis. As the chain length increases, the complexity of entanglements increases, one expects an increase of viscosity with increasing molecular weight for a given shear-rate. Properties such as molecular weight, chain length, configuration, and the degree of entanglement contribute significantly to the viscosity of the material.

Shown in Figure (IV-14) is the graph of viscosity as a function of shear-rate for the four polymer solutions studied. For the three different polymer concentrations, the viscosity increases with concentration. Also, the viscosity decreases with increasing shear-rate; a characteristic of pseudoplastic behaviour. Since the polymer solution contains long chain molecules which tend to get more entangled at higher polymer concentrations (L3 and L4). Entanglements retard the motion of the macromolecules and hence the viscosity is high. As the shearing force increases, the macromolecules

FIGURE (IV-14): Viscosity as a Function of Shear Rate for the Four Polymer Solutions Studied.

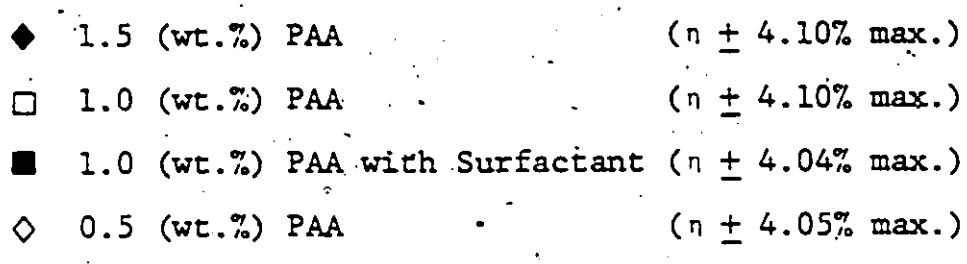

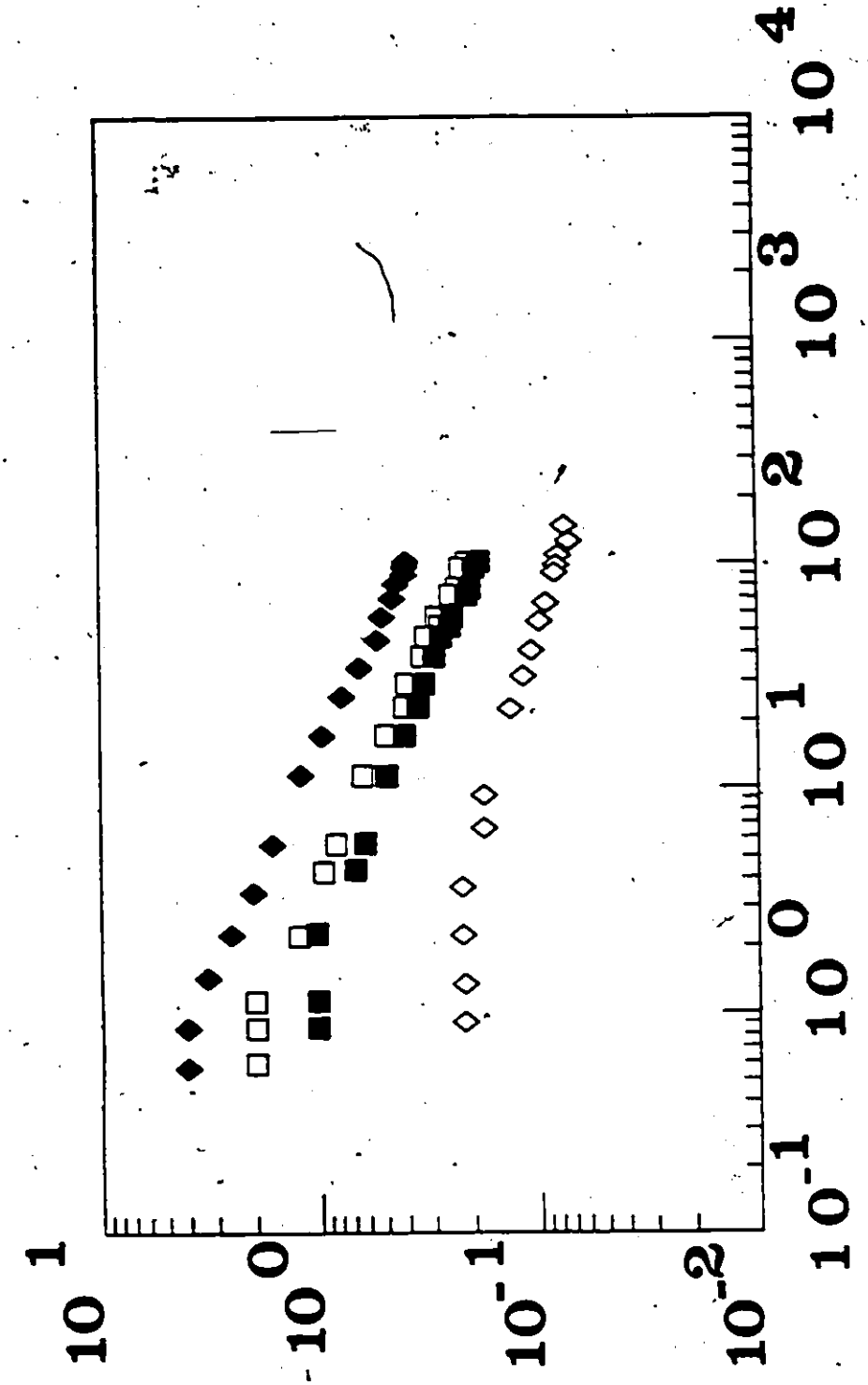
η (Pa.s)
10^1
10^0
10^-1
10^-2
10^-1
10^0
10^1
10^2
10^3
10^4
γ̇ (s^-1)

tend to slide along and disentangle, and the viscosity of the polymer solution decreases.

One of the purposes of this work is to examine the effect of the presence of a surfactant. Figure (IV-14) illustrates this effect on the viscosity behavior of the 1.0 (wt.%) PAA solution with 0.0417 (wt.%) of a surface active agent (Sorbitan Monolaurate). It was found that the viscosity was greatly reduced at low shear-rates by the surfactant and that no significant difference was exhibited at higher shear-rates in agreement with the conclusion of Vocel and Ryan (V1). A possible explanation of this phenomenon is that the surfactant being a surface active agent, would change the shape of the polymer molecule, thereby lowering the complexity of entanglements. At low shear-rates, the polymer solution with surfactant provides less resistance to shear whereas the one without surfactant shows more resistance to shear. At high shear-rates, both polymer solutions show relatively equal resistance to shear.

In modelling the viscosity, De Kee's model was used (D3). The model has the following form:

$$\eta = \sum_{p=1}^{M} \eta_p e^{-t_p \dot{\gamma}} + \eta_\infty \qquad \text{(IV-1)}$$

where

$$\eta_\infty = \sum_{p=M+1}^{\infty} \eta_p e^{-t_p \dot{\gamma}} \qquad \text{(IV-2)}$$

here $\eta_\infty = 0$ (by assumption)

and $$t_{p+1} = 0.10\ t_p \quad (p = 1,2,3,\ldots.n) \qquad \text{(IV-3)}$$

The evaluated model parameters η_p (Pa.s) and t_p(s) are given in Table (IV-1). These parameters were determined by a non-linear regression computer program presented in Appendix VI.

The limiting viscosity (η_∞) has a physical meaning, that is the value of the viscosity as the shear rate becomes very large. It is reasonable to assume that any pseudoplastic material would behave as a Newtonian fluid at high enough shear rates (C5). Carreau et al. (C5) concluded that for most engineering applications the limiting viscosity (η_∞) is very small and negligible compared to the non-Newtonian viscosity (η).

TABLE (IV-1) Evaluated Parameters Utilized in De Kee's Model

Model Parameters	Fluids			
	0.5 (wt %) PAA	1.0 (wt %) PAA with Surfactant	1.0 (wt %) PAA	1.5 (wt %) PAA
η_1 (Pa.s)	0.1180	0.7230	1.8960	3.5670
η_2 (Pa.s)	0.0775	0.3150	0.4170	1.0930
η_3 (Pa.s)	0.0496	0.2230	0.3100	0.6220
t_1 (s)	0.0780	0.2940	0.4080	0.5160

IV.4 Dimensional Analysis Considerations

The motion of gas bubbles in viscoelastic media is too complex to generate analytical solutions. Astarita (A4) presented an order-of-magnitude dimensional analysis of the problem of the motion of a spherical gas bubble through a viscoelastic Maxwell type liquid. Here we present a generalization for a non-spherical gas bubble and for a more realistic model. We will characterize the bubble motion in a viscoelastic fluid by the terminal velocity (v_t), an equivalent diameter ($D_e = [6V/\pi]^{1/3}$), and an injection period (τ).

Defining the following dimensionless parameters:

$$t^* = \frac{t}{\tau} = \text{dimensionless time} \qquad \text{(IV-4)}$$

$$\Lambda_1 = \left(\frac{v_t}{D_e}\right) t_1 = \text{dimensionless time describing the non-Newtonian influence on the bubble motion} \qquad \text{(IV-5)}$$

$$\Lambda_2 = \left(\frac{v_t}{D_e}\right) \lambda_o = \text{dimensionless time describing the elasticity influence on the bubble motion} \qquad \text{(IV-6)}$$

$$\bar{\dot{\gamma}}^* = \left(\frac{D_e}{v_t}\right) \bar{\dot{\gamma}} = \text{dimensionless shear rate tensor} \qquad \text{(IV-7)}$$

$$\eta^* = \left(\frac{\eta}{\eta_o}\right) = \text{dimensionless viscosity} \qquad \text{(IV-8)}$$

$$\bar{\bar{\tau}}^* = \left(\frac{D_e}{\eta_o v_t}\right) \bar{\bar{\tau}} = \text{dimensionless extra stress tensor} \qquad \text{(IV-9)}$$

$$\psi_1^* = \frac{\psi_1}{\eta_o \lambda_o} = \text{dimensionless primary normal stress coefficient} \qquad \text{(IV-10)}$$

where, τ = injection period, (s).

t_1 = parameter in De Kee's model (Eq. IV-1), (s).

$\bar{\bar{\dot{\gamma}}}$ = shear rate tensor, (s^{-1}).

$\bar{\bar{\tau}}$ = extra stress tensor, (Pa).

$\psi_1 = \frac{-(\tau_{11}-\tau_{22})}{\dot{\gamma}^2}$; is the primary normal stress coefficient, ($Pa.s^2$).

$-(\tau_{11}-\tau_{22})$ = primary normal stress difference, (Pa).

η_o = zero shear rate viscosity, (Pa.s).

and λ_o = rheological parameter relating the effect of elasticity on the bubble motion. It is the total time required for the fluid to recoil, (s).

As a rheological equation, we will choose an expansion of a non-linear model:

$$\bar{\bar{\tau}} = \underset{(a)}{-} \underset{(b)}{\left[\eta - \frac{D\psi_1}{Dt}\right]} \bar{\bar{\dot{\gamma}}} + \frac{1}{2} \underset{(c)}{\psi_1 \frac{\partial \bar{\bar{\dot{\gamma}}}}{\partial t}} - \frac{1}{2} \underset{(d)}{(\psi_1 + 2\psi_2)\{\bar{\bar{\dot{\gamma}}} \cdot \bar{\bar{\dot{\gamma}}}\}} + \ldots \qquad \text{(IV-11)}$$

in which the operator D/Dt is called the "substantial time derivative" or sometimes the "time derivative following the motion". The operator $\mathcal{D}/\mathcal{D}t$ is the corotational derivative or "Jaumann derivative". Different rheological models can be deduced as follows:

(a) = generalized Newtonian model.

(a) + (d) = Reiner-Rivlin model.

(a) + (c) + (d) = Ericksen model for steady viscometric flow.

(a) + (c) + (d) = with η, ψ_1, and ψ_2 constants; Coleman and Noll second order fluid.

In dimensionless form, Equation (IV-11) becomes:

$$\bar{\bar{\tau}}^* = -\eta^* \bar{\bar{\dot{\gamma}}}^* + \frac{\lambda_o}{\tau} \bar{\bar{\dot{\gamma}}}^* \left(\frac{D}{Dt}\right)^* \psi_1^* + \frac{1}{2} \frac{\lambda_o}{\tau} \psi_1^* \left(\frac{\mathcal{D}}{\mathcal{D}t}\right)^* \bar{\bar{\dot{\gamma}}}^* - \frac{2}{5} \Lambda_2 \psi_1^* \{\bar{\bar{\dot{\gamma}}}^* \cdot \bar{\bar{\dot{\gamma}}}^*\} + \cdots\cdots\cdots \quad \text{(IV-12)}$$

here we take:

$$\psi_2 = -0.10\, \psi_1 \quad \text{(IV-13)}$$

We have,

$$\frac{\eta}{\eta_o} = \eta^* (\Lambda_1^2 II^*, c) \quad \text{(IV-14)}$$

and

$$\frac{\psi_1}{\eta_o \lambda_o} = \psi_1^* (\Lambda_1^2 II^*, c) \quad \text{(IV-15)}$$

here, c = dimensionless rheological parameter,

where II^* represents the dimensionless second invariant of the rate of deformation tensor and it is defined as:

$$II^* = \left(\frac{D_e}{v_t}\right)^2 II \qquad \text{(IV-16)}$$

here, $$II = \bar{\dot{\gamma}} : \bar{\dot{\gamma}} \qquad \text{(IV-17)}$$

For an isothermal system, we propose the following correlation:

$$\frac{fRe}{16} = f(Re,\ We,\ \Lambda_1,\ \Lambda_2,\ \frac{\lambda_o}{\tau},\ c) \qquad \text{(IV-18)}$$

where, f = friction factor or drag coefficient.

and We = Weber number = $\frac{\text{inertia force}}{\text{surface tension force}}$

or $$We = \frac{\rho v_t^2 D_e}{\sigma} \qquad \text{(IV-19)}$$

In purely viscous fluids, the elastic parameters vanish and Equation (IV-18) becomes:

$$\frac{fRe}{16} = f(Re,\ We,\ \Lambda_1) \qquad \text{(IV-20)}$$

For viscoelastic fluids, the bubble motion can be classified into the following regimes:

(i) In creeping flow, (Re → 0) and the bubble motion is confined to a low shear rate (see Section IV.1). Therefore, the v_t^2 term can be neglected and Equation (IV-18) becomes:

$$\frac{fRe}{16} = f(\lambda_o/\tau,\ c) \qquad \text{(IV-21)}$$

(ii) For rapid flow (Re >> 1), the viscous forces are negligible when compared to the inertia forces and to the elastic forces. Equation (IV-18) gives:

$$\frac{fRe}{16} = f(Re,\ We,\ \Lambda_1,\ \Lambda_2,\ \frac{\lambda_o}{\tau},\ c) \qquad \text{(IV-22)}$$

The disappearance of the parameters Λ_1, Λ_2 in Equation (IV-21) is through the very low degree of pseudoplasticity encountered when the bubble is in creeping motion and the fluid did not exhibit any measurable normal stresses difference. The contribution of $\frac{\lambda_o}{\tau}$ and c terms is through the molecular disturbance caused by the bubble motion.

The Reynolds number for the purely viscous and viscoelastic fluids will be described by the following relation:

$$Re = \frac{\rho\, v_t\, D_e}{\eta_o} \qquad \text{(IV-23)}$$

where η_o is the constant zero shear rate viscosity.

V. CONCLUSIONS

The motion of gas bubbles was characterized by the fluid elasticity and viscosity, polymer ageing characteristics, and the presence of surface active agents or impurities in the test fluid. The shape of gas bubbles was controlled by the surface tension in the creeping flow regime and the polymer concentration at high Reynolds number. Consequently, the wake configurations behind ascending gas bubbles were also governed by the polymer concentration. No discontinuity was observed in the case of the log-log plots of the average terminal velocity versus bubble volume. The effect of injecting different gases was found to be predominant in the small volume range which is possibly due to the existence of electrostatic forces.

Bubble coalescence was observed to occur in three different stages for two gas bubbles injected simultaneously. In the first stage, the trailing bubble (V_f) enters the wake region behind the leading bubble (V_v). Experiencing less drag in this region, the trailing bubble accelerates significantly until collision takes place with the leading bubble. In the third stage, a process of thinning and final rupturing of the liquid film between the two touching bubbles takes place. Some of the variables associated with the coalescence process are: the height above the orifice plane at which coalescence will take place, the volume of the trailing bubble (fixed volume bubble, V_f), and the polymer concentration (c wt.%). A discontinuity in the case of the semi-log plot of V_v/V_f versus

S/H was observed as a result of increasing the orifice separation distance (S) and the larger values of V_v required in order to complete the coalescence process.

The viscosity of the 1.0 (wt.%) PAA solution was greatly reduced at low shear rates by the addition of a surfactant.

A correlation for the drag coefficient of a non-spherical gas bubble in purely viscous and viscoelastic fluids was suggested to be a function of the Reynolds number, the Weber number, time constants, and the dimensionless parameters which describe the non-Newtonian and elastic influence on the bubble motion. The bubble motion was characterized by the terminal velocity (v_t), an equivalent diameter (D_e), and an injection period (τ).

VI. RECOMMENDATIONS FOR FURTHER WORK

(i) - An experimental program is needed to connect the rheological behaviour of the viscoelastic fluids to the bubble motion, internal circulation, and the influence of the interface on the transfer of momentum and mass across it. To facilitate this study, four identical cylinders should be mounted vertically in the corners of the plexiglass tank and be allowed to rotate at certain speeds. The cylinders can be interchangeable and sets of various diameters depending on the range of shear rate desired. Internal circulation could be observed in air bubbles containing ammonium chloride (NH_4Cl) smoke. The most suitable method was to bring together streams of air containing ammonia (NH_3) and hydrogen chloride (HCl).

(ii) - Theoretical work is necessary in modelling the effect of elasticity on the transition from noncirculating to circulating gas bubbles.

(iii) - As far as mass transfer in polymer solutions is concerned, a number of tests are required with bubbles of different gases during ascend and coalescence at selected heights and orifice separation distances in the column. Also, the effects of internal circulation and surface active agents on the rate of mass transfer can be investigated.

(iv) - More experimentation is required to study the effects of surface active agents on the rheological behaviour of various elastic solutions as a function of concentration.

(v) - Creeping flow past a gas bubble could be studied

theoretically using De Kee's rheological model.

(vi) - Examination of the thinning process of a liquid film separating two coalescing bubbles is required to demonstrate the possible existence of an electroviscous effect (electrical resistance to shear) in ionic liquids.

(vii) - Triple bubble injection and bubble swarms are required to be examined.

(viii) - More experiments are needed with two bubble coalescence detailed in this work to confirm the functional dependence of the transition separation distance between orifices on the polymer concentration, height above the orifice plane at which coalescence will take place, and the volume of fixed bubble. A larger tank would therefore have to be built for measuring the coalescence under conditions of large orifice separation.

(ix) - A novel investigation could be achieved by using laser-doppler anemometry to measure the fluid velocity in the wake behind ascending gas bubbles injected from two or three orifices simultaneously at selected orifice separation distances before and after coalescence. Photographic techniques could aid the further understanding of the relationship between the bubble motion and wake configuration under the same imposed conditions. Studies so far have involved in-line coalescence only.

(x) - An electrical field could be applied gradually to the tested fluid to help explain the possible effects of

electrostatic forces between the gas and liquid phases on the velocity and stability of gas bubbles during ascend. It is also interesting to conduct the same experiment when a trace quantity of surface active agent is present.

(xi) - The mechanics of formation of bubbles of different gases from single submerged orifices within polymer solutions of various concentrations should be studied experimentally and theoretically in conjunction with bubbles hydrodynamics.

(xii) - Finally, the rheology and aging characteristics of polyacrylamide (PAA) solutions of various concentrations should be tested, specially in regard to a wide range of shear rates and temperatures.

APPENDIX I

Average Terminal Velocity Data of Air, Carbon Dioxide and Nitrogen Bubbles in the Four Polymer Solutions Studied.

TABLE (1) Average Terminal Velocity Data of Air Bubbles in 0.5 (wt.%) solution of polyacrylamide (PAA) in a 50/50 (wt.%) mixture of glycerine and water

(I.P.): 6 s

$V \times 10^6$ (m^3)	$\langle v_t \rangle \times 10^2$ (m/s)
0.02	8.65
0.034	10.33
0.056	12.36
0.072	14.56
0.096	17.15
0.15	20.81
0.20	22.05
0.25	22.12
0.35	22.79
0.55	23.29
0.75	23.86
0.90	24.06
2.50	27.10
5.00	30.38
7.50	33.85
10.00	35.65

TABLE (2) Average Terminal Velocity Data of Nitrogen Bubbles in 0.5 (wt.%) solution of polyacrylamide (PAA) in a 50/50 (wt.%) mixture of glycerine and water

(I.P.): 6 s

$V \times 10^6$ (m^3)	$\langle v_t \rangle \times 10^2$ (m/s)
0.025	7.25
0.063	13.26
0.075	14.34
0.085	15.22
0.11	17.41
0.16	19.43
0.22	20.01
0.33	21.71
0.50	22.38
0.75	23.04
0.91	23.23
1.30	23.62
2.33	26.15
3.76	28.91
5.10	30.28
6.65	31.81
8.95	33.43

TABLE (3) Average Terminal Velocity Data of Air Bubbles in 1.0 (wt.%) solution of polyacrylamide (PAA) in a 50/50 (wt.%) mixture of glycerine and water

Age: one month (I.P.): 6 s

$V \times 10^6$ (m^3)	$\langle v_t \rangle \times 10^2$ (m/s)
0.033	2.95
0.072	5.06
0.092	5.53
0.10	6.31
0.15	6.84
0.20	9.77
0.40	14.46
0.60	17.76
0.80	19.98
1.00	21.57
2.50	25.62
5.00	27.39
7.50	29.06
10.00	30.92

TABLE (4) Average Terminal Velocity Data of Air Bubbles in 1.0 (wt.%) solution of polyacrylamide (PAA) in a 50/50 (wt.%) mixture of glycerine and water

Age: eight months (I.P.): 6 s

$V \times 10^6$ (m^3)	$\langle v_t \rangle \times 10^2$ (m/s)
0.018	4.21
0.052	4.66
0.07	6.26
0.10	8.45
0.16	11.12
0.18	12.67
0.38	17.03
0.51	18.19
0.61	19.61
0.85	21.34
1.00	19.97
2.00	22.87
3.16	24.37
10.00	29.37

TABLE (5) Average Terminal Velocity Data of Air Bubbles in 1.0 (wt.%) solution of polyacrylamide (PAA) in a 50/50 (wt.%) mixture of glycerine and water

Age: ten months (I.P.): .6 s

$V \times 10^6$ (m^3)	$\langle v_t \rangle \times 10^2$ (m/s)
0.012	3.50
0.023	4.56
0.066	6.91
0.096	9.54
0.14	12.11
0.15	12.59
0.28	16.52
0.35	16.96
0.46	18.93
0.77	21.28
0.85	21.80
1.07	23.83
2.00	25.08
6.00	29.12
10.01	32.24

TABLE (6) Average Terminal Velocity Data of Air Bubbles in 1.0 (wt.%) solution of polyacrylamide (PAA) in a 50/50 (wt.%) mixture of glycerine and water (tap water)

(I.P.): 6 s

$V \times 10^6$ (m^3)	$\langle v_t \rangle \times 10^2$ (m/s)
0.04	3.11
0.052	3.69
0.061	4.16
0.078	4.96
0.096	5.35
0.12	6.43
0.16	6.83
0.20	8.99
0.25	9.13
0.33	11.50
0.40	12.40
0.65	15.47
0.82	17.88
1.50	20.85
3.00	22.86
7.50	28.37

TABLE (7) Average Terminal Velocity Data of Carbon Dioxide Bubbles in 1.0 (wt.%) solution of polyacrylamide (PAA) in a 50/50 (wt.%) mixture of glycerine and water

(I.P.): 6 s

$V \times 10^6$ (m^3)	$\langle v_t \rangle \times 10^2$ (m/s)
0.019	1.79
0.056	6.25
0.075	8.40
0.088	8.83
0.115	10.62
0.17	11.55
0.26	15.00
0.30	15.91
0.50	19.01
0.76	21.18
1.00	21.99
1.50	23.12
4.03	25.28
6.18	27.29
8.21	29.72
10.64	30.91

TABLE (8) Average Terminal Velocity Data of Carbon Dioxide Bubbles in 1.0 (wt.%) solution of polyacrylamide (PAA) in a 50/50 (wt.%) mixture of glycerine and water with surfactants

(I.P.): 6 s

$V \times 10^6$ (m^3)	$\langle v_t \rangle \times 10^2$ (m/s)
0.017	1.15
0.031	1.91
0.055	4.90
0.075	7.08
0.08	7.84
0.10	8.88
0.15	12.13
0.20	12.84
0.32	14.92
0.45	16.86
0.60	17.95
0.80	19.83
1.00	21.17
1.50	22.63
2.50	24.41
4.00	25.74
7.00	27.89
10.00	29.60

TABLE (9) Average Terminal Velocity Data of Air Bubbles in 1.5 (wt.%) solution of polyacrylamide (PAA) in a 50/50 (wt.%) mixture of glycerine and water

(I.P.): 6 s

$V \times 10^6$ (m^3)	$\langle v_t \rangle \times 10^2$ (m/s)
0.048	0.56
0.071	0.76
0.092	1.02
0.10	1.17
0.15	1.69
0.20	2.97
0.25	3.69
0.30	4.49
0.35	5.07
0.40	5.55
0.50	6.96
0.60	8.44
0.70	9.34
0.80	10.54
1.00	12.57
1.50	17.16
2.50	20.97
3.50	23.76
5.00	26.29
7.00	28.11
10.00	30.02

APPENDIX II

Values of the Transition Point from the Coalescence Data of the Four Polymer Solutions Studied.

TABLE (1) VALUES OF THE TRANSITION POINT FROM THE COALESCENCE DATA OF

0.5 (wt.%) solution of polyacrylamide (PAA) in a 50/50 (wt.%) mixture of glycerin and water

Injection Period I.P. (s)	Type of Gas	Volume of Fixed Bubble $V_\ell \times 10^6$ (m^3)	Height H(m)	Slope (i)		ln Intercept (k)		Transition Point	
				Before Transition	After Transition	Before Transition	After Transition	Separation Distance $S_t \times 10^3$ (m)	Bubble Volume $V_t \times 10^6$ (m^3)
10	Air	1	0.25	10.13	28.67	1.01	-0.84	25.03	7.58
10	Air	1	0.50	10.85	35.66	0.79	-0.61	28.34	4.10
10	Air	2	0.25	8.20	24.63	0.47	-1.23	26.08	7.60
10	Air	2	0.50	12.39	27.63	0.40	-0.55	31.24	6.48
10	Air	3	0.25	11.70	15.36	-0.022	-0.44	28.63	11.20
10	Air	3	0.50	14.95	N.T.	0.072	N.T.	N.T.	N.T.

N.T.: No Transition

TABLE (2) VALUES OF THE TRANSITION POINT FROM THE COALESCENCE DATA OF 1.0 (wt.%) solution of polyacrylamide (PAA) in a 50/50 (wt.%) mixture of glycerine and water

Injection Period I.P. (s)	Type of Gas	Volume of Fixed Bubble $V_f \times 10^6$ (m^3)	Height H(m)	Slope (t)		ln Intercept (k)		Transition Point	
				Before Transition	After Transition	Before Transition	After Transition	Separation Distance $S_t \times 10^3$ (m)	Bubble Volume $V_t \times 10^6$ (m^3)
10	Air	1	0.25	7.85	39.33	0.45	-2.59	24.25	3.39
10	Air	1	0.50	15.77	71.07	0.06	-2.55	23.71	2.26
10	Air	2	0.25	6.68	24.15	0.61	-1.69	33.06	8.99
10	Air	2	0.50	14.91	N.T.	0.30	N.T.	N.T.	N.T.
10	Air	3	0.25	6.03	18.60	0.41	-1.26	33.25	10.15
10	Air	3	0.50	14.89	N.T.	0.10	N.T.	N.T.	N.T.

N.T.: No Transition

TABLE (3) VALUES OF THE TRANSITION POINT FROM THE COALESCENCE DATA OF 1.0 (wt.%) solution of polyacrylamide (PAA) in a 50/50 (wt.%) mixture of glycerine and water with surfactant

Injection Period I.P. (s)	Type of Gas	Volume of Fixed Bubble $V_f \times 10^6$ (m^3)	Height H(m)	Slope (k)		ln Intercept (k)		Transition Point	
				Before Transition	After Transition	Before Transition	After Transition	Separation Distance $S_t \times 10^3$ (m)	Bubble Volume $V_t \times 10^6$ (m^3)
10	Air	1	0.25	10.20	34.26	0.84	-1.92	28.75	7.54
10	Air	1	0.50	31.94	78.73	-0.21	-3.13	31.23	5.96
10	Air	2	0.25	5.71	14.68	0.85	-0.22	30.25	9.39
10	Air	2	0.50	8.60	N.T.	0.74	N.T.	N.T.	N.T.
10	Air	3	0.25	4.36	11.40	0.77	-0.094	30.84	11.14
10	Air	3	0.50	7.98	N.T.	0.47	N.T.	N.T.	N.T.
10	CO_2	1	0.25	5.78	30.24	1.18	-1.51	27.59	6.20
10	CO_2	1	0.50	14.53	73.88	0.96	-2.75	31.35	6.54
10	CO_2	2	0.25	6.76	15.22	0.82	-0.16	29.29	10.10
10	CO_2	2	0.50	13.15	N.T.	0.68	N.T.	N.T.	N.T.
10	CO_2	3	0.25	3.52	11.43	0.95	-0.015	30.68	12.02
10	CO_2	3	0.50	19.52	N.T.	0.41	N.T.	N.T.	N.T.

N.T.: No Transition

TABLE (4) VALUES OF THE TRANSITION POINT FROM THE COALESCENCE DATA OF 1.0 (wt.%) solution of polyacrylamide (PAA) in a 50/50 (wt.%) mixture of glycerine and water with surfactant

Injection Period I.P. (s)	Type of Gas	Volume of Fixed Bubble $V_f \times 10^6$ (m^3)	Height H(m)	Slope (i)		ln Intercept (k)		Transition Point	
				Before Transition	After Transition	Before Transition	After Transition	Separation Distance $S_t \times 10^3$ (m)	Bubble Volume $V_t \times 10^6$ (m^3)
10	N_2	1	0.25	7.01	N.T.	1.76	N.T.	N.T.	N.T.
10	N_2	1	0.50	10.99	58.24	1.22	-1.20	25.68	5.96
10	N_2	2	0.25	7.08	N.T.	0.89	N.T.	N.T.	N.T.
10	N_2	2	0.50	9.08	34.37	0.86	-0.49	27.05	7.80
10	N_2	3	0.25	6.23	N.T.	0.79	N.T.	N.T.	N.T.
10	N_2	3	0.50	11.80	29.014	0.54	-0.43	28.27	10.05

N.T.: No Transition

TABLE (5) VALUES OF THE TRANSITION POINT FROM THE COALESCENCE DATA OF 1.5 (wt.%) solution of polyacrylamide (PAA) in a 50/50 (wt.%) mixture of glycerine and water .

Injection Period I.P. (s)	Type of Gas	Volume of Fixed Bubble $V_f \times 10^6$ (m^3)	Height H(m)	Slope (s)		ln Intercept (k)		Transition Point	
				Before Transition	After Transition	Before Transition	After Transition	Separation Distance $\delta_t \times 10^3$ (m)	Bubble Volume $V_t \times 10^6$ (m^3)
10	Air	1	0.25	2.49	N.T.	-0.026	N.T.	N.T.	N.T.
10	Air	1	0.50	4.47	N.T.	-0.050	N.T.	N.T.	N.T.
10	Air	2	0.25	13.68	37.61	-0.27	-2.37	21.93	5.03
10	Air	2	0.50	8.34	64.13	-0.096	-1.84	15.67	2.36
10	Air	3	0.25	11.63	22.47	-0.21	-1.40	27.36	8.63
10	Air	3	0.50	16.44	37.76	-0.11	-1.22	26.03	6.28
10	N_2	1	0.25	3.61	N.T.	0.028	N.T.	N.T.	N.T.
10	N_2	1	0.50	7.31	N.T.	-0.025	N.T.	N.T.	N.T.
10	N_2	2	0.25	12.34	59.41	-0.12	-4.75	24.58	5.91
10	N_2	2	0.50	15.92	102.31	-0.20	-3.86	21.16	3.20
10	N_2	3	0.25	11.33	16.98	0.11	-0.44	24.83	10.40
10	N_2	3	0.50	14.93	43.59	0.12	-1.44	27.37	7.72

N.T.: No Transition

TABLE (6) VALUES OF THE TRANSITION POINT FROM THE COALESCENCE DATA OF

1.5 (wt.%) solution of polyacrylamide (PAA) in a 50/50 (wt.%) mixture of glycerine and water

Injection Period I.P. (s)	Type of Gas	Volume of Fixed Bubble $V_f \times 10^6$ (m^3)	Height H(m)	Slope (k)		ln Intercept (k)		Transition Point	
				Before Transition	After Transition	Before Transition	After Transition	Separation Distance $S_t \times 10^3$ (m)	Bubble Volume $V_t \times 10^6$ (m^3)
10	CO_2	1	0.25	3.70	N.T.	-0.010	N.T.	N.T.	N.T.
10	CO_2	1	0.50	5.49	N.T.	-0.05	N.T.	N.T.	N.T.
10	CO_2	2	0.25	13.24	56.26	-0.16	-4.40	24.62	6.24
10	CO_2	2	0.50	10.98	90.10	-0.11	-3.26	19.88	2.75
10	CO_2	3	0.25	10.15	22.98	0.0079	-1.41	27.66	9.31
10	CO_2	3	0.50	13.57	49.41	0.10	-1.89	27.96	7.13

N.T.: No Transition

APPENDIX III

Coalescence Data of Air, Carbon Dioxide and Nitrogen Bubbles in the Four Polymer Solutions Studied.

TABLE (1) Coalescence Data of Air Bubbles in

0.5 (wt.%) solution of polyacrylamide (PAA) in a 50/50 (wt.%) mixture of glycerine and water.

(I.P.): 10 s

H = 0.50 m & V_f = 1x10^{-6} m^3		H = 0.50 m & V_f = 2x10^{-6} m^3		H = 0.50 m & V_f = 3x10^{-6} m^3	
Sx10^3 (m)	V_Vx10^6 (m^3)	Sx10^3(m)	V_Vx10^6 (m^3)	Sx10^3 (m)	V_Vx10^6 (m^3)
9.00	2.65	9.00	3.68	9.00	4.28
13.00	2.96	13.00	4.16	13.00	4.72
15.81	3.19	15.81	4.52	15.81	5.10
20.00	3.43	20.00	4.84	20.00	5.91
25.00	3.75	25.00	5.54	25.00	6.84
28.00	4.08	28.00	5.93	28.00	7.47
31.24	4.90	31.24	6.52	31.24	8.16
34.41	6.68	34.41	7.72	34.41	8.90
38.00	7.96	38.00	9.42	38.00	10.20
43.00		43.00		43.00	
H = 0.25 m & V_f = 1x10^{-6} m^3		H = 0.25 m & V_f = 2x10^{-6} m^3		H = 0.25 m & V_f = 3x10^{-6} m^3	
Sx10^3 (m)	V_Vx10^6 (m^3)	Sx10^3 (m)	V_Vx10^6 (m^3)	Sx10^3 (m)	V_Vx10^6 (m^3)
9.00	3.89	9.00	4.23	9.00	4.59
13.00	4.73	13.00	4.95	13.00	5.33
15.81	5.25	15.81	5.60	15.81	5.85
20.00	6.28	20.00	6.30	20.00	7.65
25.00	7.46	25.00	7.18	25.00	9.60
28.00	10.66	28.00	9.60	28.00	10.80
31.24	15.52	31.24	12.53	31.24	13.41
34.41	22.21	34.41	15.53	34.41	16.14
38.00	**	38.00	26.40	38.00	19.95
43.00		43.00		43.00	

**: Beyond the Capability of the Experimental Apparatus

TABLE (2) Coalescence Data of Air Bubbles in

1.0 (wt.%) solution of polyacrylamide (PAA) in a 50/50 (wt.%) mixture of glycerine and water

(I.P.): 10 s

H = 0.50 m & V_f = 1x10^{-6} m^3		H = 0.50 m & V_f = 2x10^{-6} m^3		H = 0.50 m & V_f = 3x10^{-6} m^3	
Sx10^3 (m)	V_vx10^6 (m^3)	Sx10^3(m)	V_vx10^6 (m^3)	Sx10^3 (m)	V_vx10^6 (m^3)
9.00	1.42	9.00	3.64	9.00	4.30
13.00	1.58	13.00	3.96	13.00	4.80
15.81	1.83	15.81	4.38	15.81	5.48
20.00	1.98	20.00	4.85	20.00	6.10
25.00	2.87	25.00	5.40	25.00	6.98
28.00	4.30	28.00	6.04	28.00	7.60
31.24	5.66	31.24	7.40	31.24	8.72
34.41	10.37	34.41	7.70	34.41	9.51
38.00	18.40	38.00	8.30	38.00	9.86
43.00		43.00		43.00	
H = 0.25 m & V_f = 1x10^{-6} m^3		H = 0.25 m & V_f = 2x10^{-6} m^3		H = 0.25 m & V_f = 3x10^{-6} m^3	
Sx10^3 (m)	V_vx10^6 (m^3)	Sx10^3 (m)	V_vx10^6 (m^3)	Sx10^3 (m)	V_vx10^6 (m^3)
9.00	2.13	9.00	4.70	9.00	5.56
13.00	2.36	13.00	5.20	13.00	6.20
15.81	2.60	15.81	5.70	15.81	6.90
20.00	2.91	20.00	6.43	20.00	7.32
25.00	3.53	25.00	7.34	25.00	8.20
28.00	6.40	28.00	7.92	28.00	9.00
31.24	8.98	31.24	8.38	31.24	9.64
34.41	18.75	34.41	10.24	34.41	13.20
38.00	28.80	38.00	14.49	38.00	15.60
43.00		43.00		43.00	

TABLE (3) Coalescence Data of Air Bubbles in

1.0 (wt.%) solution of polyacrylamide (PAA) in a 50/50 (wt.%) mixture of glycerine and water with surfactants

(I.P.): 10 s

H = 0.50 m & V_f = $1x10^{-6}$ m^3		H = 0.50 m & V_f = $2x10^{-6}$ m^3		H = 0.50 m & V_f = $3x10^{-6}$ m^3	
$Sx10^3$ (m)	$V_v x10^6$ (m^3)	$Sx10^3$ (m)	$V_v x10^6$ (m^3)	$Sx10^3$ (m)	$V_v x10^6$ (m^3)
9.00	1.46	9.00	4.91	9.00	5.58
13.00	1.82	13.00	5.25	13.00	5.88
15.81	2.30	15.81	5.56	15.81	6.25
20.00	2.77	20.00	5.90	20.00	6.65
25.00	4.11	25.00	6.38	25.00	7.20
28.00	4.75	28.00	6.70	28.00	7.50
31.24	6.06	31.24	7.20	31.24	7.90
34.41	9.82	34.41	7.60	34.41	8.40
38.00	17.31	38.00	8.18	38.00	8.85
43.00		43.00		43.00	
H = 0.25 m & V_f = $1x10^{-6}$ m^3		H = 0.25 m & V_f = $2x10^{-6}$ m^3		H = 0.25 m & V_f = $3x10^{-6}$ m^3	
$Sx10^3$ (m)	$V_v x10^6$ (m^3)	$Sx10^3$ (m)	$V_v x10^6$ (m^3)	$Sx10^3$ (m)	$V_v x10^6$ (m^3)
9.00	3.33	9.00	5.85	9.00	7.59
13.00	3.96	13.00	6.38	13.00	8.15
15.81	4.55	15.81	6.66	15.81	8.55
20.00	5.21	20.00	7.28	20.00	9.30
25.00	6.46	25.00	8.30	25.00	10.05
28.00	7.30	28.00	8.95	28.00	10.65
31.24	10.36	31.24	9.71	31.24	11.15
34.41	17.10	34.41	11.97	34.41	13.10
38.00	26.21	38.00	14.80	38.00	15.45
43.00		43.00		43.00	

TABLE (4) Coalescence Data of Carbon Dioxide Bubbles in 1.0 (wt.%) solution of polyacrylamide (PAA) in a 50/50 (wt.%) mixture of glycerine and water with surfactants

(I.P): 10 s

H = 0.50 m & V_f = $1x10^{-6}$ m^3		H = 0.50 m & V_f = $2x10^{-6}$ m^3		H = 0.50 m & V_f = $3x10^{-6}$ m^3	
$Sx10^3$ (m)	$V_v x10^6$ (m^3)	$Sx10^3$ (m)	$V_v x10^6$ (m^3)	$Sx10^3$ (m)	$V_v x10^6$ (m^3)
9.00	3.41	9.00	5.01	9.00	6.46
13.00	3.80	13.00	5.60	13.00	7.82
15.81	4.24	15.81	6.06	15.81	8.51
20.00	4.70	20.00	6.84	20.00	9.63
25.00	5.43	25.00	7.78	25.00	11.70
28.00	5.90	28.00	8.30	28.00	13.48
31.24	6.55	31.24	8.77	31.24	15.56
34.41	10.28	34.41	9.38	34.41	17.37
38.00	17.50	38.00	10.60	38.00	20.55
43.00		43.00	13.00	43.00	
H = 0.25 m & V_f = $1x10^{-6}$ m^3		H = 0.25 m & V_f = $2x10^{-6}$ m^3		H = 0.25 m & V_f = $3x10^{-6}$ m^3	
$Sx10^3$ (m)	$V_v x10^6$ (m^3)	$Sx10^3$ (m)	$V_v x10^6$ (m^3)	$Sx10^3$ (m)	$V_v x10^6$ (m^3)
9.00	4.04	9.00	5.75	9.00	8.80
13.00	4.45	13.00	6.60	13.00	9.35
15.81	4.70	15.81	7.03	15.81	9.68
20.00	5.15	20.00	7.68	20.00	10.57
25.00	5.84	25.00	9.23	25.00	11.10
28.00	6.30	28.00	9.80	28.00	11.61
31.24	9.48	31.24	10.46	31.24	11.98
34.41	14.63	34.41	13.78	34.41	14.25
38.00	21.50	38.00	17.15	38.00	16.80
43.00		43.00		43.00	

TABLE (5) Coalescence Data of Nitrogen Bubbles in 1.0 (wt.%) solution of polyacrylamide (PAA) in a 50/50 (wt.%) mixture of glycerine and water with surfactants

(I.P.): 10 s

H = 0.50 m & V_f = $1x10^{-6}$ m^3		H = 0.50 m & V_f = $2x10^{-6}$ m^3		H = 0.50 m & V_f = $3x10^{-6}$ m^3	
$Sx10^3$ (m)	$V_v x10^6$ (m^3)	$Sx10^3$ (m)	$V_v x10^6$ (m^3)	$Sx10^3$ (m)	$V_v x10^6$ (m^3)
9.00	4.19	9.00	5.64	9.00	6.45
13.00	4.45	13.00	5.97	13.00	6.88
15.81	4.77	15.81	6.33	15.81	7.46
20.00	5.23	20.00	6.95	20.00	8.33
25.00	5.86	25.00	7.47	25.00	9.21
28.00	6.33	28.00	7.92	28.00	9.94
31.24	11.26	31.24	10.14	31.24	10.86
34.41	16.88	34.41	13.57	34.41	14.34
38.00	24.76	38.00	16.18	38.00	17.66
43.00		43.00		43.00	
H = 0.25 m & V_f = $1x10^{-6}$ m^3		H = 0.25 m & V_f = $2x10^{-6}$ m^3		H = 0.25 m & V_f = $3x10^{-6}$ m^3	
$Sx10^3$ (m)	$V_v x10^6$ (m^3)	$Sx10^3$ (m)	$V_v x10^6$ (m^3)	$Sx10^3$ (m)	$V_v x10^6$ (m^3)
9.00	7.49	9.00	6.35	9.00	8.38
13.00	8.33	13.00	6.89	13.00	9.17
15.81	9.22	15.81	7.67	15.81	9.84
20.00	10.47	20.00	8.78	20.00	10.95
25.00	11.59	25.00	9.94	25.00	12.45
28.00	13.10	28.00	11.16	28.00	13.30
31.24	13.85	31.24	11.83	31.24	14.52
34.41	15.65	34.41	12.61	34.41	15.60
38.00	16.78	38.00	14.45	38.00	17.33
43.00		43.00		43.00	

TABLE (6) Coalescence Data of Air Bubbles in

—— 1.5 (wt.%) solution of polyacrylamide (PAA) in a 50/50 (wt.%) mixture of glycerine and water

(I.P.): 10 s

H = 0.50 m & $V_f = 1x10^{-6}$ m^3		H = 0.50 m & $V_f = 2x10^{-6}$ m^3		H = 0.50 m & $V_f = 3x10^{-6}$ m^3	
$Sx10^3$ (m)	$V_v x10^6$ (m^3)	$Sx10^3$ (m)	$V_v x10^6$ (m^3)	$Sx10^3$ (m)	$V_v x10^6$ (m^3)
9.00	1.03	9.00	2.10	9.00	3.50
13.00	1.06	13.00	2.30	13.00	4.10
15.81	1.10	15.81	2.35	15.81	4.62
20.00	1.15	20.00	2.48	20.00	5.18
25.00	1.18	25.00	2.79	25.00	5.95
28.00	N.C.	28.00	11.44	28.00	6.73
31.24	N.C.	31.24	17.50	31.24	9.15
34.41	N.C.	34.41	26.00	34.41	12.25
38.00	N.C.	38.00	**	38.00	15.28
43.00		43.00		43.00	
H = 0.25 m & $V_f = 1x10^{-6}$ m^3		H = 0.25 m & $V_f = 2x10^{-6}$ m^3		H = 0.25 m & $V_f = 3x10^{-6}$ m^3	
$Sx10^3$ (m)	$V_v x10^6$ (m^3)	$Sx10^3$ (m)	$V_v x10^6$ (m^3)	$Sx10^3$ (m)	$V_v x10^6$ (m^3)
9.00	1.07	9.00	2.50	9.00	3.65
13.00	1.10	13.00	3.00	13.00	4.36
15.81	1.14	15.81	3.58	15.81	5.17
20.00	1.19	20.00	4.71	20.00	6.20
25.00	1.25	25.00	5.83	25.00	7.50
28.00	N.C.	28.00	12.30	28.00	8.99
31.24	N.C.	31.24	21.21	31.24	12.06
34.41	N.C.	34.41	32.20	34.41	16.71
38.00	N.C.	38.00	**	38.00	22.16
43.00		43.00		43.00	

N.C.: No Coalescence
** : Beyond the Capability of the Experimental Apparatus

TABLE (7) Coalescence Data of Carbon-Dioxide Bubbles in 1.5 (wt.%) solution of polyacrylamide (PAA) in a 50/50 (wt.%) mixture of glycerine and water

(I.P.): 10 s

H = 0.50 m & $V_f = 1x10^{-6}$ m^3		H = 0.50 m & $V_f = 2x10^{-6}$ m^3		H = 0.50 m & $V_f = 3x10^{-6}$ m^3	
$Sx10^3$ (m)	$V_V x10^6$ (m^3)	$Sx10^3$(m)	$V_V x10^6$ (m^3)	$Sx10^3$ (m)	$V_V x10^6$ (m^3)
9.00	1.05	9.00	2.17	9.00	4.26
13.00	1.08	13.00	2.36	13.00	4.75
15.81	1.13	15.81	2.48	15.81	5.13
20.00	1.17	20.00	2.77	20.00	5.74
25.00	1.25	25.00	3.07	25.00	6.57
28.00	N.C.	28.00	11.88	28.00	7.15
31.24	N.C.	31.24	21.33	31.24	9.87
34.41	N.C.	34.41	**	34.41	13.45
38.00	N.C.	38.00	**	38.00	19.22
43.00		43.00		43.00	
H = 0.25 m & $V_f = 1x10^{-6}$ m^3		H = 0.25 m & $V_f = 2x10^{-6}$ m^3		H = 0.25 m & $V_f = 3x10^{-6}$ m^3	
$Sx10^3$ (m)	$V_V x10^6$ (m^3)	$Sx10^3$ (m)	$V_V x10^6$ (m^3)	$Sx10^3$ (m)	$V_V x10^6$ (m^3)
9.00	1.13	9.00	2.70	9.00	4.38
13.00	1.20	13.00	3.38	13.00	5.12
15.81	1.25	15.81	3.86	15.81	5.73
20.00	1.33	20.00	5.10	20.00	6.75
25.00	N.C.	25.00	6.19	25.00	8.40
28.00	N.C.	28.00	13.33	28.00	9.45
31.24	N.C.	31.24	27.71	31.24	13.08
34.41	N.C.	34.41	**	34.41	16.95
38.00	N.C.	38.00	**	38.00	24.30
43.00		43.00		43.00	

N.C.: No Coalescence
** : Beyond the Capability of the Experimental Apparatus

TABLE (8) Coalescence Data of Nitrogen Bubbles in

1.5 (wt.%) solution of polyacrylamide (PAA) in a 50/50 (wt.%) mixture of glycerine and water

(I.P.): 10 s

H = 0.50 m & V_f = $1x10^{-6}$ m^3		H = 0.50 m & V_f = $2x10^{-6}$ m^3		H = 0.50 m & V_f = $3x10^{-6}$ m^3	
$Sx10^3$ (m)	$V_v x10^6$ (m^3)	$Sx10^3$ (m)	$V_v x10^6$ (m^3)	$Sx10^3$ (m)	$V_v x10^6$ (m^3)
9.00	1.11	9.00	2.16	9.00	4.44
13.00	1.16	13.00	2.41	13.00	5.02
15.81	1.23	15.81	2.77	15.81	5.49
20.00	1.33	20.00	3.08	20.00	6.22
25.00	1.38	25.00	3.58	25.00	7.13
28.00	N.C.	28.00	12.96	28.00	7.90
31.24	N.C.	31.24	25.20	31.24	10.70
34.41	N.C.	34.41	**	34.41	14.55
38.00	N.C.	38.00	**	38.00	19.33
43.00		43.00		43.00	
H = 0.25 m & V_f = $1x10^{-6}$ m^3		H = 0.25 m & V_f = $2x10^{-6}$ m^3		H = 0.25 m & V_f = $3x10^{-6}$ m^3	
$Sx10^3$ (m)	$V_v x10^6$ (m^3)	$Sx10^3$ (m)	$V_v x10^6$ (m^3)	$Sx10^3$ (m)	$V_v x10^6$ (m^3)
9.00	1.17	9.00	2.70	9.00	5.13
13.00	1.23	13.00	3.36	13.00	6.03
15.81	1.29	15.81	3.82	15.81	6.96
20.00	1.37	20.00	4.90	20.00	8.22
25.00	N.C.	25.00	5.88	25.00	10.31
28.00	N.C.	28.00	13.33	28.00	12.27
31.24	N.C.	31.24	28.87	31.24	16.16
34.41	N.C.	34.41	**	34.41	19.73
38.00	N.C.	38.00	**	38.00	25.56
43.00		43.00		43.00	

N.C.: No Coalescence
** : Beyond the Capability of the Experimental Apparatus

APPENDIX IV

Viscosity Data of the Four
Polymer Solutions Studied.

TABLE (1) Viscosity Data of 0.5 (wt.%) solution of polyacrylamide (PAA) in a 50/50 (wt.%) mixture of glycerine and water

(Rheomat-30 Viscometer)

$\dot{\gamma}$ (s^{-1})	η (Pa.s)
0.90	0.22
1.35	0.22
2.25	0.22
3.60	0.22
6.76	0.18
9.02	0.18
22.55	0.13
31.57	0.11
40.59	0.11
54.13	0.09
67.66	0.09
90.22	0.08
99.75	0.08
112.77	0.07
126.30	0.07
144.35	0.07

TABLE (2) Viscosity Data of 1.0 (wt.%) solution of Polyacrylamide (PAA) in a 50/50 (wt.%) mixture of glycerine and water

(Rheomat-30 Viscometer)

$\dot{\gamma}$ (s^{-1})	η (Pa.s)
0.57	2.09
0.85	2.09
1.14	2.09
2.28	1.30
4.27	0.97
5.70	0.83
11.40	0.62
17.10	0.48
22.80	0.41
28.50	0.39
37.05	0.33
42.75	0.33
51.30	0.29
57.00	0.29
71.25	0.25
79.80	0.24
91.20	0.23
99.75	0.22

TABLE (3) Viscosity Data of 1.0 (wt.%) solution of polyacrylamide (PAA) in a 50/50 (wt.%) mixture of glycerine and water with surfactants

(Rheomat-30 Viscometer)

$\dot{\gamma}$ (s^{-1})	η (Pa.s)
0.85	1.04
1.14	1.04
2.28	1.04
4.27	0.69
5.70	0.62
11.40	0.47
17.10	0.41
22.80	0.36
28.50	0.33
37.05	0.30
42.75	0.27
51.30	0.25
57.00	0.25
71.25	0.21
79.80	0.20
91.20	0.19
99.75	0.19

TABLE (4) Viscosity Data of 1.5 (wt.%) solution of polyacrylamide (PAA) in a 50/50 (wt.%) mixture of glycerine and water

(Rheomat-30 Viscometer)

$\dot{\gamma}$ (s^{-1})	η (Pa.s)
0.57	4.18
0.85	4.18
1.42	3.34
2.28	2.61
3.42	2.09
5.70	1.67
11.40	1.25
17.10	0.97
25.65	0.79
34.20	0.67
45.60	0.57
57.00	0.52
68.40	0.47
79.80	0.44
88.35	0.41
94.05	0.41
99.75	0.40

APPENDIX V

Uncertainty Analysis of the Experimental Results of Viscosity, Bubble Terminal Velocity, and Bubble Coalescence.

By "uncertainty" we mean a possible value the error might have. Kline and McClintock (K2) presented a method of estimating uncertainty in single-sample experimental results. The method is based on a careful specification of the uncertainties in the various primary experimental measurements. We wish to estimate the uncertainty in the calculated apparent viscosity (η) on the basis of the uncertainties in the shear rate ($\dot{\gamma}$) and the shear stress (τ). The result is a given function of the independent variables $\dot{\gamma}$, $\tau\%$, κ,... Thus,

$$\eta = \eta\ (\dot{\gamma},\ \tau\%,\ \kappa, \ldots\ldots\ldots) \qquad \text{(App. V-1)}$$

here κ is a calibration constant supplied for the particular measuring system used in the Rheomat-30 viscometer and $\tau\%$ is the percent deflection.

For small variations in the independent variables, Equation (App. V-1) can be expressed in linear form as

$$\delta\eta = \frac{\partial \eta}{\partial \dot{\gamma}}\,\delta\dot{\gamma} + \frac{\partial \eta}{\partial \tau\%}\,\delta\tau\% + \frac{\partial \eta}{\partial \kappa}\,\delta\kappa + \ldots\ldots + \ldots\ldots \qquad \text{(App. V-2)}$$

Let w_η be the uncertainty in the result and $w_{\dot{\gamma}}$, $w_{\tau\%}$, w_κ,.... be the uncertainties in the independent variables. Therefore,

$$w_\eta = \left[\left(\frac{\partial \eta}{\partial \dot{\gamma}}\,w_{\dot{\gamma}}\right)^2 + \left(\frac{\partial \eta}{\partial \tau\%}\,w_{\tau\%}\right)^2 + \left(\frac{\partial \eta}{\partial \kappa}\,w_\kappa\right)^2 + \ldots + \ldots\right]^{\frac{1}{2}} \qquad \text{(App. V-3)}$$

Equation (App. V-3) can be used directly for calculating the uncertainty interval in the result.

The following is the worst possible uncertainty in the apparent viscosity presented in Appendix IV

(a) for the 0.5 (wt.%) PAA solution [Table (1)].

% deflection = 50 ± 1

we have

$$\eta = \frac{(\tau\%)(\kappa)}{\dot{\gamma}} \qquad \text{(App. V-4)}$$

where, $\dot{\gamma}$ = (rev. per min.)(constant) s^{-1}

$\tau\% = 0.50 \pm 0.02$ Pa

$\kappa = 2.384 \pm 0.001$

and $\dot{\gamma} = 0.90 \pm 0.005\ s^{-1}$.

Therefore, Eq. (App. V-3) becomes,

$$w_\eta = [(-\frac{\tau\%\kappa}{\dot{\gamma}^2} w_{\dot{\gamma}})^2 + (\frac{\kappa}{\dot{\gamma}} w_{\tau\%})^2 + (\frac{\tau\%}{\dot{\gamma}} w_\kappa)^2]^{1/2} \qquad \text{(App. V-5)}$$

$$\text{or} \quad w_\eta = [(-\frac{\eta}{\dot{\gamma}} w_{\dot{\gamma}})^2 + (\frac{\eta}{\tau\%} w_{\tau\%})^2 + (\frac{\eta}{\kappa} w_\kappa)^2]^{1/2} \qquad \text{(App. V-6)}$$

$$\therefore w_\eta = [(-(\frac{0.22}{0.90})(0.005))^2 + ((\frac{0.22}{0.50})(0.02))^2 +$$

$$+ ((\frac{0.22}{2.384})(0.001))^2]^{1/2} = \pm 0.0089 \text{ Pa.s}$$

which gives $\eta = 0.22 \pm 0.0089$ Pa.s

or % uncertainty $= \frac{0.0089}{0.22} \times 100 = \pm 4.05\%$

(b) for the 1.0 (wt.%) PAA solution [Table (2)]

$\eta = 2.09 \pm 0.0856$ Pa.s

or % uncertainty = $\pm$ 4.10%

(c) for the 1.0 (wt.%) PAA solution with surfactant [Table (3)].

$\eta = 1.04 \pm 0.0420$ Pa.s

or % uncertainty = $\pm$ 4.04%

(d) for the 1.5 (wt.%) PAA solution [Table (4)].

$\eta = 4.18 \pm 0.1712$ Pa.s

or % uncertainty = $\pm$ 4.10%

Uncertainties in the data of bubble terminal velocity and coalescence were obtained from repeated measurements. Experiments in which uncertainties are evaluated by such repetition are called multisample experiments. The uncertainty interval for these data is now written as

$$\pm \text{ uncertainty} = \frac{\text{highest value - lowest value}}{2} \qquad \text{(App. V-7)}$$

and

$$\% \text{ uncertainty} = \frac{\pm \text{ uncertainty}}{\text{average value}} \times 100 \qquad \text{(App. V-8)}$$

The following is the worst possible uncertainty (average value $\pm$ percent uncertainty):

(i) Uncertainty analysis of the terminal velocity measurements presented in Appendix I.

(a) Air Bubbles in 0.5 (wt.%) PAA [Table (1)].

$\therefore \langle v_t \rangle \pm 5.91\%$.

(b) Nitrogen Bubbles in 0.5 (wt.%) PAA [Table (2)].

$\therefore \langle v_t \rangle \pm 2.21\%$.

(c) Air Bubbles in 1.0 (wt.%) PAA [Table (3)].

$\therefore \langle v_t \rangle \pm 2.97\%$.

(d) Air Bubbles in 1.0 (wt.%) PAA [Table (4)].

$\therefore \langle v_t \rangle \pm 6.18\%$.

(e) Air Bubbles in 1.0 (wt.%) PAA [Table (5)].

$\therefore \langle v_t \rangle \pm 7.24\%$.

(f) Air Bubbles in 1.0 (wt.%) PAA with tap-water [Table (6)].

$\therefore$ $\langle v_t \rangle \pm 5.05\%$.

(g) Carbon-Dioxide Bubbles in 1.0 (wt.%) PAA [Table (7)].

$\therefore$ $\langle v_t \rangle \pm 4.16\%$.

(h) Carbon-Dioxide Bubbles in 1.0 (wt.%) with Surfactant [Table (8)].

$\therefore$ $\langle v_t \rangle \pm 3.48\%$.

(i) Air Bubbles in 1.5 (wt.%) PAA [Table (9)].

$\therefore$ $\langle v_t \rangle \pm 5.98\%$.

(ii) Uncertainty analysis for the coalescence data presented in Appendix III.

(a) Air Bubbles in 0.5 (wt.%) PAA [Table (1)].

for H = 0.50 m:

$V_f = 1 \times 10^{-6}\ m^3$ $\therefore V_v \pm 18.67\%$

$V_f = 2 \times 10^{-6}\ m^3$ $\therefore V_v \pm 10.07\%$

$V_f = 3 \times 10^{-6}\ m^3$ $\therefore V_v \pm 7.31\%$

for H = 0.25 m:

$V_f = 1 \times 10^{-6}\ m^3$ $\therefore V_v \pm 9.14\%$

$V_f = 2 \times 10^{-6}\ m^3$ $\therefore V_v \pm 8.85\%$

$V_f = 3 \times 10^{-6}\ m^3$ $\therefore V_v \pm 7.19\%$

(b) Air Bubbles in 1.0 (wt.%) PAA [Table (2)].

for H = 0.50 m:

$V_f = 1 \times 10^{-6}\ m^3$ $\therefore V_v \pm 8.15\%$

$V_f = 2 \times 10^{-6}\ m^3$ $\therefore V_v \pm 7.14\%$

$V_f = 3 \times 10^{-6}\ m^3$ $\therefore V_v \pm 6.98\%$

for H = 0.25 m:

$V_f = 1 \times 10^{-6}\ m^3$ $\therefore V_v \pm 7.63\%$

$V_f = 2 \times 10^{-6}\ m^3$ $\therefore V_v \pm 9.53\%$

$V_f = 3 \times 10^{-6}\ m^3$ $\therefore V_v \pm 12.66\%$

(c) Air Bubbles in 1.0 (wt.%) PAA with Surfactant [Table (3)].

for H = 0.50 m:

$V_f = 1 \times 10^{-6}$ m^3 $\therefore V_v \pm 7.54\%$

$V_f = 2 \times 10^{-6}$ m^3 $\therefore V_v \pm 5.91\%$

$V_f = 3 \times 10^{-6}$ m^3 $\therefore V_v \pm 5.56\%$

for H = 0.25 m:

$V_f = 1 \times 10^{-6}$ m^3 $\therefore V_v \pm 7.74\%$

$V_f = 2 \times 10^{-6}$ m^3 $\therefore V_v \pm 6.96\%$

$V_f = 3 \times 10^{-6}$ m^3 $\therefore V_v \pm 6.08\%$

(d) Carbon-Dioxide Bubbles in 1.0 (wt.%) PAA with Surfactant [Table (4)].

for H = 0.50 m:

$V_f = 1 \times 10^{-6}$ m^3 $\therefore V_v \pm 6.74\%$

$V_f = 2 \times 10^{-6}$ m^3 $\therefore V_v \pm 5.79\%$

$V_f = 3 \times 10^{-6}$ m^3 $\therefore V_v \pm 5.26\%$

for H = 0.25 m:

$V_f = 1 \times 10^{-6}$ m^3 $\therefore V_v \pm 19.86\%$

$V_f = 2 \times 10^{-6}$ m^3 $\therefore V_v \pm 9.04\%$

$V_f = 3 \times 10^{-6}$ m^3 $\therefore V_v \pm 8.86\%$

(e) Nitrogen Bubbles in 1.0 (wt.%) PAA with Surfactant [Table (5)].

for H = 0.50 m:

$V_f = 1 \times 10^{-6}\ m^3$ $\therefore V_v \pm 6.67\%$

$V_f = 2 \times 10^{-6}\ m^3$ $\therefore V_v \pm 6.20\%$

$V_f = 3 \times 10^{-6}\ m^3$ $\therefore V_v \pm 5.89\%$

for H = 0.25 m:

$V_f = 1 \times 10^{-6}\ m^3$ $\therefore V_v \pm 9.73\%$

$V_f = 2 \times 10^{-6}\ m^3$ $\therefore V_v \pm 10.51\%$

$V_f = 3 \times 10^{-6}\ m^3$ $\therefore V_v \pm 8.88\%$

(f) Air Bubbles in 1.5 (wt.%) PAA [Table (6)].

for H = 0.50 m:

$V_f = 1 \times 10^{-6}\ m^3$ $\therefore V_v \pm 9.71\%$

$V_f = 2 \times 10^{-6}\ m^3$ $\therefore V_v \pm 7.62\%$

$V_f = 3 \times 10^{-6}\ m^3$ $\therefore V_v \pm 6.71\%$

for H = 0.25 m:

$V_f = 1 \times 10^{-6}\ m^3$ $\therefore V_v \pm 9.35\%$

$V_f = 2 \times 10^{-6}\ m^3$ $\therefore V_v \pm 6.93\%$

$V_f = 3 \times 10^{-6}\ m^3$ $\therefore V_v \pm 19.40\%$

(g) Carbon-Dioxide Bubbles in 1.5 (wt.%) PAA [Table (7)].

for H = 0.50 m:

$V_f = 1 \times 10^{-6}\ m^3$ $\quad \therefore V_v \pm 11.43\%$

$V_f = 2 \times 10^{-6}\ m^3$ $\quad \therefore V_v \pm 9.22\%$

$V_f = 3 \times 10^{-6}\ m^3$ $\quad \therefore V_v \pm 7.04\%$

for H = 0.25 m:

$V_f = 1 \times 10^{-6}\ m^3$ $\quad \therefore V_v \pm 10.62\%$

$V_f = 2 \times 10^{-6}\ m^3$ $\quad \therefore V_v \pm 8.41\%$

$V_f = 3 \times 10^{-6}\ m^3$ $\quad \therefore V_v \pm 6.85\%$

(h) Nitrogen Bubbles in 1.5 (wt.%) PAA [Table (8)].

for H = 0.50 m:

$V_f = 1 \times 10^{-6}\ m^3$ $\quad \therefore V_v \pm 10.11\%$

$V_f = 2 \times 10^{-6}\ m^3$ $\quad \therefore V_v \pm 8.80\%$

$V_f = 3 \times 10^{-6}\ m^3$ $\quad \therefore V_v \pm 6.76\%$

for H = 0.25 m:

$V_f = 1 \times 10^{-6}\ m^3$ $\quad \therefore V_v \pm 9.36\%$

$V_f = 2 \times 10^{-6}\ m^3$ $\quad \therefore V_v \pm 7.69\%$

$V_f = 3 \times 10^{-6}\ m^3$ $\quad \therefore V_v \pm 5.25\%$

APPENDIX VI

Non-Linear Regression Computer Program
Used in Evaluating Parameters Utilized
in De Kee's Rheological Model.

Note: DPENLN in statement 12 is a computer library subroutine.

```
1.      //DAJAN    JOB  (GOGC,GS1),'    NURIA      ',CLASS=Z
2.      //  EXEC  WATFIV
3.      //GO.SYSIN  DD  *
4.      $JOB    WATFIV
5.      C       ABDULHAMID EL-MABRUK DAJAN
6.      C       TITLE 1.0(wt.%) POLYACRYLAMIDE (PAA) IN A 50/50(wt.%) MIXTURE
7.      C       OF GLYCERINE AND WATER WITH SURFACTANT .
8.      C       DATA OF VISCOSITY & SHEAR-RATE
9.      C       NON-LINEAR REGRESSION PROGRAM
10.     C       DETERMINATION OF CONSTANTS UTILIZED IN DE KEE'S MODEL
11.     C       ***************************************************************
12.             CALL DPENLN
13.             STOP
14.             END
15.             SUBROUTINE SUBZ(Y,X,B,PRNT,NPRNT,N)
16.             DIMENSION Y(50),X(50,1),B(10),PRNT(2)
17.             NPRNT=1
18.             RETURN
19.             END
20.             SUBROUTINE PCODE(P,X,B,PRNT,F,I)
21.             DIMENSION P(10),X(50,5),B(10),PRNT(2)
22.             P(1)=EXP(-B(2)*X(I,1))
23.             P(2)=-B(1)*X(I,1)*EXP(-B(2)*X(I,1))
24.             P(3)=EXP(-0.10*B(2)*X(I,1))
25.             P(4)=EXP(-0.01*B(2)*X(I,1))
26.             RETURN
27.             END
28.             SUBROUTINE FCODE(Y,X,B,PRNT,F,I)
29.             DIMENSION Y(50),X(50,1),B(10),PRNT(2)
30.             F=B(1)*EXP(-B(2)*X(I,1))+B(3)*EXP(-0.10*B(2)*X(I,1))
31.            C+B(4)*EXP(-0.01*B(2)*X(I,1))
32.             PRNT(1)=X(I,1)
33.             RETURN
34.             END
35.     $ENTRY
36.     015  4  0001000
37.          0  0  0    0000
38.
39.     0.67       0.34       0.32       0.28
40.     (F12.6,3X,F12.6)
41.           1.046      1.140
42.           0.897      4.275
43.           0.827      5.700
44.           0.471      11.400
45.           0.418      17.100
46.           0.366      22.800
47.           0.335      28.500
48.           0.306      37.050
49.           0.279      42.750
50.           0.256      51.300
51.           0.251      57.000
52.           0.218      71.250
53.           0.209      79.800
54.           0.196      91.200
55.           0.191      99.750
56.
57.     $IBSYS
```

```
 178.     0****PARAMETERS***   0.72287633E 00   0.29350023E 00   0.31489933E 00
.22344743E 00
 180.
 181.          Y OBS          Y PRED       (OBS-PRED)          X1              X2
 182.
 183.          1.0460         1.0446        0.14486E-02      1.1400
 184.         0.68700        0.70455       -0.75616E-02      4.2750
 185.         0.62700        0.62181        0.51923E-02      5.7000
 186.         0.47100        0.46691        0.40879E-02      11.400
 187.         0.41600        0.40793        0.10074E-01      17.100
 188.         0.38600        0.37115       -0.51498E-02      22.800
 189.         0.33500        0.34211       -0.71105E-02      28.500
 190.         0.30600        0.30659       -0.58544E-03      37.050
 191.         0.27900        0.28690       -0.78972E-02      42.750
 192.         0.25600        0.26208       -0.60816E-02      51.300
 193.         0.25100        0.24813        0.28706E-02      57.000
 194.         0.21800        0.22019       -0.21852E-02      71.250
 195.         0.20900        0.20706        0.19411E-02      79.800
 196.         0.19600        0.19263        0.33660E-02      91.200
 197.         0.19100        0.18359        0.74103E-02      99.750
```

REFERENCES

A1. Astarita, G. and Apuzzo, G., A.I.Ch.E.J., 11, 815 (1965).

A2. Acharya, A., Mashelkar, R.A., and Ulbrecht, J., Chem. Eng. Sci., 32, 863 (1977).

A3. Acharya, A. and Ulbrecht, J., A.I.Ch.E.J., 24, 348 (1978).

A4. Astarita, G., Ind. Eng. Chem. Fundl., 5, 549 (1966).

A5. Adamson, A.W., "Physical Chemistry of Surfaces", John Wiley, New York, (1982), 4th Edition.

A6. Atkins, P.W., "Physical Chemistry", Freeman, San Francisco (1982), 2nd Edition.

B1. Barnett, S.M., Humphrey, A.E., and Litt, M., A.I.Ch.E.J., 12, 253 (1966).

B2. Bhaga, D. and Weber, M.E., Chem. Eng. Sci., 35, 2467 (1980).

B3. Bailar, John C., Moeller, T., Kleinberg, J., Guss, Cyrus O., Castellion, Mary E., and Metz, Clyde, "General Chemistry", Academic Press, New York, (1978).

B4. Bird, R.B., Chem. Eng. Sci., 6, 123 (1957).

B5. Bird, R.B., Stewart, W.E., and Lightfoot, E.N., "Transport Phenomena", John Wiley, New York, (1960).

B6. Borisenko, A.I. and Tarapov, I.E., "Vector and Tensor Analysis with Applications", Dover, New York, (1979).

B7. Bennett, C.O. and Myers, J.E., "Momentum, Heat, and Mass Transfer", McGraw-Hill, New York, (1982), 3rd Edition.

B8. Butterworth, D. and Hewitt, G.F., "Two-Phase Flow and Heat Transfer", Oxford University Press, Oxford, (1979).

C1. Calderbank, P.H., Johnson, D.S.L., and Loudon, J., Chem. Eng. Sci., 25, 235 (1970).

C2. Crabtree, J.R. and Bridgwater, J., Chem. Eng. Sci., 26, 839 (1971).

C3. Clift, R., Grace, J.R., and Weber, M.E., "Bubbles, Drops, and Particles", Academic Press, New York,(1978).

C4. Caswell, B. and Schwartz, W.H., J. Fluid Mech., 13, 417 (1962).

C5. Carreau, P.J., DeKee, D., and Daroux, M., Can. J. Chem. Eng., 57, 135 (1979).

D1. de Nevers, N. and Wu, J.L., A.I.Ch.E.J., 17, 182 (1971).

D2. de Nevers, N., "Fluid Mechanics", Addison-Wesley, Reading, Massachusetts, (1977).

D3. DeKee, D. and Carreau, P.J., J. non-Newtonian Fluid Mech., 6, 127 (1979).

D4. DeKee, D. and Carreau, P.J., J. Rheology, 28, 109 (1984).

D5. Daily, J.W. and Harleman, D.R.F., "Fluid Dynamics", Addison-Wesley, Reading, Massachusetts, (1973).

G1. Garner, F.H. and Hammerton, D., Chem. Eng. Sci., 3, 1 (1954).

G2. Gillespie, T. and Rideal, E.K., Trans. Faraday Soc., 52, 1973 (1956).

G3. Goldstein, S., "Modern Developments in Fluid Dynamics", Vols. I and II, Dover, New York, (1965).

H1. Huang, W.S. and Kintner, R.C., A.I.Ch.E.J., 15, 735 (1969).

H2 Hughes, R.R. and Gilliland, E.R., Chem. Eng. Prog., 48, 497 (1952).

H3. Hewitt, G.F., "Measurement of Two Phase Flow Parameters", Academic Press, New York, (1978).

J1. Johnson, A.I. and Hamielec, A.E., A.I.Ch.E.J., 6, 145 (1960).

K1. Kawase, Y. and Ulbrecht, J.J., J. non-Newtonian Fluid Mech., 8, 203 (1981).

K2. Kline, S.J. and McClintock, F.A., Mech. Eng., 75, 3 (1953).

L1. Leal, L.G., Skoog, J., and Acrivos, A., Can. J. Chem. Eng., 49, 569 (1971).

L2. Levan, M.D. and Newman, J., A.I.Ch.E.J., 22, 695 (1976).

L3 Lodge, Arthur S., "Body Tensor Fields in Continuum Mechanics: With Applications to Polymer Rheology", Academic Press, New York, (1974).

L4. Lodge, Arthur S., "Elastic Liquids", Academic Press, New York, (1964).

L5. Lamb, H., "Hydrodynamics", Dover, New York, (1945), 6th Edition.

M1. Marrucci, G., Chem. Eng. Sci., 24, 975 (1969).

M2. Mendelson, H.S., A.I.Ch.E.J., 13, 250 (1967).

M3. Mordarski, J., M.A.Sc. Thesis, University of Windsor (1984).

M4. Miller, D.N., A.I.Ch.E.J., 29, 312 (1983).

M5. Markovitz, H. and Williamson, R.B., Trans. Soc. Rheo., 1, 25 (1957).

M6. Maxwell, J.C., Phil. Trans., 157, 49 (1866).

N1. Naik, S.C., Lee, J.C., and Richardson, J.F., Can. J. Chem. Eng., 55, 90 (1977).

N2. Narayanan, S., Goosens, L.H.J. and Kossen, N.W.F., Chem. Eng. Sci., 29, 2071 (1974).

S1. Shima, A. and Tsujino, T., Chem. Eng. Sci., 36, 931 (1981).

S2. Skelland, A.H.P. and Caenepeel, C.L., A.I.Ch.E.J., 18, 1154 (1972).

S3. Stokes, G.G., Camb. Phil. Trans., 7, 339 (1842).

S4. Stokes, G.G., Camb. Phil. Trans., 8, 105 (1843).

S5. Stokes, G.G., Brit. Ass. Report (1847).

S6. Stokes, G.G., Camb. Phil. Trans., 9, 166 (1850).

S7. Schraub, F.A., Kline, S.J., Henry, J., Runstadler, Jr., P.W., and Littell, A., Trans. ASME "J. Basic Eng.", 64 WA/FE-20, 1 (1964).

S8. Slattery, J.C., J. Colloid Sci., 16, 431 (1961).

S9. Sy, F., Taunton, J.W., and Lightfoot, E.N., A.I.Ch.E.J., 16, 386 (1970).

S10. Synge, J.L. and Schild, A., "Tensor Calculus", Dover, New York, (1978).

S11. Schlichting, H., "Boundary-Layer Theory", McGraw-Hill, New York, (1979), 7th Edition.

S12. Sears, F.W., Salinger, G.L., "Thermodynamics, Kinetic Theory, and Statistical Thermodynamics", Addison-Wesley, Reading, Massachusetts, (1975), 3rd Edition.

S13. Shames, I.H., "Mechanics of Fluids", McGraw-Hill, New York, (1982), 2nd Edition.

T1. Ting, R.Y., A.I.Ch.E.J., 21, 810 (1975).

V1. Vocel, J. and Ryan, J.T., Can. J. Chem. Eng., 49, 425 (1971).

V2. Vennard, J.K., and Street, R.L., "Elementary Fluid Mechanics", John Wiley, New York, (1982), 6th Edition.

V3. Virk, P.S. and Baher, H., Chem. Eng. Sci., 25, 1183 (1970).

W1. Wallis, G.B., (1970) Annular Two-Phase Flow. Part 1: A Simple Theory. Part 2: Additional Effects. J. Basic Eng., 92(1), 59.

W2. Wallis, G.B., "One-Dimensional Two-Phase Flow", McGraw-Hill, New York, (1969).

W3. Westerheide, D.E. and Westwater, J.W., A.I.Ch.E.J., 7, 357 (1961).

W4. White, F.M., "Viscous Fluid Flow", McGraw-Hill, New York, (1974).

W5. Wood, B.D., "Applications of Thermodynamics", Addison-Wesley, Reading, Massachusetts, (1982), 2nd Edition.

W6. Wrede, R.C., "Introduction to Vector and Tensor Analysis", Dover, New York, (1972).

W7. Wylie, C.R., "Advanced Engineering Mathematics", McGraw-Hill, New York, (1975), 4th Edition.

VITA AUCTORIS

ABDULHAMID MABRUK FADHIL DAJAN
Department of Mechanical Engineering
University of Windsor
Windsor, Ontario, Canada
N9B 3P4

***

February 18, 1954:	Born in Derna, Libya.
1973:	Completed high secondary school at Ibrahim Al-Osta Omar Secondary School, Derna, Libya.
1978:	Received Bachelor of Engineering Science (B.E.Sc.) in Mechanical Engineering from the University of Garyounis, Benghazi, Libya.
1979:	Mechanical Engineer at the Ammonia Plant, Marsa El-Brega, Libya.
1980:	Teaching Assistant at the University of Garyounis, Benghazi, Libya.
1985:	Currently, a candidate for the degree of Master of Applied Science (M.A.Sc.) in Mechanical Engineering at the University of Windsor, Windsor, Ontario, Canada, N9B 3P4.